THE CHARACTERIZATION OF FRECKLE CASTING DEFECTS IN DIRECTIONALLY SOLIDIFIED NICKEL-BASE SUPERALLOY TURBINE BLADES

By

ERIK M. MUELLER

A THESIS PRESENTED TO THE GRADUATE SCHOOL
OF THE UNIVERSITY OF FLORIDA IN PARTIAL FULFILLMENT
OF THE REQUIREMENTS FOR THE DEGREE OF
MASTER OF SCIENCE

UNIVERSITY OF FLORIDA

2003

This document is dedicated to everyone across the world who dreams and hopes for a better world.

ACKNOWLEDGMENTS

I would like first and foremost to thank my parents and God for giving me the opportunity to attend the University of Florida and receive a higher education. Many people across the world are unable to receive such a gift, so I hope I have made the best use of my years at school. I would also like to thank my sister, Melissa, and all my grandparents, aunts, uncles, and cousins for their continual support throughout my life. My good friends, Andy, Chris, and Julio, have also been there to show me what real friendship is like and to support me during this time. Of chief importance is Dr. Michael Kaufman, who has guided me through this project and has also been there as a friend for me when I needed help. Dr. Amelia Dempere was instrumental in providing me with the monetary support to be in graduate school to do this project. Without her and the Major Analytical Instrumentation Center (MAIC), this project would never have been possible. I would also like to Dr. Richard Connell for introducing me to materials engineering and Dr. Gerhard Fuchs for introducing me to superalloys.

TABLE OF CONTENTS

LIST OF TABLES

Table page

LIST OF FIGURES

Figure page

Abstract of Thesis Presented to the Graduate School
of the University of Florida in Partial Fulfillment of the
Requirements for the Degree of Master of Science

THE CHARACTERIZATION OF FRECKLE CASTING DEFECTS
IN DIRECTIONALLY SOLIDIFIED
NICKEL-BASE SUPERALLOY TURBINE BLADES

By

Erik M. Mueller

August 2003

Chair: Dr. Michael Kaufman
Major Department: Materials Science and Engineering

The purpose of this project was to characterize equiaxed grains, or freckles, that appear on the surface of directionally solidified superalloy turbine blades. There has been extensive work on modeling the formation of freckle defects on castings using mathematical models and 3-dimensional imaging. Unfortunately, not all the model predictions can explain every microstructure and defect created in a system with upwards of ten components. During a post-casting etch, much of the surface of these castings is lost—this project analyzed two castings with unaltered, unetched surfaces in an attempt to observe the microstructure in these regions. Stereology was also used to quantify the purported increase in various microstructural features near the freckles. Indeed a marked increase in porosity, η, and $\gamma + \gamma'$ eutectic colonies was seen in freckled regions of the castings. Several morphologies of γ' were observed, including grain boundary γ', γ' adjacent to grain boundaries, and eutectic γ'. It will be shown that these eutectic colonies

do not form by eutectic growth, but rather by cellular solidification. Further, there appears to be no preferred orientations of the freckle grains relative to the casting. Although not exclusive to freckle regions, the surface of the casting has an external alumina layer that is likely the result from a reaction between the ceramic mold and the Al in the liquid metal. Further, there are an unusually large number of MC carbides immediately underneath the alumina layer. These reactions, the freckle characteristics, and the microstructural evolution during single crystal growth will be described in some detail.

CHAPTER 1
INTRODUCTION

Today's modern jet aircraft, both military and civilian, demand higher performance, efficiency, and endurance from their engines. For many decades, the aerospace industry has believed that ceramics would eventually fill the role as the material of choice for turbine blades and vanes in jet engines. However, no available ceramic has both the toughness and high temperature strength requirements necessary in these sometimes corrosive environments. Therefore, the material of choice continues to be superalloys, particularly those of alloyed nickel.

Materials that provide relatively high strength and environmental resistance at elevated temperatures have been lumped into the category of high-temperature materials. When this subject is broached, materials that come to mind are usually ceramics, steels, refractory metals, superalloys, and certain carbon composites. However, one must take into account as to how one defines the phrase "high temperature." Can a specific temperature threshold be assigned, or is it relative to each material? For example, 2024 aluminum begins to melt at 502°C, and significant creep occurs above 300°C. This could obviously not be used in critical aircraft engines that operate in excess of 1000°C.

Therefore, the general rule is to base the designation of "high-temperature" to 30 to 50% of the melting point of a material. Above this 50% melting point, diffusion and other atomic motion mechanisms accumulate and the material loses usefulness. Therefore, it takes careful materials selection to find a suitable material for this

application. For the aforementioned turbine blade, one would choose a superalloy material. Other materials would likely be ruled out because

- Ceramics would not have the fracture toughness to withstand the high stresses in the turbine
- Refractory metals would oxide too fast
- Steels would creep and yield under these conditions.

Thus, for these applications, Ni-based superalloys are unique in that they not only possess the high strength and toughness at high temperatures, but they also have effective resistance against oxidation and corrosion if properly alloyed.

For aircraft turbine engines, the goal is to maximize the efficiency. By increasing the inlet temperature 56°C (100°F), the power output will increase 4%.[1] Nickel-base superalloys are distinctive in that, unlike most materials, they can operate at temperatures near 85% of their melting temperature. Today, aircraft engine manufacturers are busy trying to increase the engine output, which in turn requires better composition control. Nickel-base superalloys outperform cobalt-base superalloys because of the coherent precipitate phase, Ni_3Al. This phase increases the strength and rupture life of a turbine blade dramatically, especially as temperature increases.[2]

Besides alloy chemistry, there are other techniques to improve temperature capabilities—directional solidification and thermal barrier coatings. Directional solidification (DS) greatly improves the rupture strength and life of a turbine blade by reducing the number of grain boundaries normal to the applied stress. These grain boundaries are the reason for failure at elevated temperatures due to grain boundary fracture. A step above DS superalloys is blades cast as single crystals. Single crystal processing eliminates grain boundaries altogether, and these parts have been shown to

operate at temperatures 25-50°C higher than the same alloys directionally solidified. In addition, fatigue life is improved as well.

In spite of their superior properties, a major problem with using nickel-base superalloys is that they are extremely expensive. Many of the alloying elements (such as tantalum, rhenium, and ruthenium) cost in excess of $400 a pound. Add to the fact that the DS and single crystal casting methods are difficult to perform, and the price soars astronomically. Therefore, it is crucial to increase the quality control of the casting process and reduce the amount of material that has to be scrapped. A major problem in the turbine blade industry has been the formation of casting defects exclusive to DS and single crystal castings. These include scale and freckles. Superalloy scale is a rough raised layer on the casting surfaces that typically contains oxides and other undesirable phases—this can usually be removed by sandblasting or low-pressure water blasting. Freckles and other internal defects, though, cannot be removed as their depth is considerably greater.

Freckles in single crystal and DS castings appear as long chains of equiaxed grains that run vertically along the sides of the castings. They ruin the enhancements of the DS and single crystal processes by acting as failure sites for creep rupture. To detect freckles, the as-cast turbine blades are etched and visually inspected; if a freckle trail is discovered, the entire casting must be scrapped. Therefore, it is of significant importance to the jet propulsion and gas turbine industries to determine the cause of freckle defects and prevent their formation.

Consequently, the goal of this project is to characterize these freckle defects in DS superalloy castings and understand the mechanism of their formation. There has been

extensive work on modeling the formation of freckle defects on castings using mathematical models and 3-dimensional imaging. Unfortunately, not all of the model predictions correlate exactly to the actual castings defects. One of the major drawbacks is the etching process used to remove the surface of the casting to reveal freckles. A good portion of the surface layer is removed during this process, which may yield clues to the origin of these freckle defects.

Furthermore, many researchers have commented on the increase in various microstructural features near the freckled areas of the castings. However, no true quantitative measurements have yet been made. In this study stereological methods will be applied to the castings to determine what, if any, differences exist in the volume fraction of microstructural features in and near freckles relative to the rest of the casting. Other characterization techniques will also be employed to investigate these features qualitatively—shape, size, and relative location. The orientation of these features and the freckle grains themselves, with respect to the casting, will be investigated as well.

CHAPTER 2
LITERATURE REVIEW

As stated in Chapter 1, most of the research in characterizing freckle defects in nickel-base superalloys and correlating them with the mathematical modeling results has already been produced. This section will explain, in depth, about nickel base superalloys, their processing, chemistry, and the nature and theory behind their defects including freckles.

2.1. Nickel-Base Superalloys

Nickel base superalloys are often used for applications that require high strength and fracture toughness at elevated temperatures. These alloys are especially useful for the hottest areas of aircraft engines and industrial gas turbine engines (IGTs). This is because, in addition to being strong and tough, they are resistant to fatigue, oxidation, creep, and hot corrosion. These properties stem from the microstructure of the γ and γ' phases of nickel-base superalloys, the addition of various elements, and the casting processes and heat treatments used.

2.1.1. Chemical Composition

What makes superalloys unique is the coherent interface between the austenitic FCC γ structure and the $L1_2$ γ' structure of Ni_3Al (see Figure 1).[3] Both have nearly identical lattice parameters creating extremely low mismatch (see Figure 2).[2] The morphology of the γ' is determined by the mismatch: spheres occur from 0 to 0.2% and cubes appear from 0.5 to 1%.[2] The amount of misfit can be controlled, in part, by the concentration of other γ' formers. In fact, up to 60% of the Al in Ni_3Al can be substituted

by Ti, Ta, and Nb. The γ' phase is a superlattice that shows long-range ordering (LRO) to its melting point. Since this is the primary source of Ni superalloy strength, the volume percentage of γ' will greatly affect the strength of the alloy. Current commercial cast alloys have greater than 50% γ', which results in higher creep strength but dramatically reduces their hot workability. This increase in creep strength with increasing temperature is due to an anomalous increase of flow stress with temperature.[1]

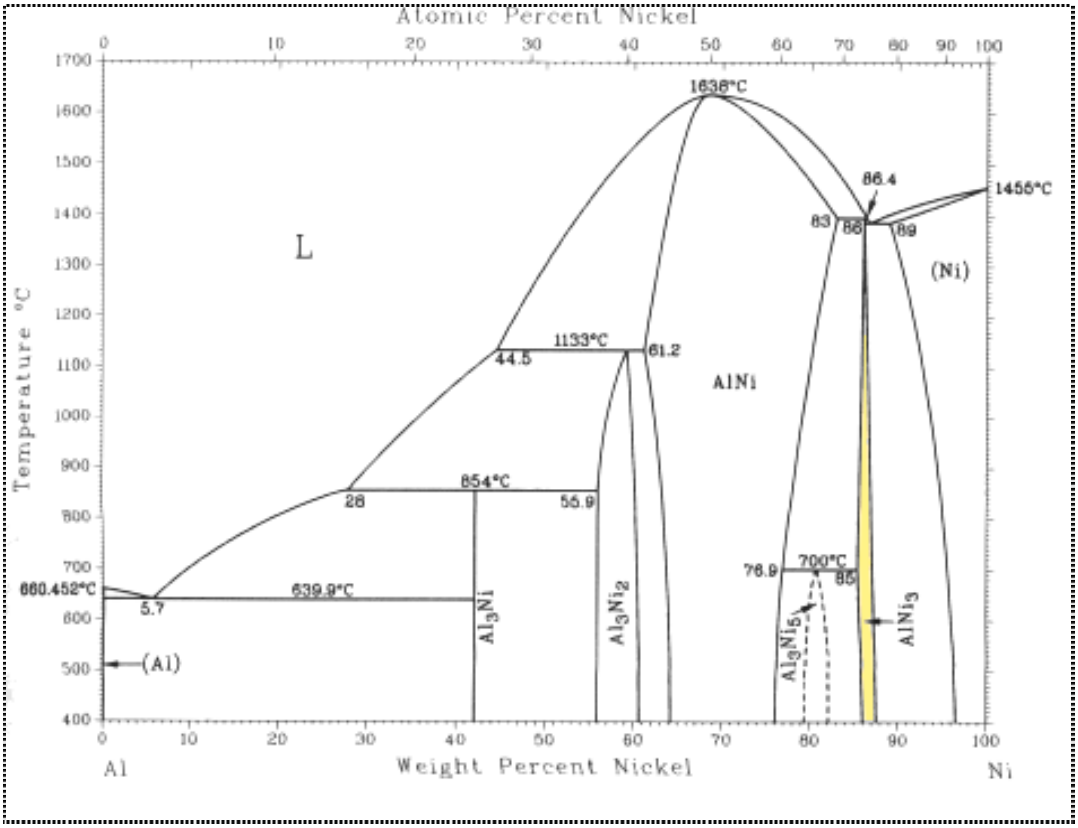

Figure 1 - Binary phase diagram of Ni and Al

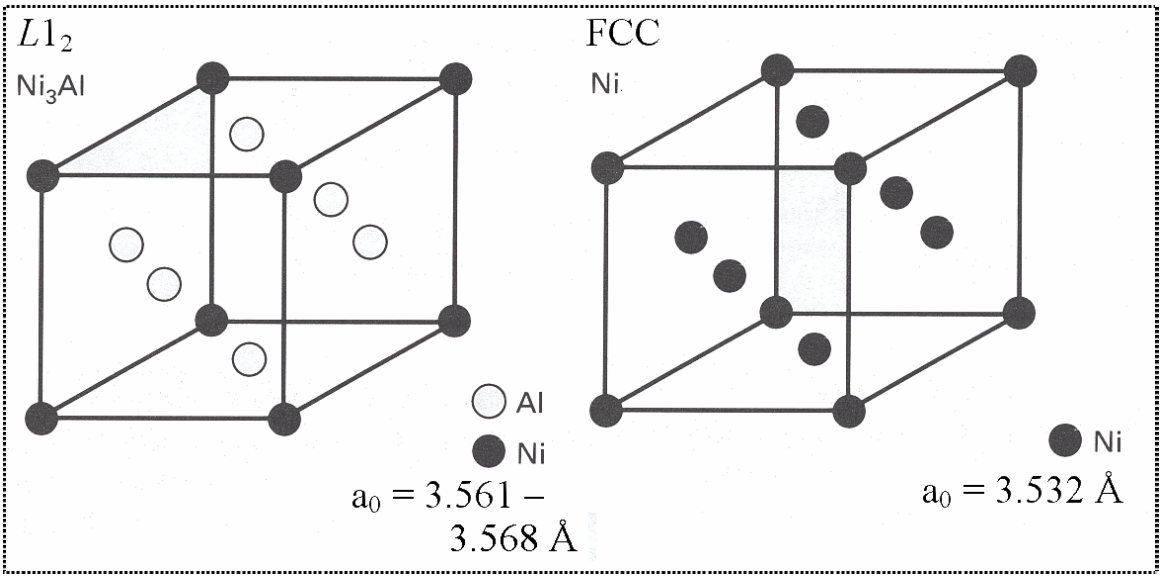

Figure 2 - Crystal structures of FCC Ni, γ, and Ni_3Al, γ'

2.1.2. Role of Alloying Elements

Modern superalloy compositions contain 8 or more elements, creating a very complex system to describe thermodynamically. It would be extremely difficult to construct and interpret an 8 to 10-dimensional phase diagram.[4] Furthermore, many of the sought after phases and microstructures of nickel-base superalloys are metastable and must be developed through careful heat treatments. Finally, many of these elements tend to segregate to different areas of the casting—either the dendrite core or the interdendritic regions.

One of the base elements for any nickel-base alloy is chromium, and in fact, the original superalloy was Ni-20Cr. Cr is an important element in that its primary function is to protect the alloy from oxidation and other forms of corrosion. Cr will form a protective oxide layer on the surface that will adhere well to the surface with a matching coefficient of thermal expansion. Cr is particularly effective in preventing hot corrosion and sulfidation. Unfortunately, the Cr_2O_3 layer is only effective until about 900°C. Cr also acts as a solid solution strengthener and carbide former.[2]

Another major element used to environmentally protect nickel-based superalloys is aluminum. Al, like Cr, forms a protective layer on the surface, but is more stable than Cr_2O_3 at higher temperatures. However, Al_2O_3 does not protect well in corrosive environments, such as sulfur intensive hot corrosion, so both Al and Cr are needed in relatively high quantities to protect the part. The primary function of Al, though, is to strengthen the alloy by forming γ'.

While being a solid-solution strengthener, Co also alters the γ' solvus temperature and aids in expanding the temperature window for heat treatments. Co also reduces the stacking fault energy (SFE) of the alloy, which improves creep resistance and makes dislocation cross slip around γ' particles more difficult.[1,5]

Ti, Ta, Nb, W, Re, and Mo are all used as solid-solution strengtheners. Ta, Ti, and Nb strengthen the γ' precipitates by enhancing the anti-phase boundary (APB) energy, while W, Re, and Mo strengthen the γ matrix. These elements, along with Cr, also react with carbon to form the various carbides present in superalloys. For various reasons usually stemming from corrosion and oxidation resistance, recent trends in DS and single crystal castings favor using more Ta, W, and Re for strengthening, as opposed to Mo and V, which were used in older alloy designs. Mo and V lower oxidation resistance while Re and W show synergistic effects in strengthening the γ/γ' interface. Ta strengthens γ', and has been shown to reduce freckle formation,[6] as will be discussed later. The concentration of these refractory elements must be controlled, however, as they increase the density, cost, and likelihood of forming deleterious topologically close-packed (TCP) phases.

C, B, Zr, and Hf are added to strengthen and stabilize grain boundaries. C reacts with Hf, Zr, and other elements of the casting (Ta and Ti) to form MC carbides, which retard grain boundary sliding and alleviate residual stresses in the casting. Hf and Zr are particularly effective in that they react with deleterious impurities, such as S and P, before all other elements. B, likewise, forms borides that also strengthen the grain boundaries. However, due to directional solidification and single crystal casting technologies, the need for grain boundary strengtheners and stabilizers has diminished.

2.1.3. Other Phases in Nickel-Base Superalloys

Besides the γ and γ' phases, there are many other phases that may be present in superalloys. Some, like carbides, are desired under certain conditions. However, the majority are detrimental phases that initiate fast fracture and reduce service life.

The C in superalloys tends to react with one or more alloying elements in solution to form carbides. Carbides serve as excellent grain-boundary strengtheners improving creep rupture life dramatically. They also strengthen the rest of the casting and act as traps for harmful elements such as P and S. Carbides formed in superalloys can be classified as either primary or secondary. Primary carbides are those that form from the melt and are almost always the MC phase (eg. TaC, TiC) with an NaCl structure. These carbides are randomly oriented with the matrix and are located both inter- and intragranularly. MC carbides tend to be extremely stable such that they typically survive various heat treatment schedules. Their morphology can be either script, cuboidal, or blocky.[2]

Secondary carbides are those that form from solid solution, usually during lower-temperature heat treatments or during service. Their constitution and structure depend on

overall alloy composition and include $M_{23}C_6$, M_7C_3, and M_6C carbides. These carbides usually appear at grain boundaries and can be created and altered in reactions between MC carbides and the γ matrix. M_7C_3 carbides are trigonal, form in low Cr concentrations, and are unstable. They usually decompose into $M_{23}C_6$ carbides, which have complex cubic structures and usually form in alloys with higher Cr concentrations. $M_{23}C_6$ are created either as a product of M_7C_3 decomposition, or as a reaction of MC and γ. The M_6C carbides are similar to that of the $M_{23}C_6$ in structure and morphology, except that they tend to form at higher levels of W and Mo. M_6C appear to be more stable at higher temperatures than $M_{23}C_6$.[1]

Borides, like carbides, act as excellent grain boundary strengtheners. They are usually hard, blocky particles of tetragonal M_3B_2, and form at small concentrations of B (<0.03 wt %). However, single crystal alloys usually lack carbon and boron due to the absence of grain boundaries. The philosophy behind most single crystal processing is to increase the amount of γ' for strengthening. However, as will be discussed later, carbon may have other beneficial effects on single crystal (SX) and DS superalloy castings.

In alloys with high concentrations of Nb, the γ" phase will form. This is a coherent body-centered tetragonal (bct) phase of Ni_3Nb. This phase strengthens the alloy primarily because of its high lattice mismatch strains with the matrix. Similar to γ', γ" will provide high strength at low temperatures, but unlike γ', it is a metastable phase which becomes unstable above 650°C. Furthermore, one must ensure a carefully controlled heat treatment to prevent the formation of the stable δ-phase of Ni_3Nb. This is an incoherent orthorhombic phase that can strengthen grain boundaries in small amounts, but in large amounts (more volume percent than γ") is detrimental to the alloy.

The hexagonal η-phase ($D0_{24}$) of $Ni_3(Ti,Ta)$ is often found in superalloys with high (Ti+Ta)/Al ratios, especially after considerable service life. The η phase can also form during solidification after the γ + γ' eutectic[7] and can appear in a pearlite structure of alternate lamellae with γ or as a ribbon-like Widmanstätten pattern.[2] In either case, the η phase grows slowly, but can eventually grow larger than the γ' particles. Usually occurring near grain boundaries, this incoherent brittle phase will reduce the ductility and rupture strength of the alloy. There has been limited investigation into η formation. This phase has been found to be a component in the scale that forms on castings of PWA 1483.[7] This η was found to contain a percentage of Si that dissolved from the mold. It was also found that the precipitation of MC carbides reduced η formation due to the reduction in the remaining Ti and Ta contents in the alloy.[7]

There are a myriad of TCP phases that can be present in a casting that are detrimental to the performance of the part. These phases are complex in nature, incoherent, and brittle resulting in a lowered rupture life, ductility, and creep resistance. These include μ, Laves, σ, P, and G phase.[1,2,8] The μ phase is rhombohedral and forms at high temperatures in alloys with high W and Mo. The tetragonal σ phase, which also appears in stainless steels, forms elongated, irregular globules with a structure similar to M_6C carbides and appears during service at elevated temperatures. Laves, P, and G phases are all complex, irregularly-shaped globules, which are strongly promoted by silicon and greatly reduce fatigue and creep resistance.[8,9] With all TCP phases, including η, only a slight change in local composition is is needed to force the composition past the stability threshold.

Besides these TCP phases, a variety of nitrides, oxides, hydrides, and other ceramic impurities can form and thus reduce the desired properties not only by acting as crack initiation sites, but also by removing alloying elements from solid solution. Therefore, it is imperative to control the chemistry of each casting and protect the environment during casting.

2.2. Processing of Superalloys

Nickel-base superalloys need to be processed under special conditions. They must be cast at high temperatures due to their high melting temperature (T_M), but must also be cast in a vacuum to prevent excessive oxidation and contamination. Those alloys with high concentrations of solid-solution strengtheners, especially γ' formers, cannot be hot or cold worked and must therefore be cast.

The casting or forging of nickel-base superalloy parts is a multistage process in controlled environments. First, the raw materials and reused scrap are vacuum induction melted (VIM). VIM involves melting of the material in a vacuum to prevent the formation of slag and control the reactivity of the elements. This melting step produces ingots with coarse, non-uniform grain sizes that must be refined for forged components. Either vacuum arc remelting (VAR) or electroslag remelting (ESR) are performed to refine the ingot. Both of these processes remelt the original VIM ingot to improve the microstructure and purify the alloy.[2] ESR differs from VAR in that it can be carried out in air. For castings, though, only the VIM process is necessary.

2.2.1. Investment Casting

Due to the complex shapes often required for blades and vanes, many superalloy components are best produced by lost-wax investment casting (see Figure 3).[10] Lost wax investment casting involves the creation of a replica made of wax that must be designed

to compensate for shrinkage. Any desired holes or cavities are produced by ceramic cores inserted into the wax pattern. The wax pattern is then assembled with other patterns to form a 'tree.' The tree is then dipped repeatedly into slurry baths while rotating to insure complete coverage and uniform thickness. When a sufficient slurry coating has been applied, the mold is covered with coarse stucco particles. This way, fine and smooth ceramic particles conform to the wax shape inside of the mold, whereas the stucco provides strength and prevents cracking and excess runoff of the wet slurry. This process is repeated several times until the mold is sufficiently thick.

The ceramic mold is then dried and placed into an oven for the dewaxing process. Here, the mold is heated to remove the wax and leave the hollow ceramic shell. It is important to control the rate of temperature change to prevent cracking in the mold. After the dewaxing process, the mold is sintered.

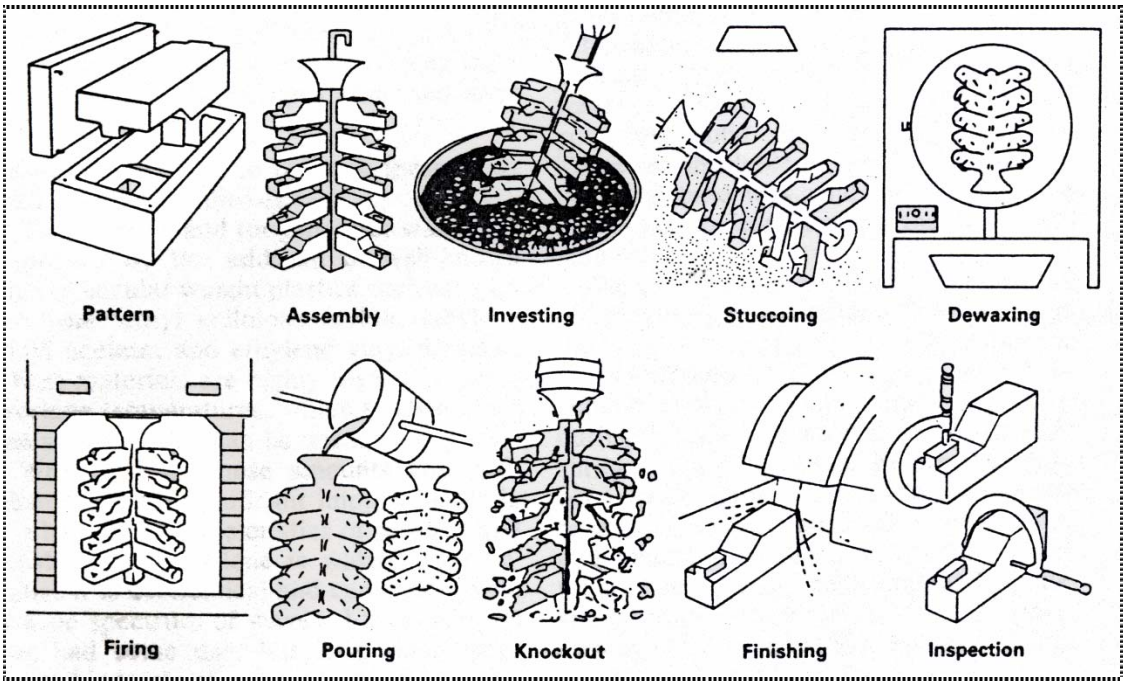

Figure 3 – The investment casting process

To make the actual casting, the ingots of superalloy are melted and poured into a preheated ceramic shell. After cooling, the ceramic shell is removed and usually destroyed, and the metal parts are machined off the 'tree.' However, for DS and SX castings, considerably more care (and cost) must be added to the investment casting process.

2.2.2. Directional Solidification (DS)

The process of directional solidification (DS) helped to revolutionize the development of modern nickel-base superalloys. DS alloys have higher creep rupture life in addition to improved fatigue resistance and ductility. This is due to the vast reduction in grain boundary surface area, which acts as an initiation site for creep failure. Fatigue resistance is maximized due to the <100> preferred growth direction of the DS grains (the <100> orientation has the lowest modulus, as opposed to other growth directions).[2,5]

The DS process for superalloy components involves an investment procedure but, in this case, a special furnace is used. The ceramic mold must be heated to above the liquidus temperature of the alloy in the furnace. The bottom of the mold is placed onto a chill plate of Cu or some other conductive metal that is water-cooled. After filling the shell with molten alloy, it is slowly withdrawn from the furnace, which is also above the liquidus temperature. This allows the original <100> grains to continuously grow throughout the casting (see Figure 4).[2]

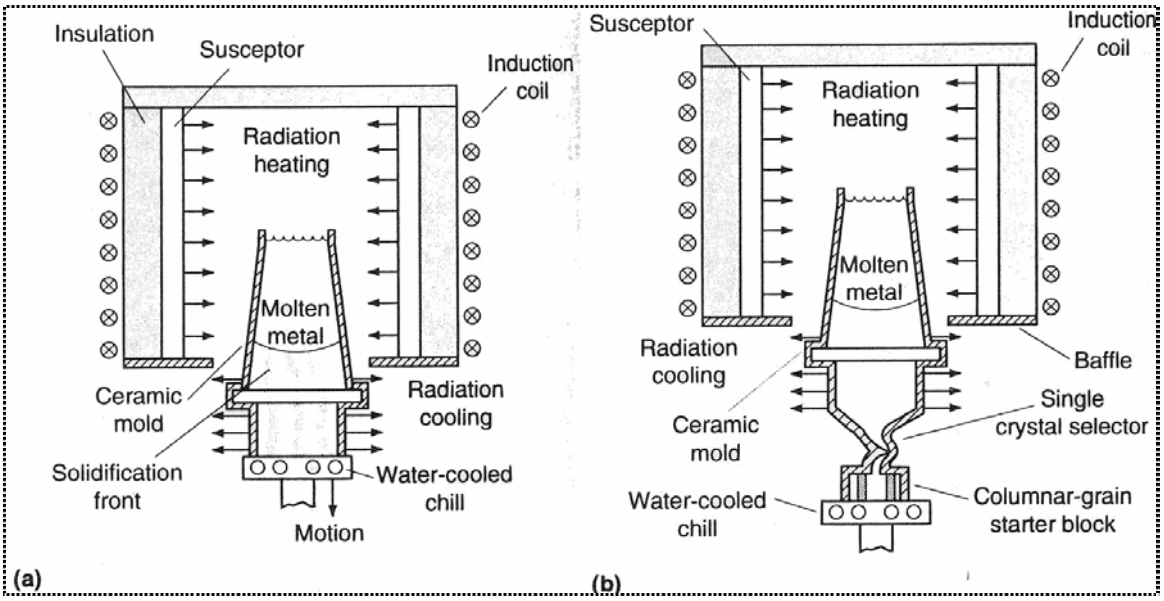

Figure 4 - Schematics of (a) a DS furnace and (b) a single crystal furnace

It is important to control the processing conditions of DS components in order to prevent a myriad of defects. Upon contact with the water-cooled chill, the molten alloy immediately solidifies and a thermal gradient (G) is established. This gradient is controlled and influenced by the temperature of the chill, the size of the casting, the temperature of the upper and lower chambers of the furnace, and other variables. The casting cannot be withdrawn until the solid dendrites have reached the area of the casting at the liquidus temperature. Because of the low thermal conductivity of Ni, the effect of the chill is small and the majority of heat must be dissipated by other means: conduction through the casting, conduction from the ceramic mold, and radiation emanating from the mold. At steady-state conditions, the thermal gradient is controlled by the size of the casting and the baffle. To ensure that the growth of columnar grains does not break down, G and the withdrawal velocity (R) must be carefully controlled.

Defects frequently occur in these castings and include grain boundary cracking, bulging, non-metallic inclusions, and recrystallization. Grain boundary cracking is caused by a hoop stress from ceramic cores during cooling and can be prevented by

adding Hf to the alloy. Bulging is caused by creep of the mold shell, causing flat surfaces in the casting to bulge out.[11] This distorts the ceramic mold, and inclusions are formed from parts of the mold that break off when the molten alloy is poured into the mold. Both of these defects can be resolved with better mold design and construction. However, the defects of chief concern are those involving the nucleation of equiaxed grains. Any recrystallization or nucleation of new grains defeats the purpose of the DS process and results in the part being scrapped. Freckles, spurious grains, and columnar-to-equiaxed transitions are a few of the defects that can occur. These will be discussed in Section 2.3.

A further advancement to DS casting was the development of SX castings with Ni-based superalloys. The same DS process is used, except that a seed or grain selector is added. Often helical in shape, the grain selector allows the <100> direction to dominate and eventually be the only grain growing into the component. An alternate method involves using a previously cast SX piece as a seed. The seed is allowed to partially melt and then the new solidification follows the growth direction of the seed. The advantage of the seed is that it allows any direction and orientation about that direction to be grown, though this process must be more rigidly controlled. The defects involved with SX castings are the same as those for DS except for grain boundary cracking. The absence of grain boundaries allows the removal of C, B, Hf, and Zr from alloy design. This increases the incipient melting temperature of the alloy and is one of the reasons for enhanced creep rupture life.

2.2.3. Microstructural Features

The microstructure of these DS alloys, and most solidified structures, stems from supercooling issues. As the liquid cools, the solidification front, which is initially a flat

surface, releases its latent heat of fusion at the interface. This increases the temperature on the liquid side of the interface, which creates a temperature inversion and results in cellular growth. This thermal supercooling, which exists in other solidification processes, is not as valid for DS as constitutional supercooling.[12] Here, the alloying elements partition—the solid that forms has a different composition from that of the original liquid. The liquid at the interface contains excess solute, which shifts the equilibrium liquidus temperature. If above the actual liquid temperature, it causes the solidification front to break down forming perturbations that lead to the formation of cells and dendrites. Eventually, more solute is built up in the lateral directions, forming perturbations on the advancing cells. These secondary perturbations lead to the formation of both secondary and tertiary dendrite arms on the already existing primary dendrite arms.[12,13] The spacing of the primary dendrite arms (λ) is related to the temperature gradient (G) and growth velocity (R) in the casting:

$$\lambda = K \cdot G^n \cdot R^m \quad (1)$$

K is a constant specific to the alloy, and $m \approx 0.25$ and $n \approx -0.5$ for many nickel-base alloys.[14-16]

In nickel-base superalloys, Cr, W, Re, and Mo segregate to the dendrite core while Ta, Ti, and Al remain in the interdendritic liquid.[2] Thus, the dendrite arms are γ, and MC carbides begin to precipitate as cooling proceeds (usually 5-30°C below the liquidus[2,17,18]). The solidification concludes with the $\gamma + \gamma'$ eutectic that occurs over a small, 5°C window.[19] The γ' precipitates in the γ regions spread throughout the γ dendrites and large amounts of $\gamma + \gamma'$ eutectic remains where the interdendritic fluid solidified last.

The dendritic structure of the castings is not always perfectly aligned with respect to the bottom of the chill. This is due to the development of curvature in the liquidus isotherm that occurs when the conduction of heat through the casting is much less than the conduction and radiation of heat out of the mold walls. The opposite effect occurs in VAR ingots in that there is more heat on the outside than inside, causing a convex upward liquidus isotherm. Since the dendrites tend to grow normal to the solidification front (or antiparallel to the direction of heat flux), the dendrites will bend somewhat when the isotherm curves. This is the cause of "splaying" of dendrites and can cause the part to be rejected if the deviation from <100> is severe enough (usually around 10° from other subgrains).

As described above, alloying elements partition and microsegregate during dendritic solidification. Another process called macrosegregation occurs when solute is transported over large distances. Macrosegregation is a result of convection caused by density differences in the casting. A form of macrosegregation, called inverse segregation, can occur in DS castings from the back flow of solute-enriched interdendritic liquid through the interdendritic channels in the casting as it cools.[20] In Al-Cu alloys, the Cu solute can actually emanate from the chill surface and alongside the casting.[21-22] This backflow of interdendritic fluid is controlled by the viscosity and permeability of the fluid. As the primary dendrite arm spacing (PDAS) increases, the permeability through the dendritic mushy zone will increase. The PDAS is inversely proportional to the thermal gradient and withdrawal rate, so segregation will be favored at low G and R.

2.3. Freckles

Freckle casting defects have been discovered in many kinds of various DS alloys besides superalloys. They were found originally in iron-base superalloys and have been seen in steels, solders, and various other alloys near the eutectic composition.[23] They have been observed in both castings and ingots.[23-24] In all these alloys, the freckle defects were found to be long chains of equiaxed grains parallel to the primary dendrite arms whose composition was close to that of the interdendritic regions. They have been found on the surface of castings and near the midradius of ingots. The number of, and even presence of, freckle chains has been found to increase as the diameter of the casting increases. Consistent with this observation, there is a minimum diameter or size at which freckle chains will not form—even if conditions are ideal for freckling.

Freckle chains begin to form at a certain length above the chill in DS and SX castings. The chains commonly converge as one moves up the casting, but divergence does not occurs. It was observed by Giamei that the freckle chains are as deep as they are wide—approximately 1-2 mm.[23] Freckle grains are observed to be replete with misoriented grains, eutectic, carbides, and porosity. Unfortunately, there is no quantitative or stereological data to confirm this and most reports are based on qualitative observations only.

In superalloys such as CMSX4, Waspaloy, Mar-M 200, and PWA 1480, the freckle grains are purportedly enriched in those elements that partition to the liquid during solidification, such as Al, Ta, Nb, and Ti. There is also a lack of those elements that segregate to the dendrite core in freckles (Co, Cr, and other refractory elements). In fact, freckling often occurs in those alloys with high concentrations of W and Re. However,

additions of Ta and sometimes Nb have been shown to reduce the propensity for freckle formation in these castings.

Besides castings, freckles have been found in VAR processed ingots of Waspaloy.[24] The freckles in this case occur at the midradius rather than the surface. This is one of the largest problems with freckles in ingots in that they cannot be detected, even by ultrasound, unless they are cut open. Due to the large size of these ingots, this is an undesirable solution. Characterization of these ingot freckles resulted in large quantities of script carbides and η-phase with a Widmanstätten morphology. This explains the increased hardness in the freckle areas and the propensity for fatigue and fracture initiation sites. Even though VAR ingots eventually are forged into polycrystalline parts, the presence of these ingot freckles greatly reduces uniformity in the ingot and can be a source of fracture during processing.

2.3.1. Theories of Freckle Formation

From the earliest research into freckle formation, it was immediately noticed that freckle chains would always form at a distance away from the chill, where the thermal gradient and growth velocity of the mushy zone had decreased.[23] In addition, the compositional shift towards the eutectic composition in the freckle chains pointed to a clue of the origin of these defects. Copley was the first to see freckle chains actually forming by using a solution of water and NH_4Cl near eutectic composition.[25] The solution was directionally solidified on a chill cooled with liquid nitrogen. As was soon discovered, interdendritic liquid from inside the mushy zone tended to "jet" upward from the mush into the liquid layer. The liquid would remain immiscible due partly to its cooler temperature. Along the way, these jets would erode dendrites and break them

apart where they would redissolve into the liquid or act as nucleation sites for equiaxed grains.

It was also shown that the jets emanate from the highest part of the mushy zone. In castings, the mushy zone is concave upward due to the surface being cooler than the rest of the interior. Thus, the freckle trails appear on the surface. In VAR ingots where the mushy zone is convex upward, the jet plumes emanate to the casting interior. The jet trails are also always parallel to the direction of gravity. Figure 5 show vectors of channel flow calculated for a solder alloy.[26] Solute from the mushy zone flows up, forcing the liquid above the mush down into it. If a casting is directionally solidified at an angle so that the mushy zone is tipped (since primary dendrites always grow opposite to the direction of heat flux), the jet plumes will still grow parallel to gravity.[25]

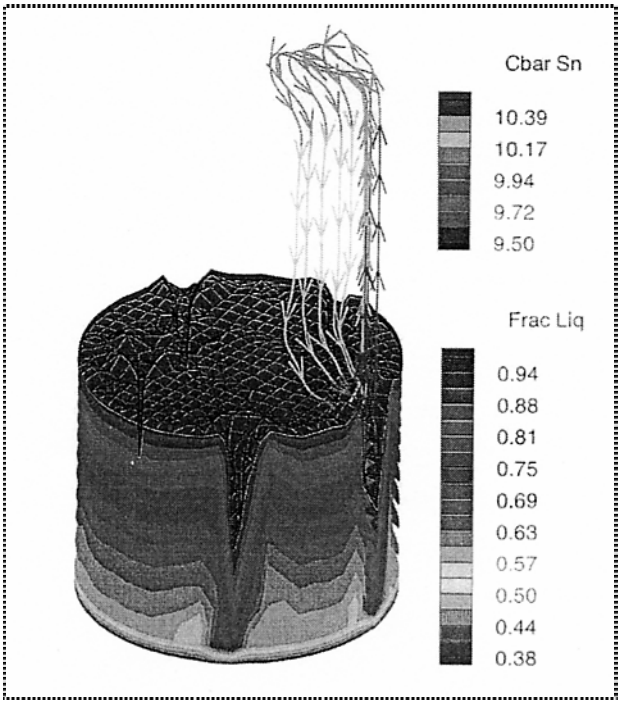

Figure 5 - Isosurfaces of volume fraction and stream traces emerging from a channel

The relation of this H_2O-NH_4Cl system to superalloy solidification was made in later research. The freckle grains tended to have an increase in both Al and Ti, but lacked

the heavier W and Re, which were found in the dendrite core.[6] Therefore, it was found that in nickel-base superalloys, excess segregation of the heavier refractory elements into the dendrite core and lighter γ' formers into the interdendritic fluid create a density inversion. At a critical G and R, a pressure increase in the interdendritic fluid forces it out at the highest point of the mushy zone as small jet plume. During this process, named thermosolutal convection, the plumes break off dendrite arms as they shoot upward.[6,27] The interdendritic fluid does not readily mix with the rest of the liquid due to its difference in density and temperature between the two liquids. This interdendritic plume eventually solidifies as a chain of small, equiaxed grains where the nuclei are purportedly the dendrite arms removed by the plumes. Figure 6 shows a model of these plumes and how they remain immiscible in the liquid.[26]

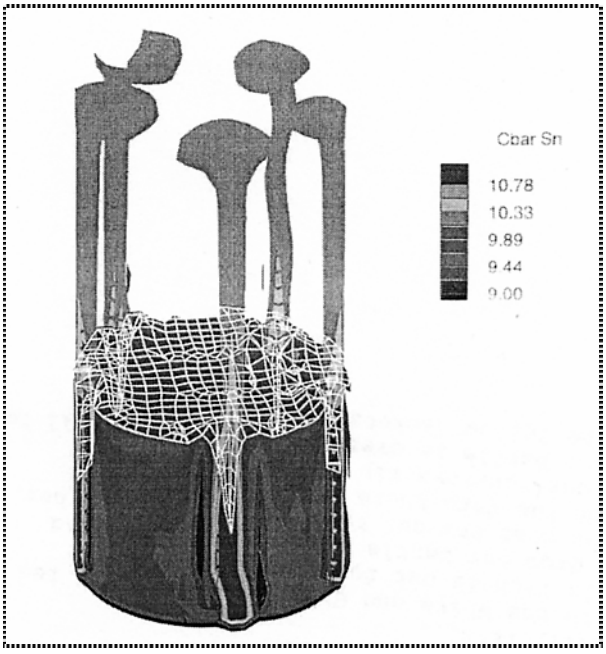

Figure 6 – Isosurfaces of solute concentration, showing solute enrichment within channels and the emerging plumes.

Knowing the cause, the question was then figuring out how to prevent the formation of freckles. Copley proposed controlling the R and G. At high R, the amount

of heat released into the mushy zone must be less than what is conducted through the solid to maintain the flow of heat out of the casting. Thus, the growth rate can be defined as

$$R = \frac{K_T * G_S}{\Delta H} \tag{2}$$

where K_T and G_S are the conductivity and temperature gradient of the solid, respectively, and ΔH is the heat of fusion.[25] Under equilibrium, freckle formation is controlled by the difference in temperature between the liquidus and solidus (ΔT), the minimum time necessary to produce freckles (Δt), and the gradient, G. Therefore, the growth rate can be defined as

$$R = \frac{\Delta T}{\Delta t}\frac{1}{G} \tag{3}$$

As Copley discovered, above a critical thermal gradient (G*) the mushy zone becomes too small to accommodate the convective currents that would produce freckles (see Figure 7).[25]

Other solutions, though, involved altering the alloy chemistry. The major cause of freckle formation stems from substantial segregation of the heavier elements to the dendrite core. Reducing the concentration of W and/or Re would reduce the propensity to form freckles. However, in doing so the strengthening effects of these elements are sacrificed. In castings with high Ta contents (or Ta to W + Re ratios), few, if any, freckle chains appear. Ta partitions to the interdendritic liquid, which helps to increase its density and hinder thermosolutal convection.[6,28]

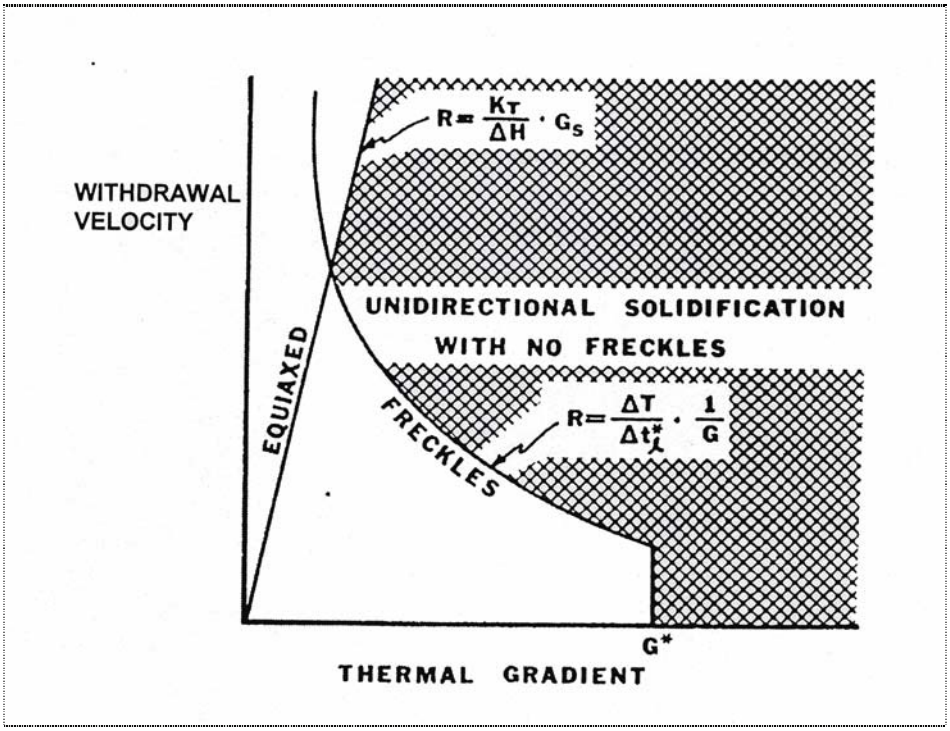

Figure 7 - The effect of growth velocity (R) and thermal gradient (G) on freckle formation.

Most SX alloys contain no C since there are no grain boundaries to strengthen. However, small additions of C have been shown to hinder freckle formation by altering the segregation behavior of certain elements.[29] It was shown that MC carbides, while containing no W, reduced it from segregating to the dendrite core. More likely, though, the carbides that formed increased the permeability in the interdendritic fluid by increasing the drag force and, due to their high density, stave off the density inversion that occurs in the mushy zone.[29]

2.3.2. Modeling

While a change to the chemistry of these alloys helps prevent the onset of freckling, this may not be acceptable for all castings. As previously shown, castings with high Ta concentrations have the tendency to form η. Therefore, returning to the fine-tuning of processing conditions was investigated. Consequently, a large amount of effort has been

placed into modeling the situation of thermosolutal convection and what impact various conditions have on the process. This has led to the creation of models and criteria that attempt to describe the conditions that promote freckle formation during solidification.

The first mathematical constructions of freckle channel formation were originally developed by Sarazin and Hellawell on a variety of solder alloys.[27] These binary Pb-Sn and Pb-Sb systems were chosen due to their simplicity (rather than the multicomponent superalloys). Their research attempted to use permeability and thermodynamic data to calculate various dimensionless fluid mechanics numbers. Using these numbers, one could determine the conditions necessary for thermosolutal convection to occur. It was discovered that there is a critical Rayleigh number below which freckling will not occur. More recently, research has been slated towards three-dimensional modeling of freckle-forming binary alloys.[26,30]

The Rayleigh number (Ra) is a dimensionless number used for convection and is officially defined as the driving force to flow over the resistance to flow or

$$Ra = \frac{g \cdot \alpha \cdot \Delta T \cdot h^3}{\nu \cdot D_T} \tag{4}$$

where g is gravitational acceleration, α the coefficient of thermal expansion, ν the dynamic viscosity, D_T the thermal diffusivity, and h some length or dimension.[31] Above a critical Rayleigh number (Ra*), turbulent flow will commence. There have been differing opinions of how to define and apply the Rayleigh criterion to freckle formation—using mathematical criteria[25,27-28,32] or conservation equations.[33-35] Auburtin et al. believed conservation equations cannot be practically applied to industry and derived their Ra criterion from mathematical standards.[36] Their version,

$$Ra = \frac{g \cdot d\rho / dz \cdot h^4}{\nu \cdot D_T} \tag{5}$$

uses the density inversion (dρ/dz) instead of a temperature difference. One of the difficult parts in applying this criterion to superalloy castings is how to define the characteristic length, h. Here, Auburtin defines it as the primary dendrite arm spacing. Beckermann et al., however, define their Rayleigh criterion through conservation equations:[37]

$$Ra = \frac{g \cdot \Delta\rho / \rho_0 \cdot \overline{K} \cdot h}{\nu \cdot D_T} \tag{6}$$

Beckermann uses the mean permeability ($\overline{K}$) in his equation and defines the characteristic length as the mushy zone height. It is believed that this approach is more applicable to a large variety of casting conditions. Nevertheless, both authors have determined how to use Rayleigh criteria to predict freckling:

- Determine the local Rayleigh number (Ra^{MAX}) from the local G and R either through thermocouple measurements or analyzing primary dendrite arm spacings.
- Determine the critical Rayleigh number (Ra*) below which freckling will not occur.
- Ensure that $Ra^{MAX} < Ra^*$.

It should be noted that Ra* will only predict at what point freckling *will not* occur; it cannot predict freckle formation.[36,37] Even if the local Ra is higher than Ra*, freckles may not form due to small casting cross sections, complex shapes, or small vertical heights. Likewise, Ra* will not predict where or how many freckle chains will form. Both authors also discovered that tilting the casting significantly decreases Ra*, increasing the likelihood of freckle formation.[25,36,37]

Schneider et al. continued the work of Beckermann et al. by using the conservation equations with several computer simulators previously used by the steel industry.[35] The simulations included tracking the concentrations of various elements in the convective channels in castings with various thermal gradients and growth velocities, which were combined here as cooling rate:

$$\dot{T} = G \cdot R \tag{7}$$

Most importantly, a critical PDAS was found above which the system becomes unstable and convection occurs. For CMSX2, the critical primary dendrite arm spacing was 320 μm.[35]

Pollock and Murphy also correlated the formation of convective jets to the columnar-to-equiaxed transition (CET) in DS and SX alloys. This transition is a breakdown of the single crystal or columnar grains caused by a blockage of columnar growth brought on by contact with the melt walls, remelting, and fragmentation of dendrite arms, or some other mechanism.[28] Freckling and CET occur under similar conditions. In both, it was found that at low G, secondary and tertiary dendrite arms remelt, detach, and fragment. These dendrite fragments serve as nucleation sites for new grains. Furthermore, the detached arms also impede the advancing solidification front, reducing R as well. This complicates the situation but allows a total transition from single or columnar to small, equiaxed grains.

CHAPTER 3
METHODS AND MATERIALS

3.1. Materials

The materials used for this procedure were two nickel-base superalloy castings directionally solidified from the Howmet Corporation in Hampton, VA. Due to proprietary concerns, the composition and processing variables were not disclosed. It was therefore a challenge to try to compare compositions of the materials and to determine if any elements had segregated. Energy dispersive spectroscopy (EDS), which will be discussed later, was used to ascertain the chemistries, and compare them to similar industrial compositions from literature.

3.2. Optical Microscopy

The purpose of the optical microscopy was to examine the microstructural features, and to measure the PDAS. The main goal was to try to discover if there was more porosity, eutectic, and other features around the freckled region than in the rest of the casting. Furthermore, the amounts microstructural features inside and near the freckle grains were contrasted with the rest of the casting.

The PDAS was found using the optical microscope at low magnifications (usually 50X) on specimens cut perpendicular to the growth direction of the primary dendrite. The PDAS was then measured from one dendrite core to the nearest diagonal dendrite core. This process was repeated multiple times to reduce the variance in the results.

3.3. Preparation of Samples

The samples for optical microscopy were cut using a wire electrical discharge machine (EDM). The samples were ground in sequence with 120, 240, 320, 400, 600, 800, and 1200-grit SiC polishing paper. The fine polishing was performed using a 1.0 μm alumina suspension. The surface features were brought out by using an etchant of 80 mL hydrochloric acid, 2 mL nitric acid, 11 mL water, and 16g FeCl.[38] These samples were then viewed through the Leco Neophot 21 optical microscope.

The process of cutting the bars was difficult, especially for the DS-2 samples. A wire EDM was chosen over a cut-off wheel because when the cutoff blade was deep into the sample, the sample would move causing the blade to shatter. Similar problems were encountered with the wire EDM. As the wire cut deeper into the sample, the cut metal around the wire would close in on itself, pinching the wire off (see Figure 8). This may have been due to residual stresses in both castings. Therefore, careful, slow, and repetitious EDM cuts had to be made for the each desired specimen.

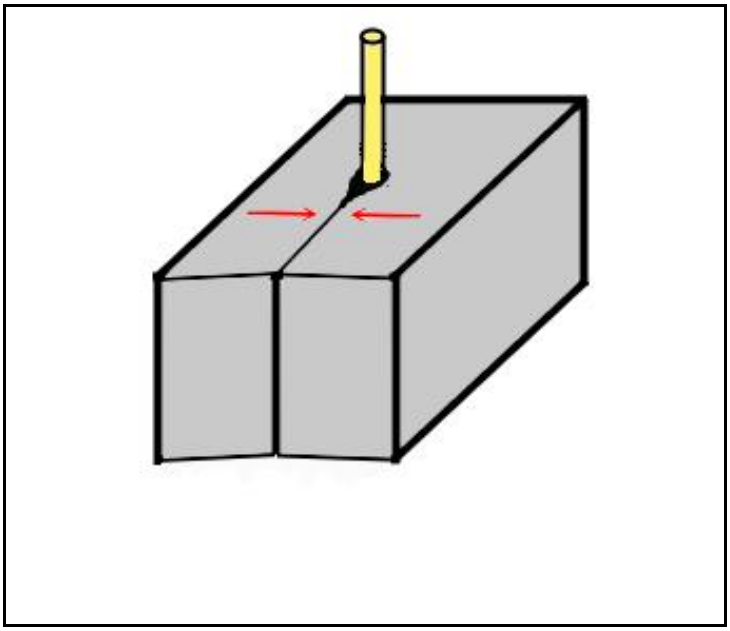

Figure 8 - Illustration showing the castings pinching back on itself after being cut by the wire EDM

Another complication was that the only regions of interest in these bulky samples was near the surface containing the freckle chains and extended only a few millimeters into the surface. Therefore, carefully designed cuts were made in the freckled regions from and were less than 10 mm into the sample. In order to get the best picture to characterize the samples, cuts were made in three directions (see Figure 9):

1. Parallel to the growth direction and parallel to the casting surface
2. Parallel to the growth direction and perpendicular to the casting surface
3. Perpendicular to the both growth direction and the casting surface.

In reality, however, Cut 1 is not really a cut, but rather the surface polished and etched to reveal the grain structure.

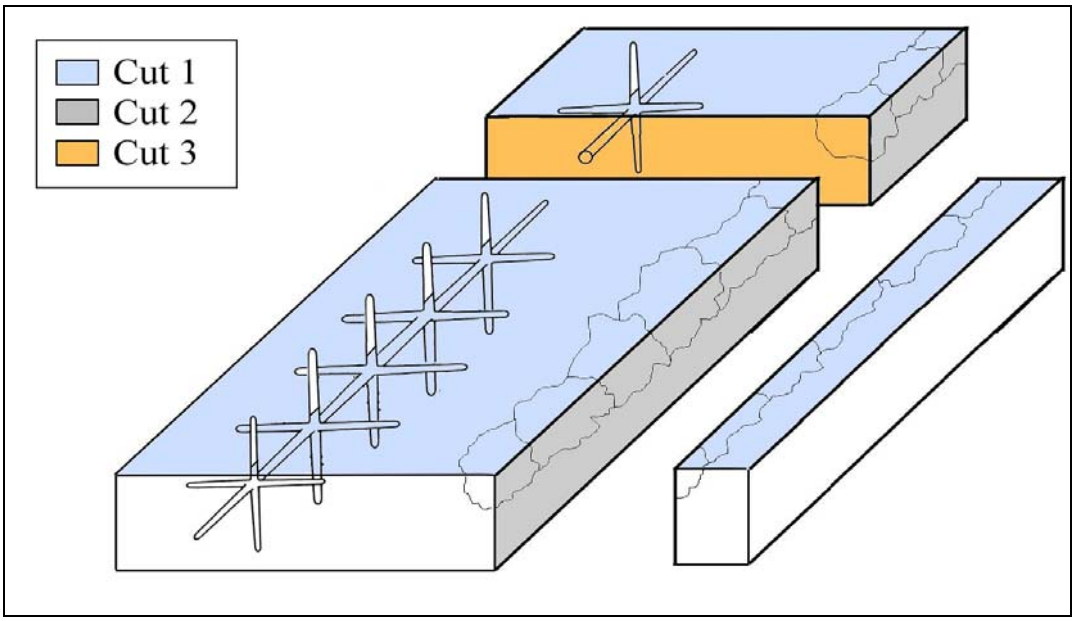

Figure 9 - Illustration of the directions cut in relation to the primary dendrite arms (not to scale).

3.4. Stereology

In order to quantify the microstructural features in the alloys, stereological methods were used. Stereology involves using information from a two dimensional image to find three-dimensional properties. This includes using point, line, and area probes and

running the data through expected value theorems to get geometric properties of the structure.[39] For example, from a count of points, one can infer the volume fraction of a microstructural feature. Some of the probing techniques are shown in Figure 10. These probes are then used to find properties of the microstructure (see Table 1). This project used these techniques to determine

- The quantitative volume percentages of microstructural features inside the freckles
- The quantitative volume percentages of microstructural features in freckled regions (so as to include the grain boundary areas)

The microstructural constituents of interest are eutectic, porosity, carbides, and η-phase. These were contrasted with the measurements found in the rest of the casting. The stereological measurements were taken from optical photographs as well as scanning electron microscope (SEM) micrographs (see below).

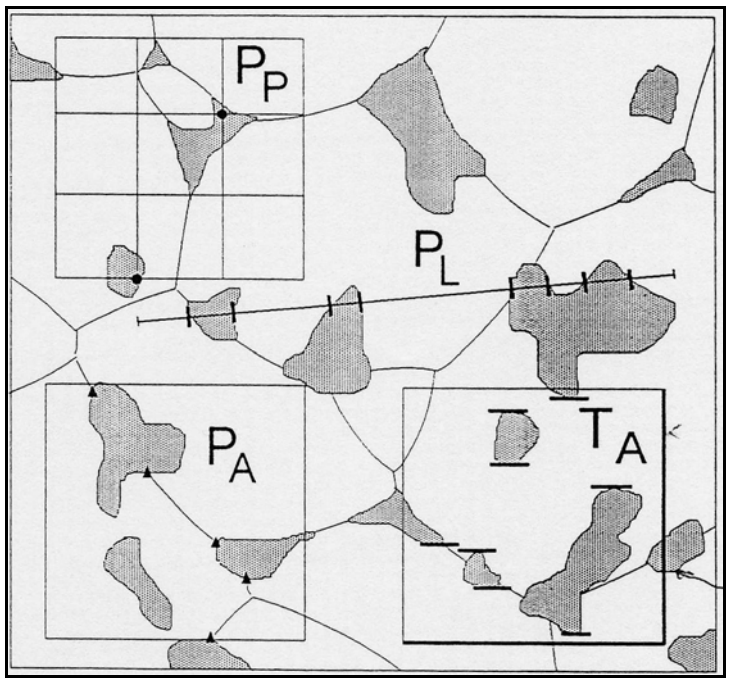

Figure 10 - Manual counting methods used for stereology

Table 1 - Common stereological formulas and relations to microstructural features

Probe Count	Relation	Property Found
Point Count	$<P_P> = V_V$	Volume Fraction
Line Intercept Count	$<P_L> = 0.5\ S_V$	Surface Area Density
Area Point Count	$<P_A> = 0.5\ L_V$	Length Density
Feature Count	$<N_A> = M_V/2\pi$	Total Curvature
Area Tangent Count	$<T_A> = M_V/\pi$	Total Curvature

It is important to ensure that the probe set used is isotropic, uniform, and random.[39] In addition, the correct number of probes must be used to ensure proper data collection and filter out noise. Part of the problem for this project was that the target for sampling was in and near the freckle grains. This reduces the chance of a random set of fields being sampled and can throw off the actual volume percent of the desired constituents.

Therefore, for this project, a set of 20 fields, each with 324 point grids were chosen to take volume fraction measurements in random spots inside the freckled area, and in areas in which freckles existed. These were contrasted with a sampling amount for areas in the casting, near the surface, that showed no freckle formations. There was a difference noted between the probes inside the freckle and those outside for those fields that encompassed freckled and non-freckled regions. Furthermore, the results from the position of the freckle chains were compared. If no trend can be associated with the position, then any cross-section will be random and uniform. Otherwise, an extra interpretive factor must be added.

3.5. SEM and TEM

Samples were prepared for SEM and transmission electron microscope (TEM) similar to those fashioned for optical microscopy—they were cut using the EDM. The samples were also polished with 120, 240, 320, 400, 600, 800, and 1200-grit SiC polishing paper. Fine polishing was done with 1.0 μm alumina suspension. An etching

solution from Van der Voort was used contained 80 mL hydrochloric acid, 2 mL nitric acid, 11 mL water, and 16g FeCl.[38] These samples were preheated at 180°F in hot water before etching. The SEM used was a JEOL SEM 6400 equipped with Oxford Link ISIS EDS and Oxford OPAL electron backscattered secondary electron detector (EBSD).

The samples prepared for TEM were ground and polished in a similar manner to those for SEM and optical microscopy. However, these thin slices were ground to approximately 100 μm before polishing mechanically. The thin polished specimens were pressed to form 3 mm disks. These disks were then electropolished in a solution of 50 mL perchloric acid, 100 mL of ethylene glycol, and 350 mL of methanol at -20°C, 10 mV, and 1 to 5 A until a small hole appeared. The area around the hole needed to be sufficiently thin to be electron transparent. If not, the specimens were ion milled at a low angle (~12°) to thin the regions near the hole. The TEMs used were a JEOL TEM200CX and a Philips TEM420 equipped with an EDAX EDS system.

3.6. Electron Backscattered Diffraction

As previously mentioned, the JEOL SEM 6400 is fitted with an Oxford OPAL system. Similar to convergent beam diffraction patterns, the EBSD technique collects data to create a Kikuchi map, which contains crystallographic data along with information on orientation relationships and grain misorientation. This is done when the detector, which is a phosphor-coated screen, collects backscattered electrons and forms a pattern of lines whose configurations are determined by the orientation and structure of the crystal. The samples for EBSD are 10 mm wide and less than 1 mm thick and are placed at 70° to the detector. The accelerating voltage used was 20 kV.

3.7. Nanoindentation

A Hysitron Triboindenter nanoindenter was used to determine the hardness and moduli of different microconstituents in the castings. The Triboindenter, which is controlled by a Triboscan transducer, works by affixing a nanotip to an electrostatically held plate between two other plates (see Figure 9). The outer plates are fixed to electrodes where a potential is created by adding an AC current 180° out of phase. As the center plate moves, the potential changes allowing for displacement measurement. Force is measured by a DC current applied to the center plate.

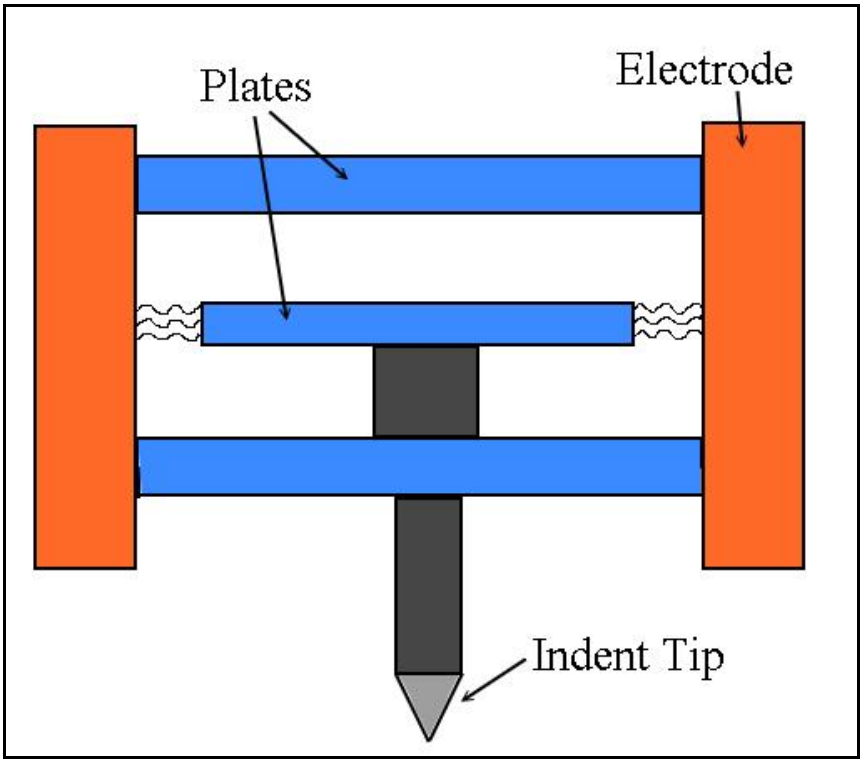

Figure 11 - Illustration of indent head mechanism in the Triboindenter .

Using the nanoindenter, nanohardness measurements and modulus mapping could be performed. Nanoindentation involves forcing the tip into the surface with a known load. The depth is monitored and force is measured as the tip is released to give hardness and relaxed modulus measurements. Multiple indents were performed on various

constituents in both castings with a Berkovich indenter at loads ranging from 500 to 5000 μN. This range of loads was used to counteract problems associated at both extremes: small loads can produce results with increased scatter due to the greater impact of noise, and large loads can create indents too large to accurately characterize small phases. Modulus mapping was performed by oscillating the tip to collect force and phase measurements while also gathering topographical data.

CHAPTER 4
RESULTS

The results acquired are divided into four parts. The first discusses the SEM and optical pictures showing and describing the microstructure and morphology of the superalloy samples. The next section shows the stereological data of the microstructure. The third section details the grain orientations and results found from the EBSD data. The last section discusses data found from the nanoindenter.

4.1. Microstructural Characterization

There were two large samples obtained from the Howmet Corporation. One, which will be herein designated DS-1, is a section off of an airfoil approximately 300 mm tall, 70 mm wide, and up to 25 mm thick (see Figure 12). The second sample set is from a larger 1.2 m long industrial gas turbine blade, 300 mm wide, and 120 mm thick, with two hollow cavities running through the middle (see Figure 13). This specimen was cut from the top of the DS casting. Close examination of Figure 13 reveals freckle chains on the side of the castings—some of these are pointed out in the figure.

The primary difference between the two castings is that the DS-1 casting had been etched to reveal freckle grains, whereas the DS-2 castings had not—they still had their original, undisturbed surface. While this was intriguing to study the possible surface effects of the second casting, it also presented a problem when using the wire EDM to cut them. Specifically, the "virgin" surface was not sufficiently conductive to be spark cut due to the remnant oxide/ceramic that remained after casting. This was overcome by scratching the surface to be cut and having the wire cut at precisely that location.

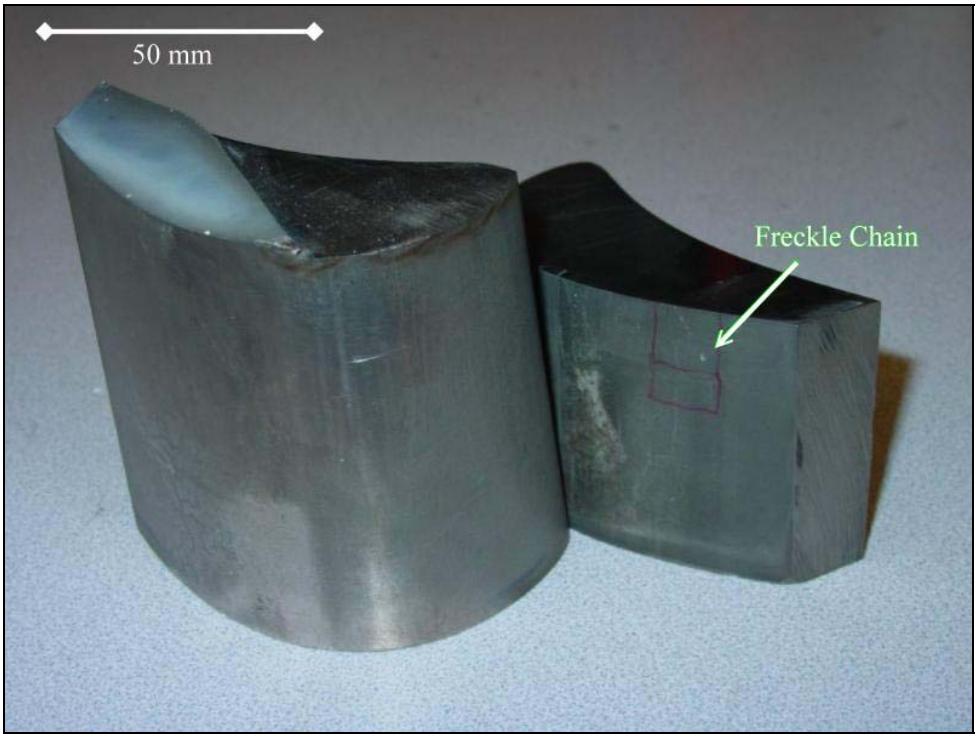

Figure 12 - Photograph of the DS-1 castings and a labeled freckle chain.

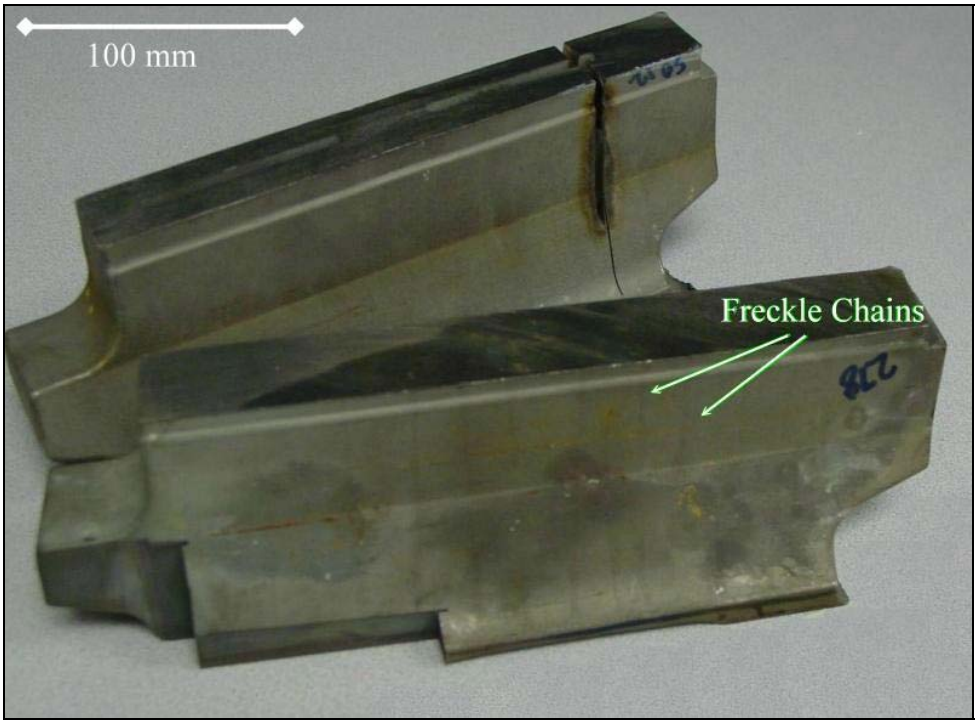

Figure 13 - Photograph of the DS-2 castings with some visible freckle chains labeled.

4.1.1. Compositions

The overall compositions of the DS-1 and DS-2 castings were not revealed by Howmet due to their proprietary nature. In an effort to determine both global and local compositional information, EDS spectra were obtained from the samples at low magnifications in an area, not point, mode in order to accommodate as much area as possible. These scans included the freckled regions, and were large enough to incorporate all the phases and constituents to prevent biasing the results from the segregation of elements. Multiple scans were run in order to minimize deviations. Figure 14 shows an EDS spectrum from the DS-2 casting. Spectra from the DS-1 casting were similar to the DS-2 and had the same elements present.

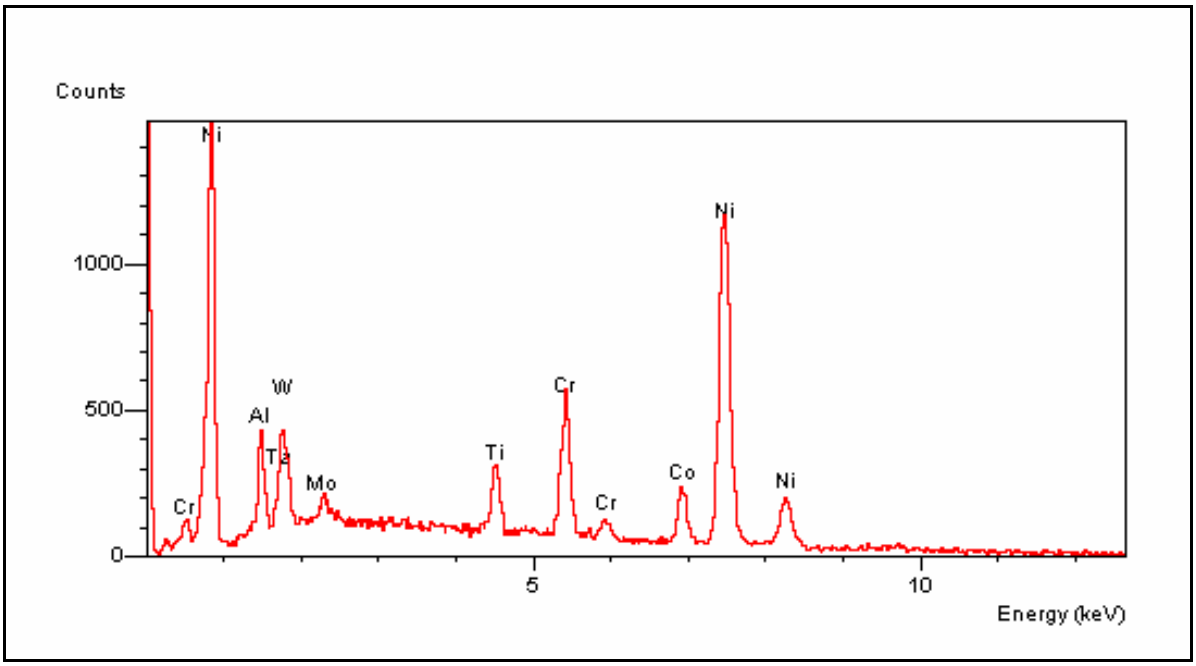

Figure 14 - EDS spectrum of DS-2 alloy at 15 kV.

Using the atomic number, absorption, and fluorescence (or ZAF) correction software on the EDS system, a semi-quantitative analysis was performed on the qualitative data in the EDS spectra. This technique uses matrices, summations, and formula integrations to estimate weight and atomic percent of a sample based on peak

height, elements found, etc.[40] The weight percentages for both DS-1 and DS-2 alloys, excluding carbon, are shown in Table 2. The resulting analysis suggested that the DS-2 casting is similar to a Rene N4 alloy minus Nb and Hf, and DS-1 seemed comparable to PWA 1483.[2]

Table 2 - Estimated nominal compositions of DS-1 and DS-2 alloy. These compositions are compared to that of Rene N4 and PWA 1483.

C	Al	Ti	Cr	Co	Ni	Mo	Ta	W	Nb	Hf
DS-1 (Small Airfoil)										
xxxxx	2.9	6.1	12.8	9.3	59.1	1.8	3.2	4.8		
PWA 1483										
0.07	3.6	4	12.8	9	60.8	1.9	4	3.8		
DS-2 (Large Pieces)										
xxxxx	2.9	3.5	9.9	7.8	64	1.3	4.2	6.3		
Rene N4										
0.06	4.2	3.5	9.8	7.5	62	1.5	4.8	6	0.5	0.15

In addition, semi-quantitative EDS analysis was performed at a higher magnification to contrast compositions in the freckled regions with that of the rest of the casting (or matrix). The results, without carbon, are shown in Figure 15 for DS-1 and Figure 16 for DS-2. For both alloys, the freckled regions were higher in Al, Ti, and Ta, and lower in Cr, Co, W, and Mo. It should be noted that ZAF semi-quantitative analysis is susceptible to error during the EDS collection, and from the nature of the ZAF correction itself.

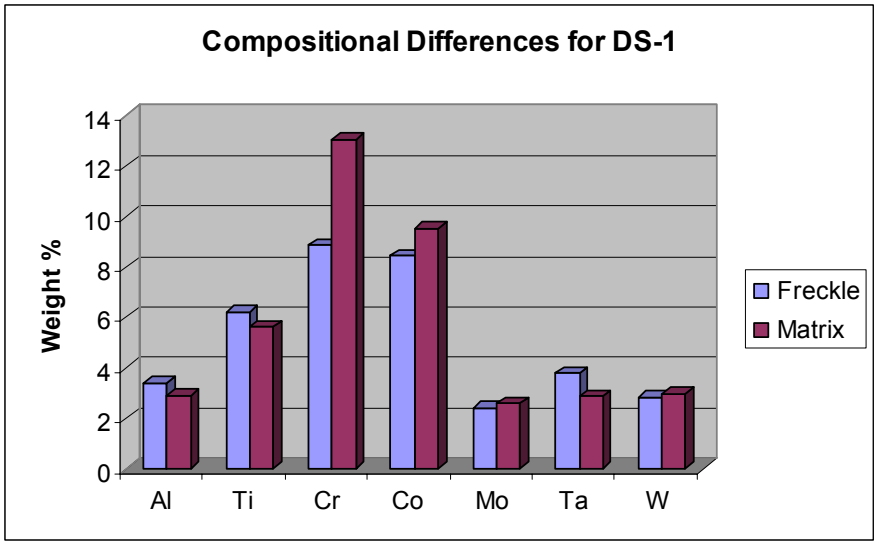

Figure 15 - Comparison of freckle chain and matrix compositions in weight percent from DS-1 alloy without Ni.

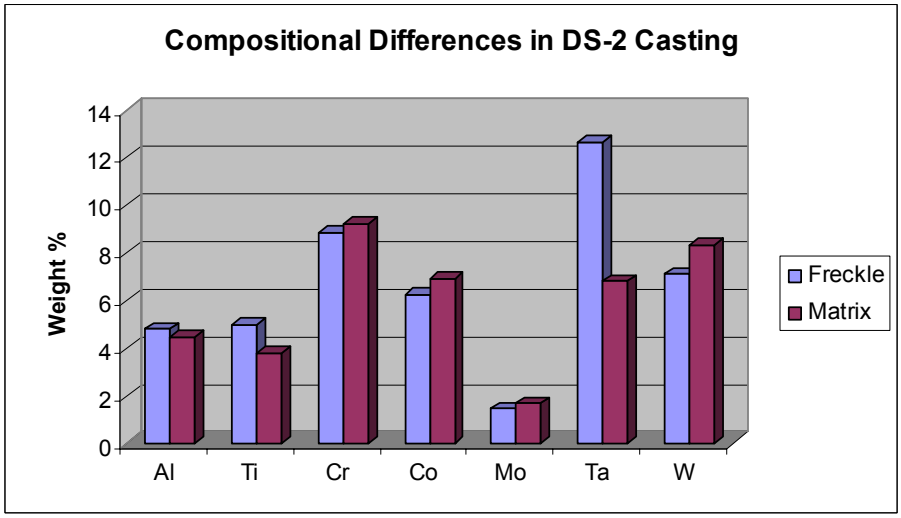

Figure 16 - Comparison of freckle chain and matrix compositions in weight percent from DS-2 alloy without Ni.

The freckles in the DS-1 casting about the same Al, Ti, Cr, and Mo amounts as DS-2, but the amounts of Co, Ta, and W and were different. The Co and W differences between the freckle grains of the two castings correspond to the compositional differences between the two alloys as a whole. However, the freckle Ta differences are too great to associate with composition and likely indicates substantial Ta segregation in DS-2 to the interdendritic during solidification.

4.1.2. Surface of the Castings

The freckle chains were observed visually on the surface macroscopically, and were studied microscopically as well. The dendritic structure was revealed in Figure 17 for DS-1 and in Figure 18 for DS-2. The primary (and secondary) dendrites are all arranged in a <100> type direction. Here, as shown in Figure 17, the dendritic structure of the freckle grains is more randomly oriented, and no direct relation could be determined by visual inspection alone. The orientations were identified later using EBSD.

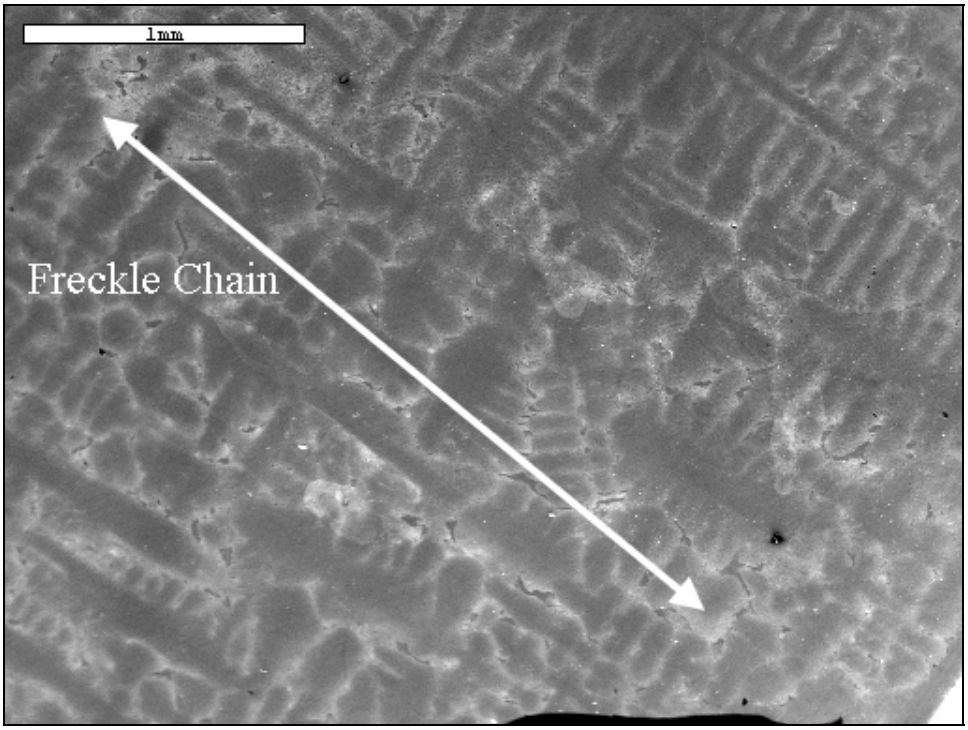

Figure 17 - SEM (Scanning Electron Micrograph) of etched DS-1 surface showing dendritic structure. Freckle grains run diagonal from top left to bottom right (35X).

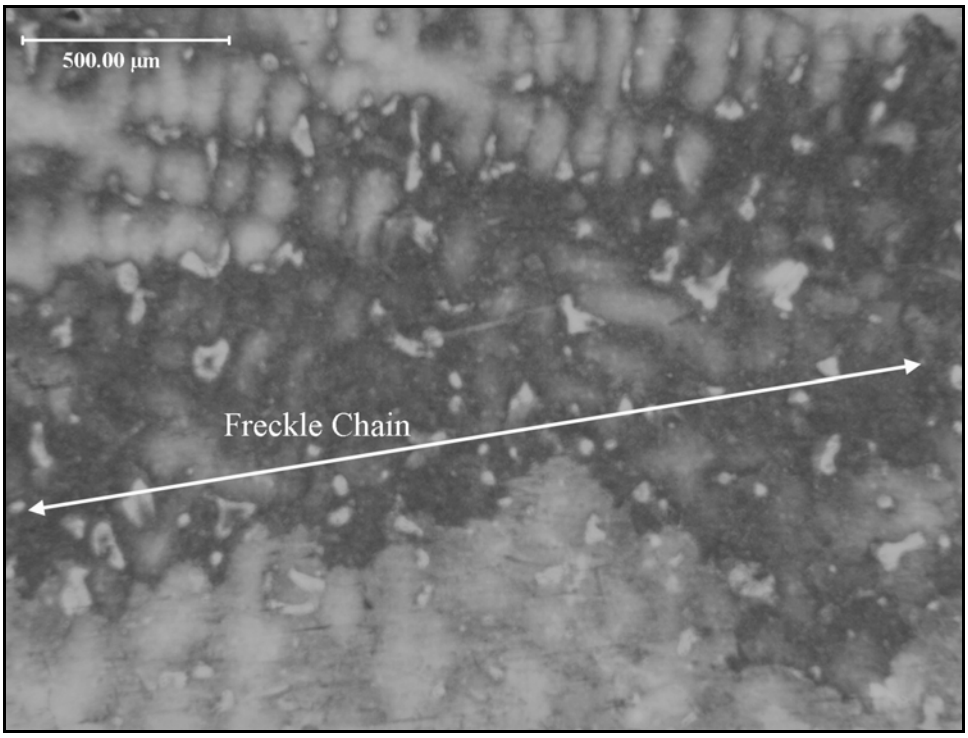

Figure 18 - SEM of etched surface of DS-2 casting revealing dendritic structureof freckle chain. The chain runs left to right in the middle of the picture (50X).

As noted above, the surface of the DS-2 castings was initially unaltered after it was broken out of the mold. This "virgin" surface (see Figure 19) exhibits charging non-metallic phases approximately 100 to 400 µm in size. Further inspection of this phase (see Figure 20) in the backscattered mode shows the charging particles are of low atomic weight, and also revealed some smaller, high atomic weight phases (see Figure 21). The X-ray map (see Figure 22), reveals the larger charging phase to be alumina while the smaller, brighter phase is likely (Ta,Ti)C carbide. Traces of ZrO_2 were also found on the surface, most likely left over from the ceramics mold.

It was discovered that the overall composition of the surface differed in the freckled regions and in the rest of the casting (here called "matrix"). From Figure 23, one can see these compositional differences. There may have been a larger percentage of alumina in the freckled regions, or it might just reflect the results from Figure 16.

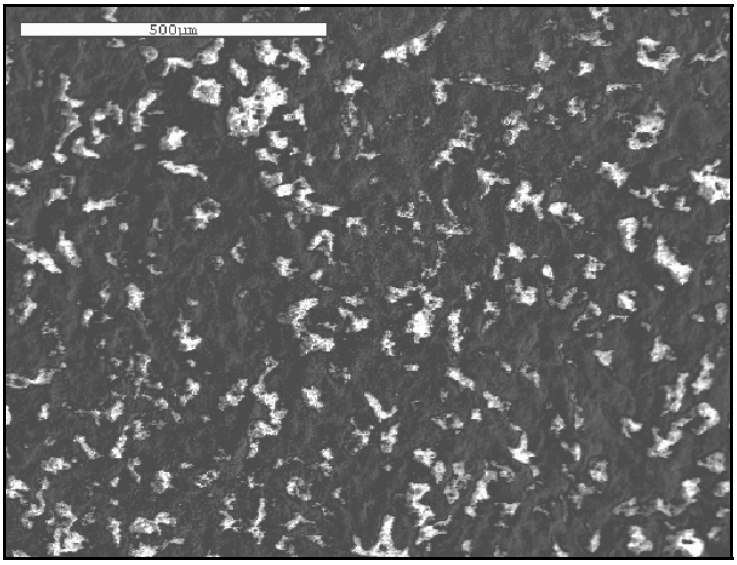

Figure 19 - SEM of unaltered DS-2 alloy surface (100X).

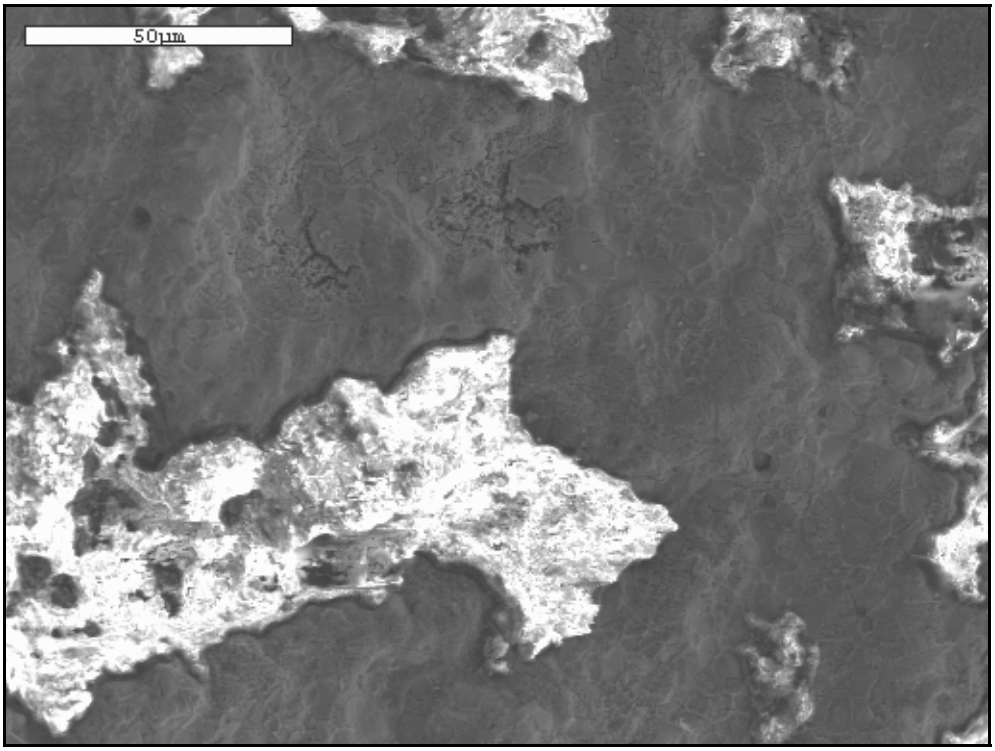

Figure 20 - SEM of surface of DS-2 casting showing charging alumina phase (650X).

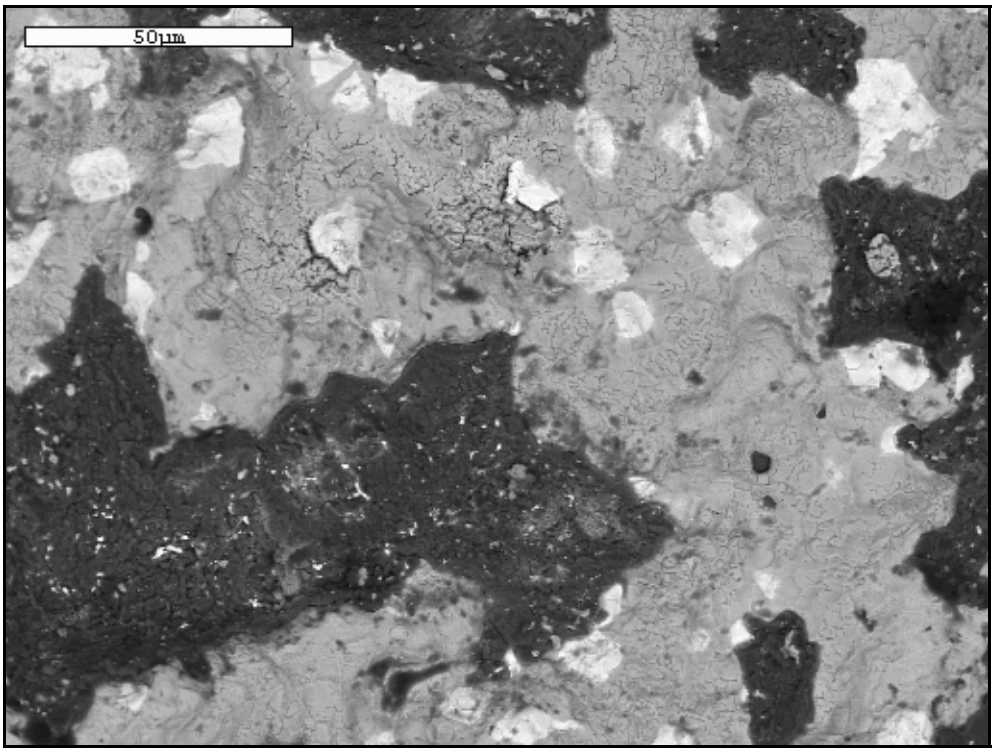

Figure 21 - BSE (Backscattered Electron) SEM of Figure 20. The brighter areas have elements with higher atomic numbers (high Z).

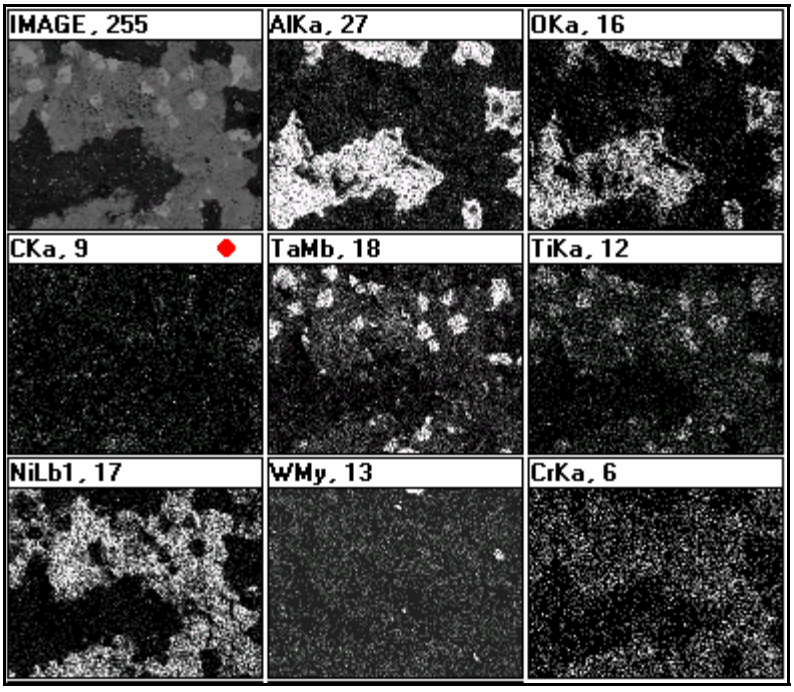

Figure 22 - X-Ray map of Figure 21 revealing the Al enrichment in the charging phase and the Ta and Ti enrichment in the high Z phase.

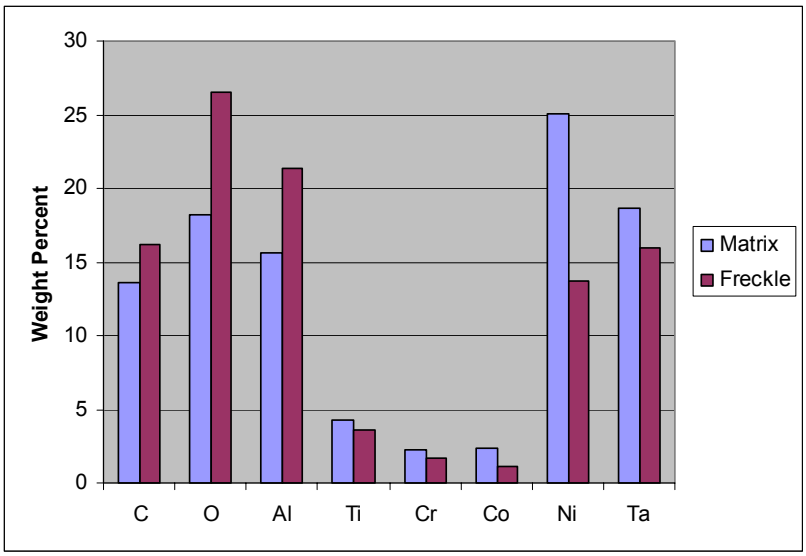

Figure 23 - Comparison of EDS data from matrix and freckle regions of unaltered surface of DS-2 alloy.

4.1.3. Eutectic Colonies and Porosity

Large amounts of eutectic were found in and near the freckle grain boundaries. Qualitatively, the volume percent seemed larger at and around the freckles than the rest of the casting. Quantitative data describing these differences are in Section 4.2.

The microstructure of the eutectic colonies in the current castings and in other cast Ni-base superalloys, when cross-sectioned, appears as a fan of small γ rods or plates in a "pool" of γ'. This is shown in Figure 24. The γ structure can also take up other forms, such as a web (see Figure 25). From other planes, such as the surface cut in Figure 26, the eutectic colony may show a different structure. In the current alloys, the eutectic is believed to be the last liquid to freeze, and thus has the highest content of those elements that partition away from the dendrite core (Al, Ta, Ti). Furthermore, in the DS-2 castings, there was porosity near the eutectic colonies in the freckle chain (as well as elsewhere in the casting). This is shown in the optical micrograph in Figure 27. In the DS-1 alloy, though, porosity is also associated with the hexagonal η, or $Ni_3(TaTi)$, phase

at the eutectic/matrix boundaries (see Figure 28). The η phase will be discussed in Section 4.1.5.

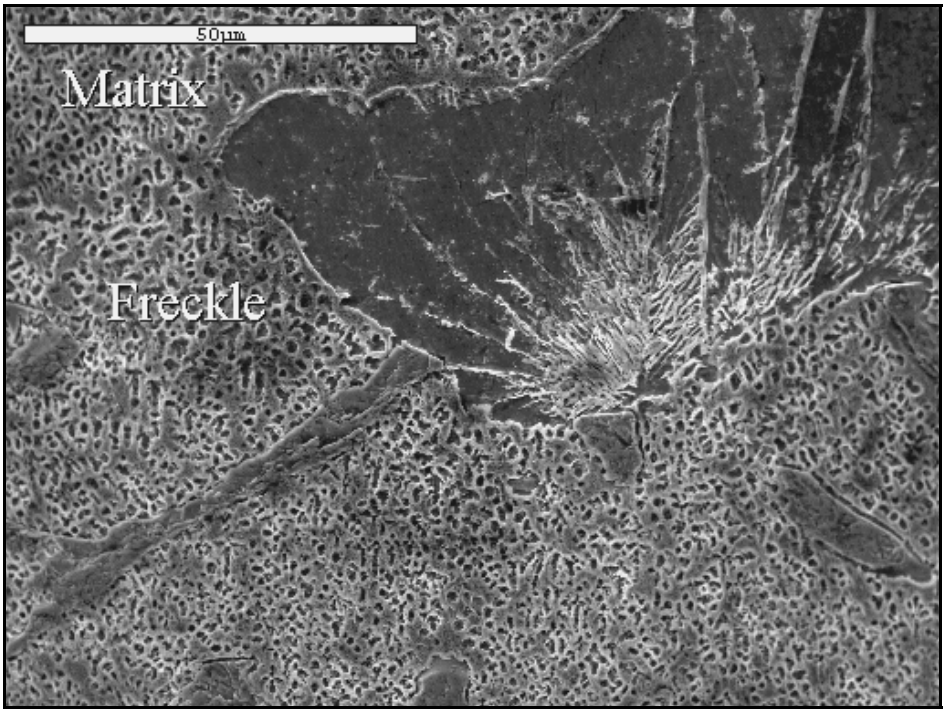

Figure 24 – SEM of eutectic colony at a freckle boundary in DS-2 alloy (1000X).

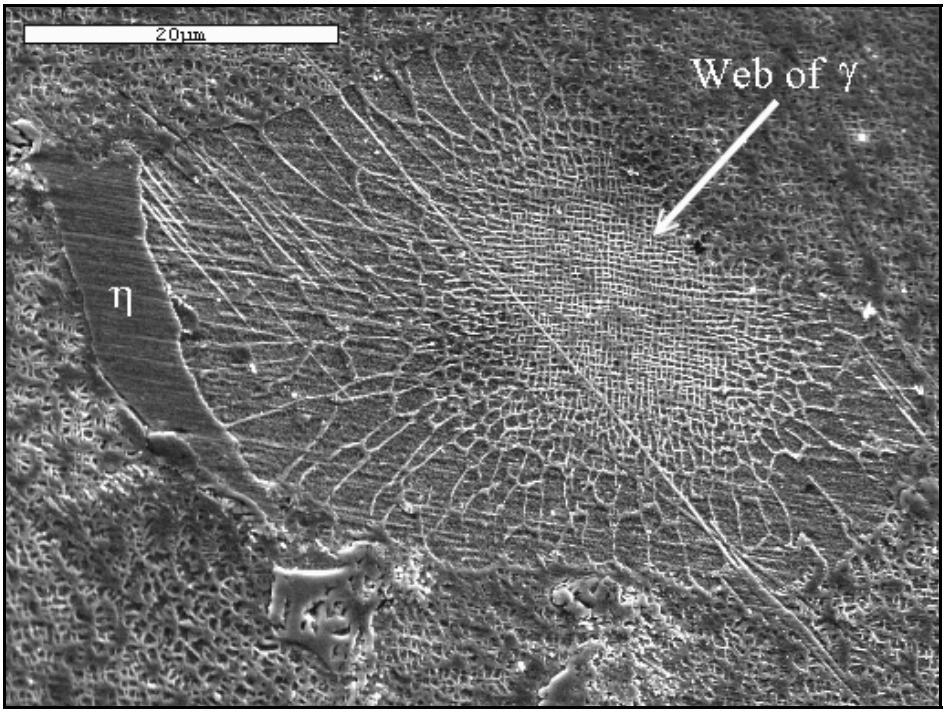

Figure 25 – SEM of a eutectic colony in DS-1. Note the web-like morphology of the γ (2000X).

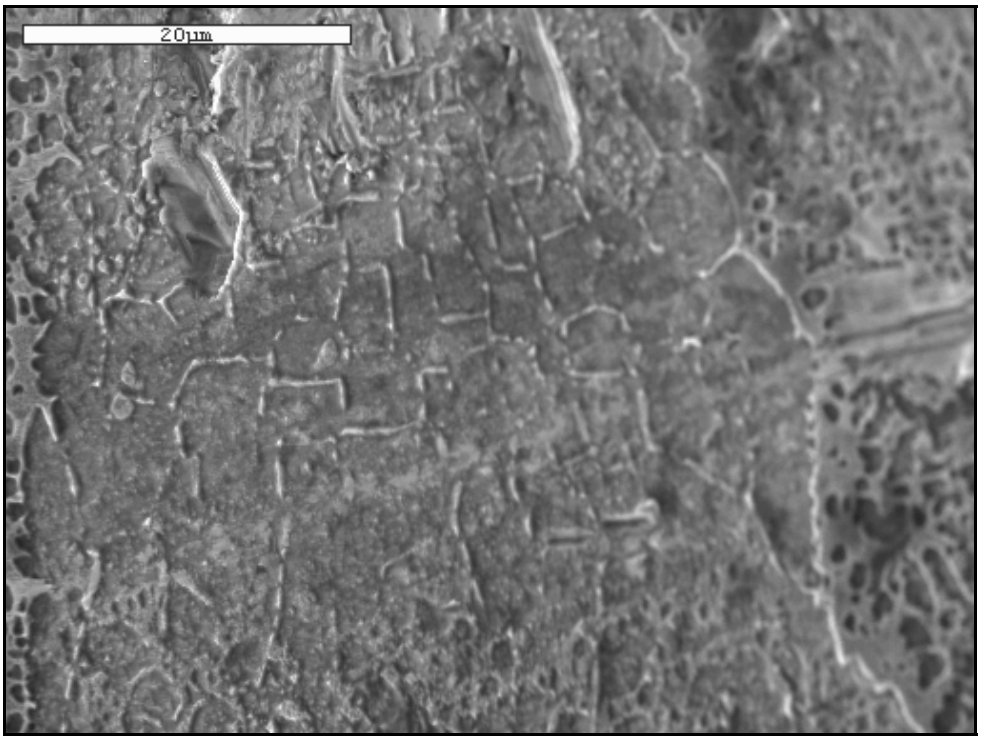

Figure 26 – SEM of different section of eutectic in DS-2 alloy at the casting surface. The eutectic is in the middle (2000X).

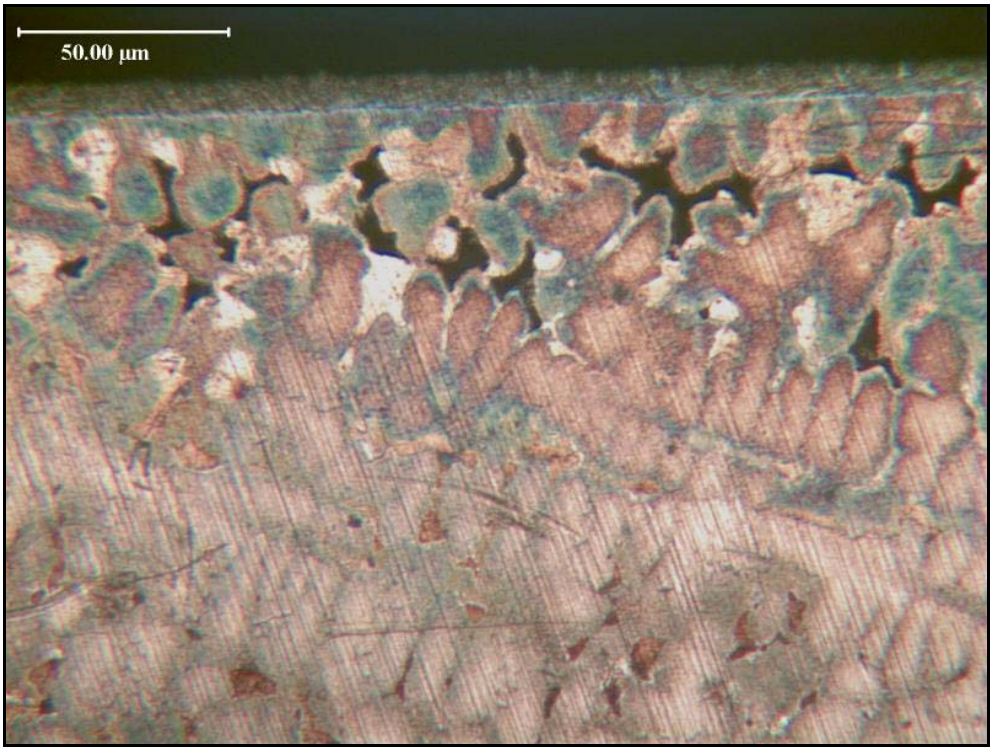

Figure 27 - Optical micrograph of cross section of DS-2 casting. In the freckle chain on the left, the dark spots are porosity next to the white eutectic colonies (50X).

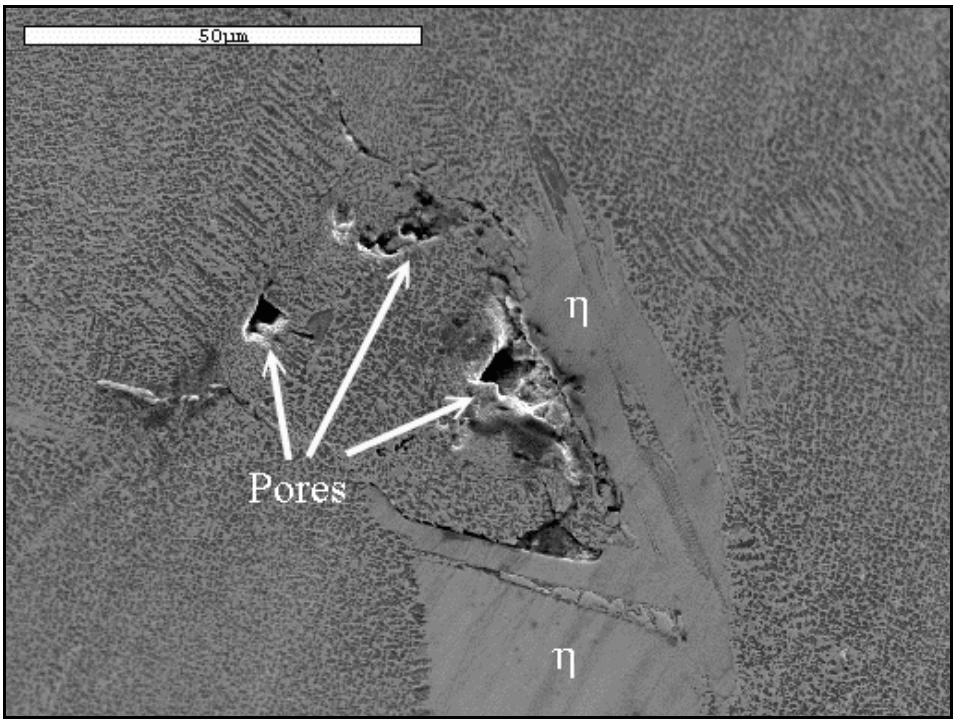

Figure 28 – SEM of porosity near a colony of η at a freckle grain boundary (1000X).

4.1.4. Eutectic at Grain Boundaries

One of the more interesting solidification structures is shown in Figure 29. Nearing the boundary between the freckle and the matrix, the γ' appears to be elongated. While certain castings have been shown to contain a film of γ' at grain boundaries, this morphology was unexpected and was found in both alloys (see Figure 30). This elongated structure was also seen near η and carbides at the freckle-freckle and freckle-matrix boundaries. The DS grain boundaries, while having some carbides and eutectic at the boundaries, never exhibited the elongated structure of γ', and often there were no other phases present besides γ and γ' (see Figure 31).

Besides the elongated γ' morphology, blocky γ' was found at the grain boundaries involving freckles when there are no other intergranular constituents, such as eutectic, η, or carbides, present (see Figure 32). The grain boundary γ' is approximately 5 to 10

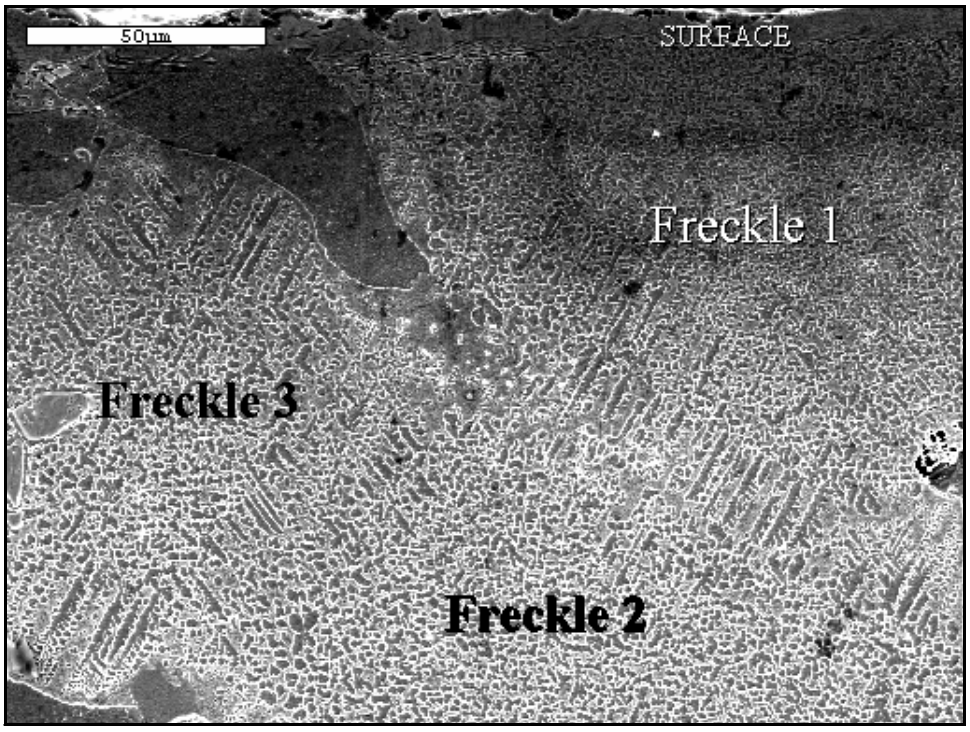

Figure 29 - SEM of DS-2 alloy near surface showing elongated γ' at the boundaries between three freckles.

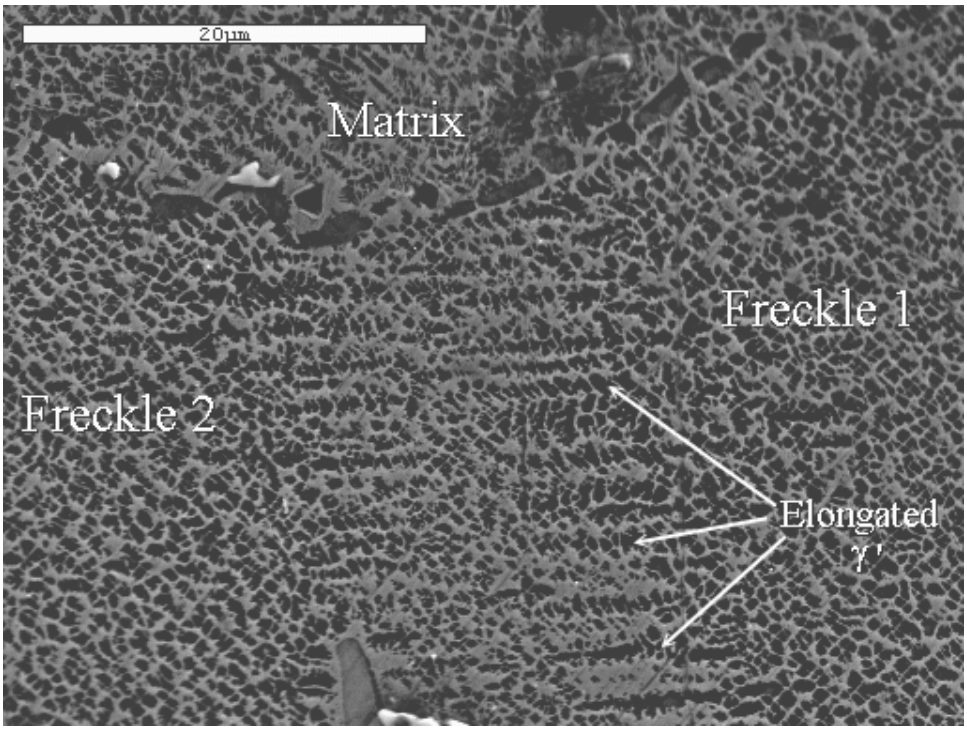

Figure 30 – SEM of DS-1 alloy at boundary of freckle grains and matrix. The γ' "elongates" at the freckle boundary.

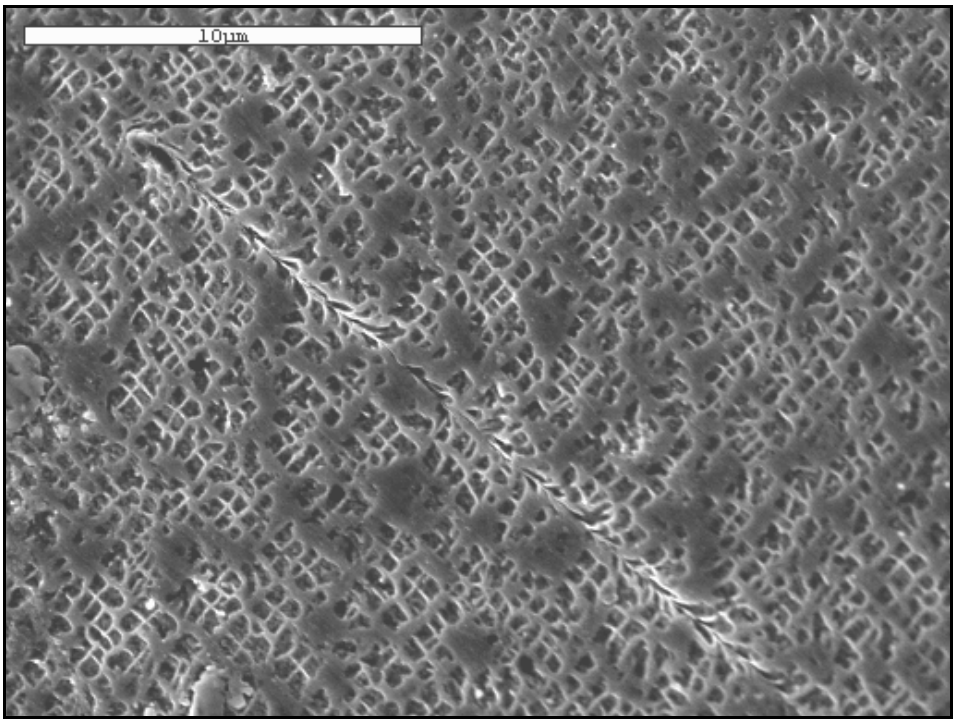

Figure 31 – SEM of DS boundary in DS-1 (5500X).

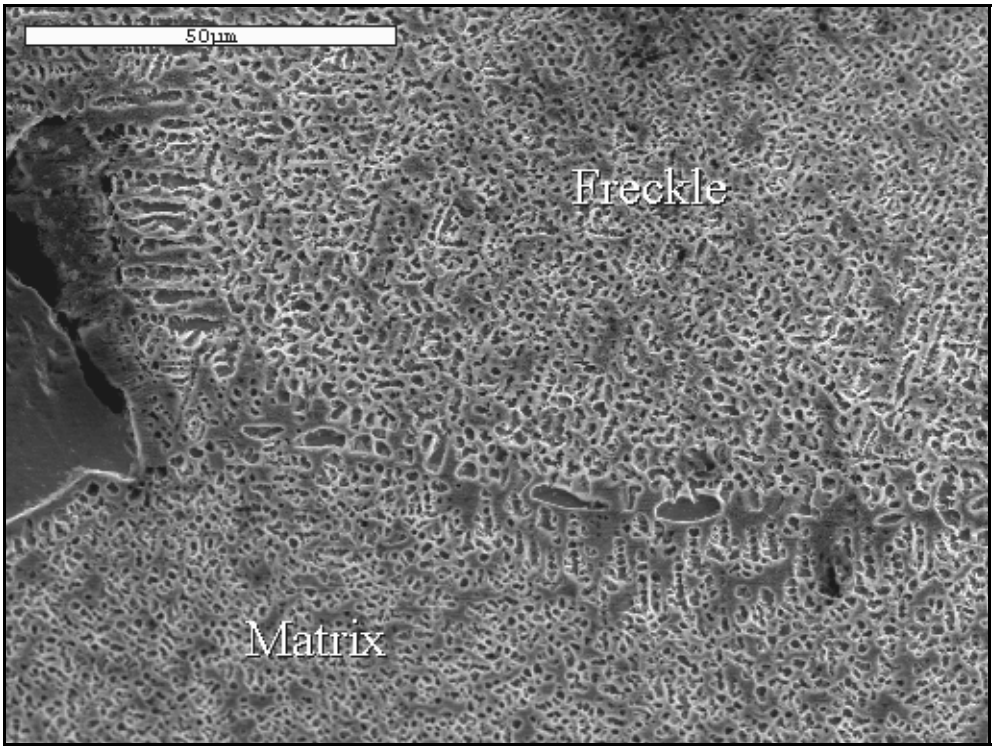

Figure 32 - SEM showing intergranular γ' at a freckle grain boundary in DS-2 (900X).

times larger than the intragranular γ' and is rectangular is shape, rather than cuboidal. In Figure 33, one can see more of the elongated γ' and the blocky γ' at a freckle-matrix boundary.

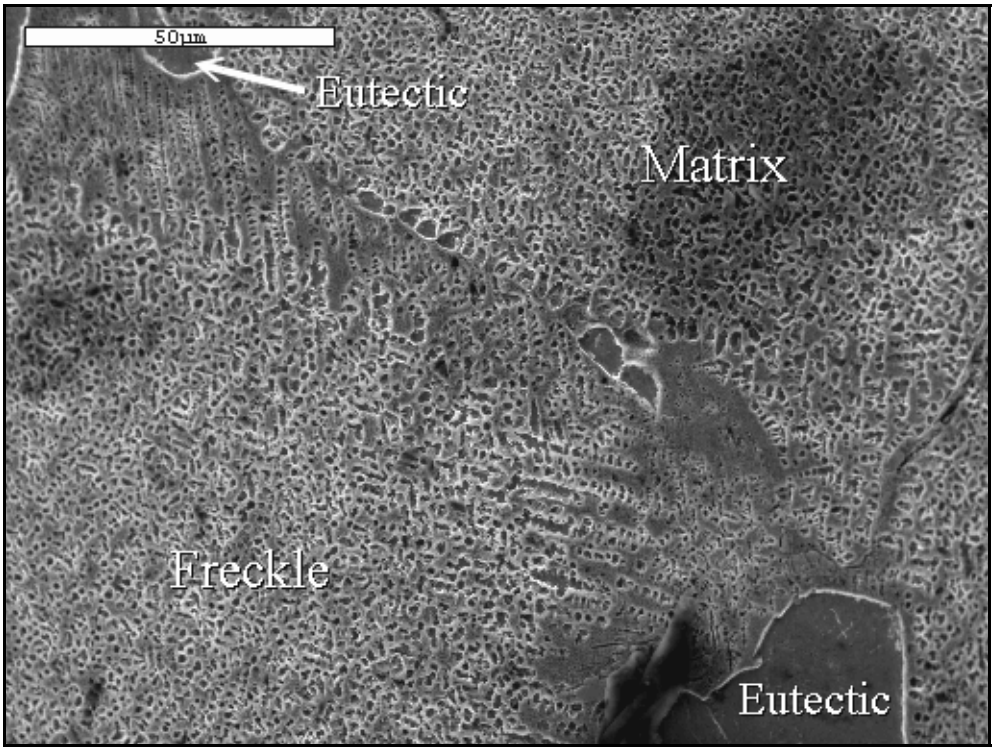

Figure 33 – SEM of intergranular γ' between two eutectic colonies at a freckle grain boundary from DS-2. Note the elongated γ' inside the freckle grain at the boundary (750X).

4.1.5. Eta Phase Formation

Upon investigation in the SEM, the η phase was frequently observed in one of the castings. Figure 34 is an optical image showing some of this η phase around a freckle grain in the DS-1 alloy. Figure 35 is an SEM image of the same freckle grain. This phase was found primarily at the boundary between the freckle and the rest of the casting (as shown in Figure 35), but was also found inside the freckle grain itself. Furthermore, as stated previously, there were large eutectic regions near these freckled regions as well.

It is important to distinguish between the η phase and the carbides, since in backscattered mode, both appeared lighter than the γ + γ' matrix (see Figure 36). This distinction was made from EDS and X-ray mapping. The η phase, or $Ni_3(Ti,Ta)$, usually has little solubility for Al or Cr. Likewise, the MC carbides have little solubility for Ni. An X-ray dot map of Figure 36 is shown on Figure 37 and shows regions enriched in Ni and Ti, and depleted in Cr. This is shown again in an area with more η (Figure 38), and its X-ray map clearly shows the enrichment in Ni and Ti, as well as low Mo, Al, and Cr amounts (see Figure 39). To differentiate the η phase from the primary carbides, an SEM micrograph and corresponding X-ray dot maps of a primary MC carbide is shown in Figures 40 and 41, respectively. This phase is high in Ta and Ti, while being low in Ni and Cr, indicating it is an MC carbide. The compositions of the different phases in Figure 36 are given in Table 3.

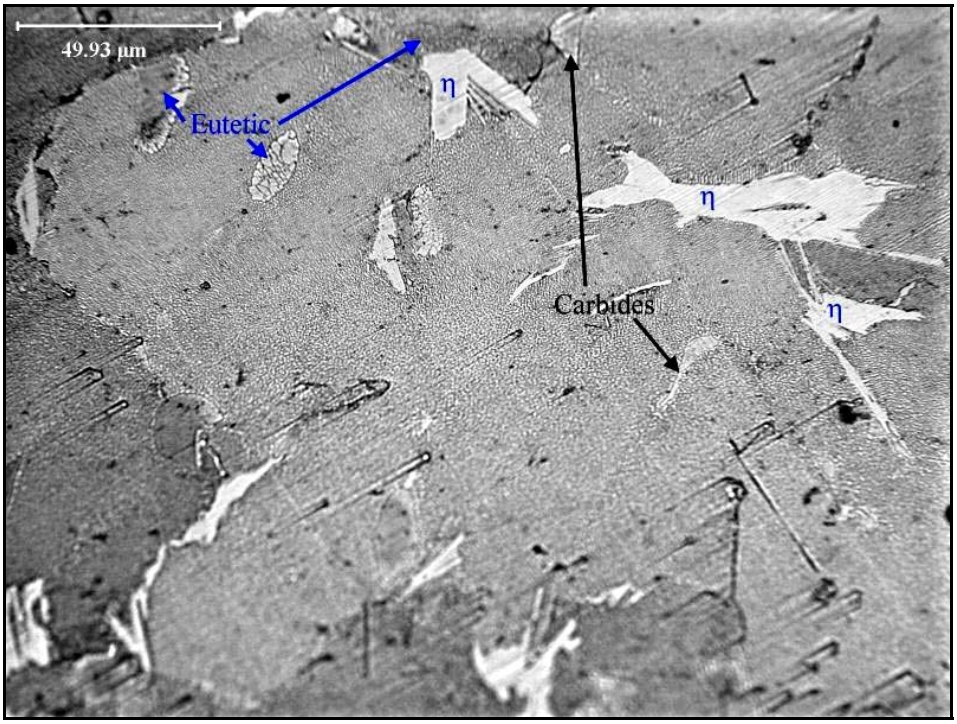

Figure 34 - Optical image of a freckle grain in DS-1 casting showing various phases (50X).

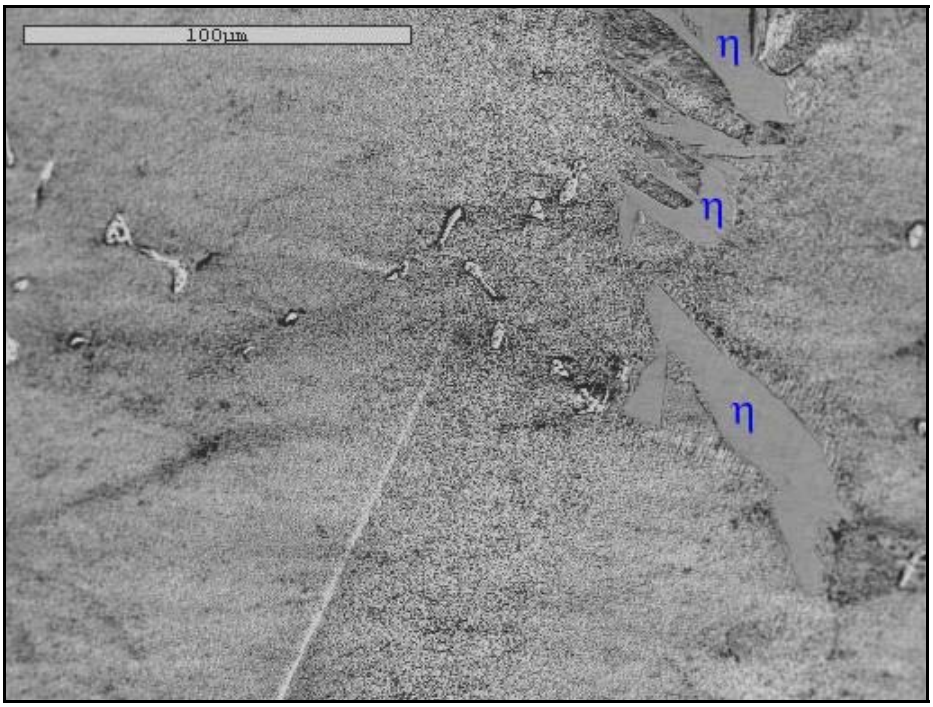

Figure 35 - BSE SEM of freckle boundary in the DS-1 showing η phase (500X).

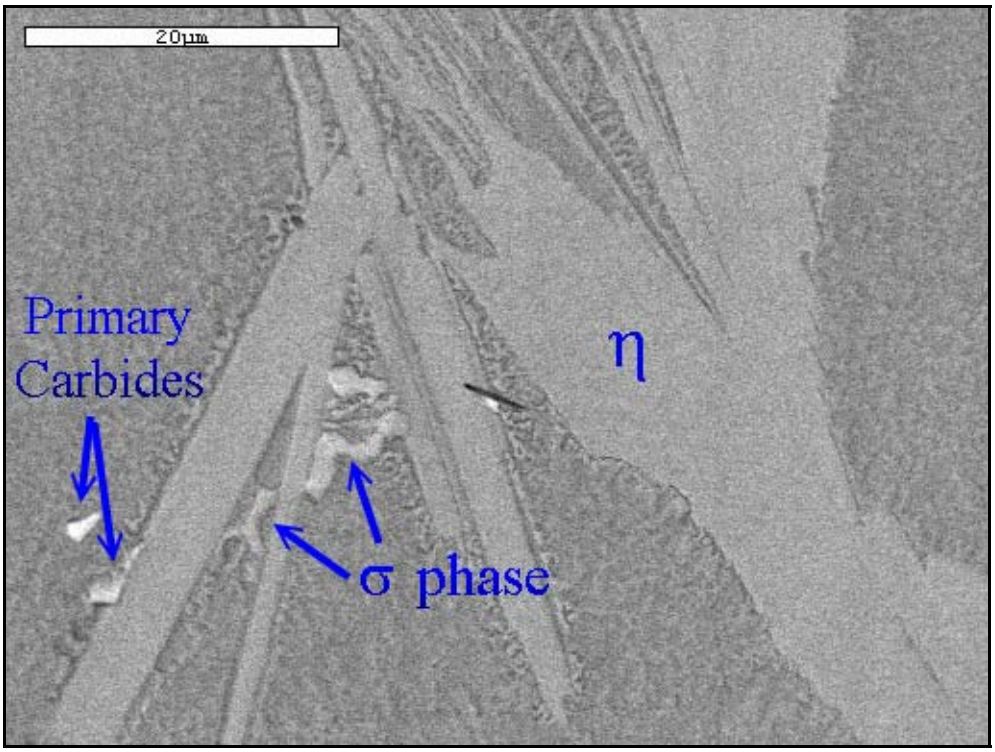

Figure 36 - BSE SEM showing η phase, carbides, and TCP phase at a DS-1 freckle boundary (1900X).

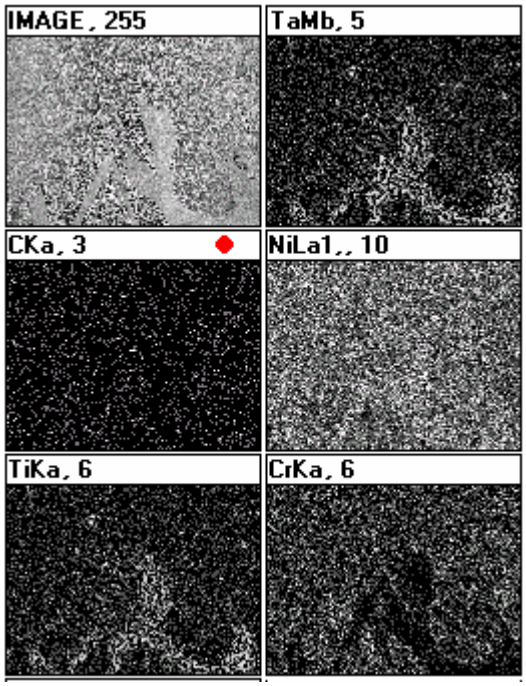

Figure 37 - X-ray map of Figure 36, showing elements common to η phase.

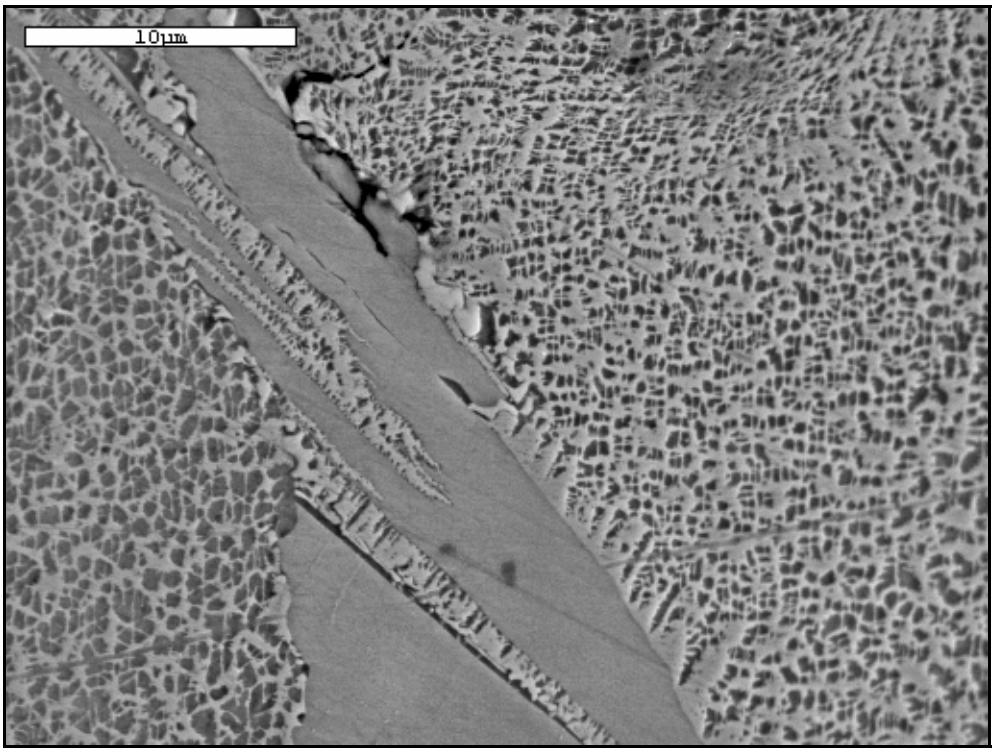

Figure 38 – SEM of η Phase (3300X).

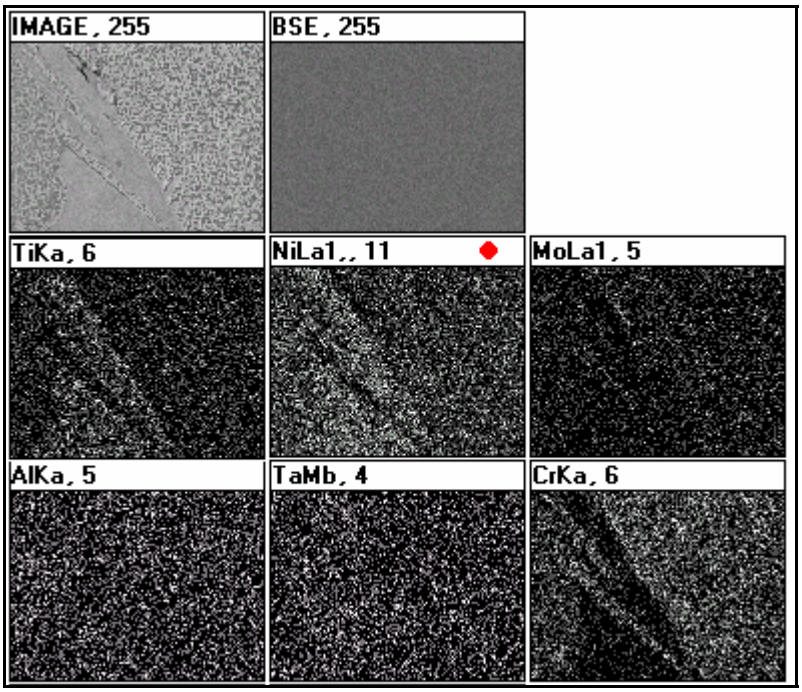

Figure 39 - X-ray map of Figure 38, showing elements common to η phase.

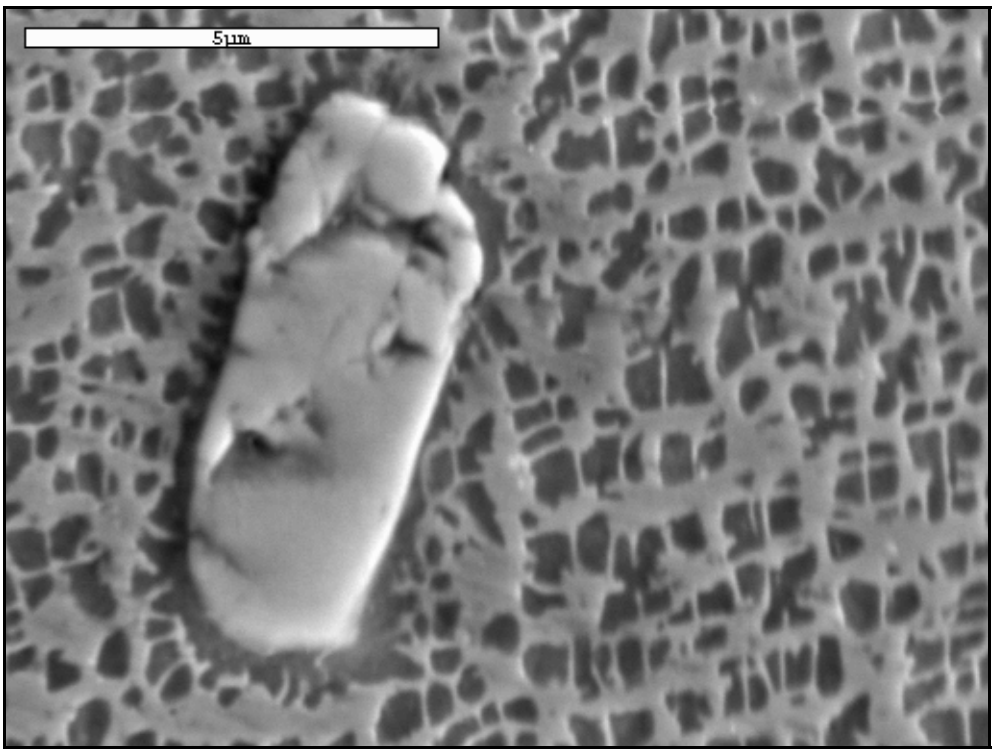

Figure 40 – SEM of MC carbide in matrix (10000X)

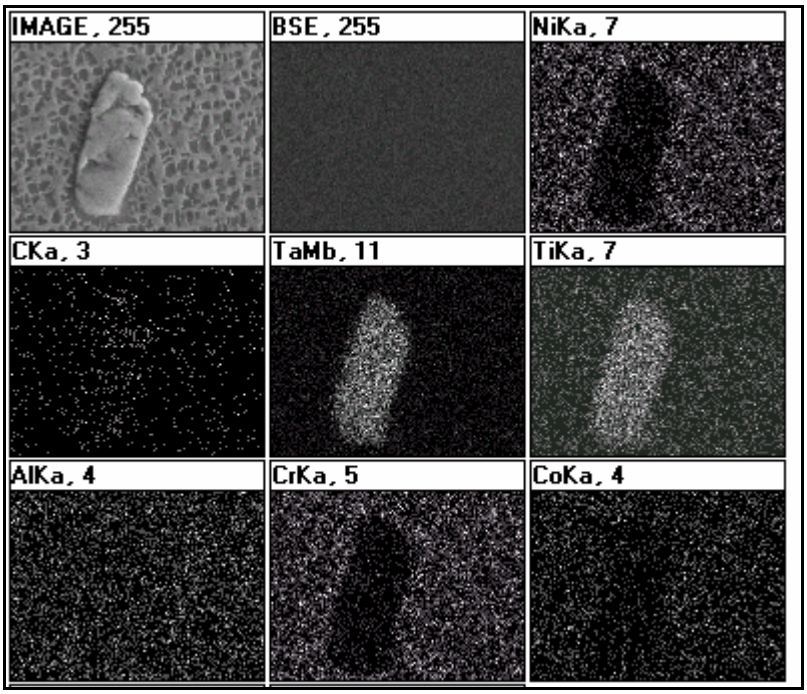

Figure 41 - X-ray map of MC carbide in Figure 40.

Table 3 - EDS weight percents of elements for phases in Figure 36.

Constituents	Al	Ti	Cr	Co	Ni	Mo	Ta	W
MC Carbide	0.2*	30.0	1.2	0.5*	3.9	4.2	49.3	10.7
σ phase	0.1*	2.7	44.8	1.3	3.4	30.5	1.5	15.5
η Phase	3.5	12.2	3.6	6.3	63.6	0.9	7.4	2.5
Matrix (γ + γ')	3.3	5.7	20.3	9.9	51.6	2.8	2.3	4.0

* - No significant amount present

The η present in the DS-1 casting appeared to be plate-like in morphology. There also seemed to be more of the aforementioned elongated γ' near the η plates at the freckle-matrix border. From TEM micrographs, η was found to contain stacking faults and to be located near a carbide (see Figures 42 and 43). EDS analysis in the area of the stacking faults showed mostly Ni and Ti, and little of the other elements. TEM also showed stacking faults in γ' that was near η.

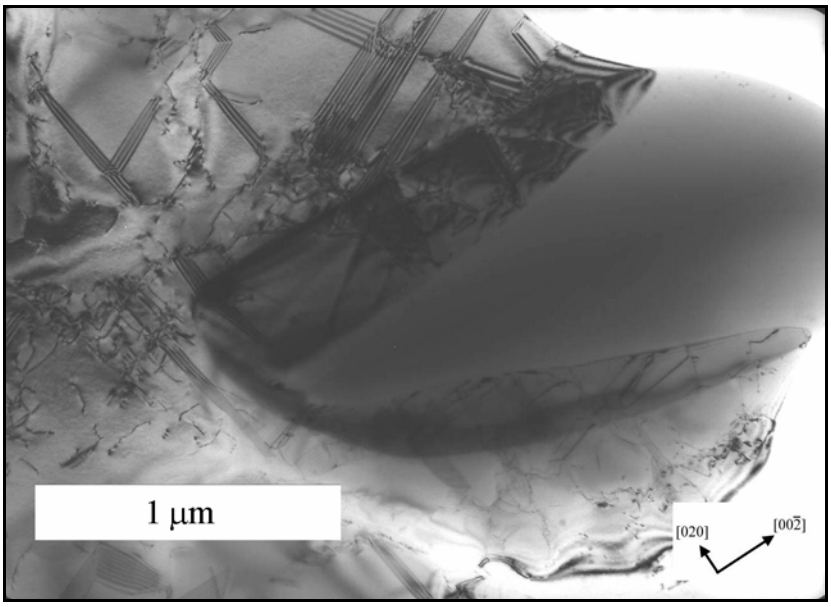

Figure 42 - BF TEM image of η containing stacking faults stacking faults near a carbide (30000X).

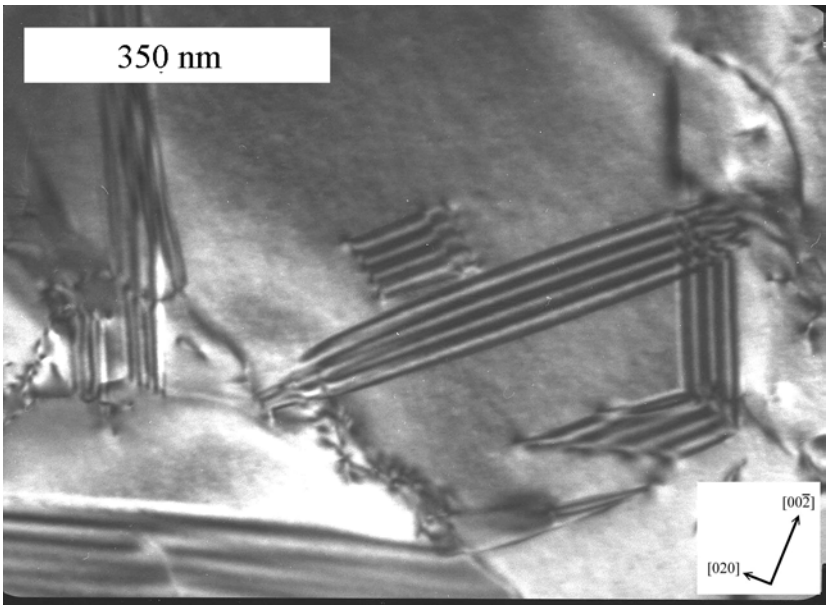

Figure 43 - BF TEM closeup of stacking faults above the carbide from Figure 42 (100000X).

4.1.6. Morphology and Microstructure of Constituents near Surface

As previously mentioned, the surfaces of the DS-2 castings were not modified prior to investigation. This meant that the surface of these castings had been in contact with the ceramic mold during the DS process. The actual surface was characterized as

described in Section 4.1.1. In this section, a freckle chain was cross-sectioned (Cut 2) and examined to investigate its microstructure near the surface.

There appears to be an 8 μm thick layer at the surface that does not contain the cuboidal γ' (see Figure 44). Near the surface, large amounts of eutectic were present, as seen in Figure 45. Figure 46 shows another large eutectic colony with the γ layer above it. There is also a large pore and carbides present. These colonies are commonly seen in cast superalloys, but rarely of this size. Another large eutectic area is seen in Figure 47. In this case, a large MC carbide is located in the middle of the eutectic colony and the γ' plates appear in a "starburst" pattern emanating from the carbide. The typical matrix γ + γ' structure is present between the carbide and the surface. It should be noted that EDS was performed on all the constituents discussed above to properly identify each phase.

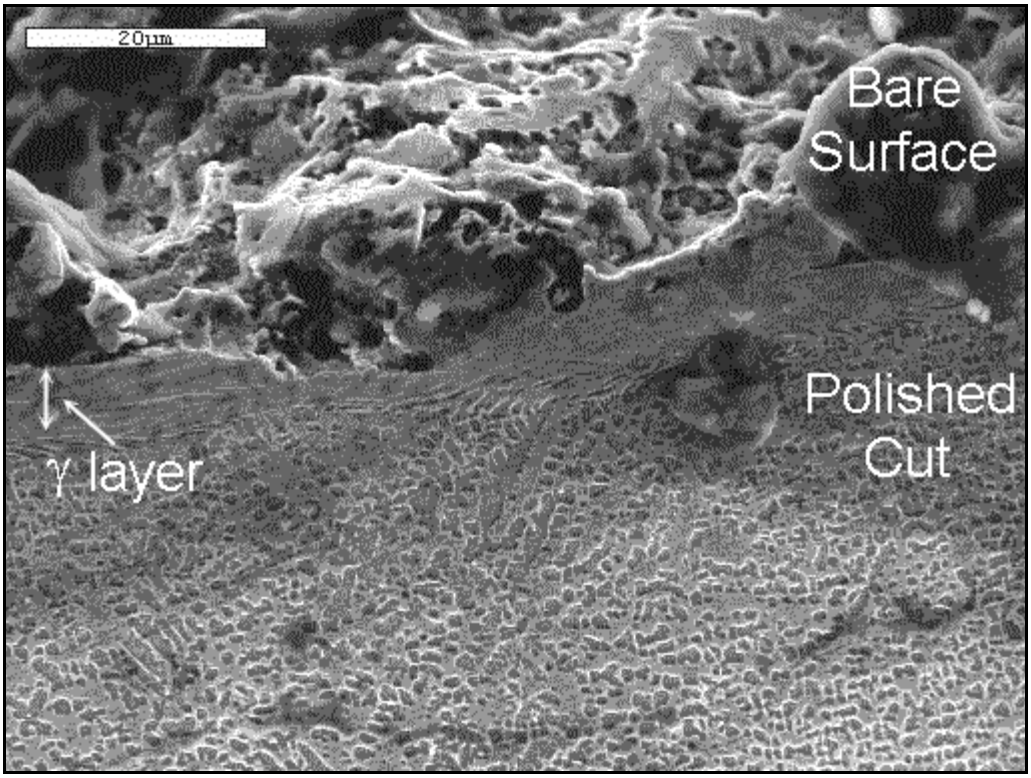

Figure 44 - SEM of a cross section of the DS-2 casting surface at a freckle chain (1400X).

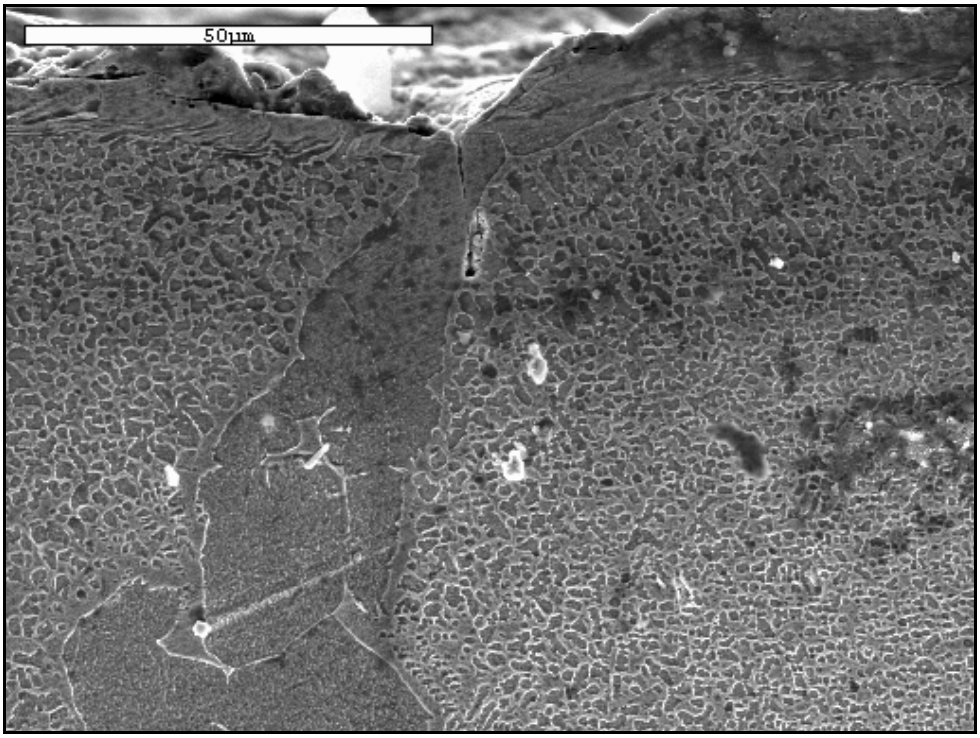

Figure 45 – SEM of a large eutectic colony near the external surface of the DS-2 casting (1000X).

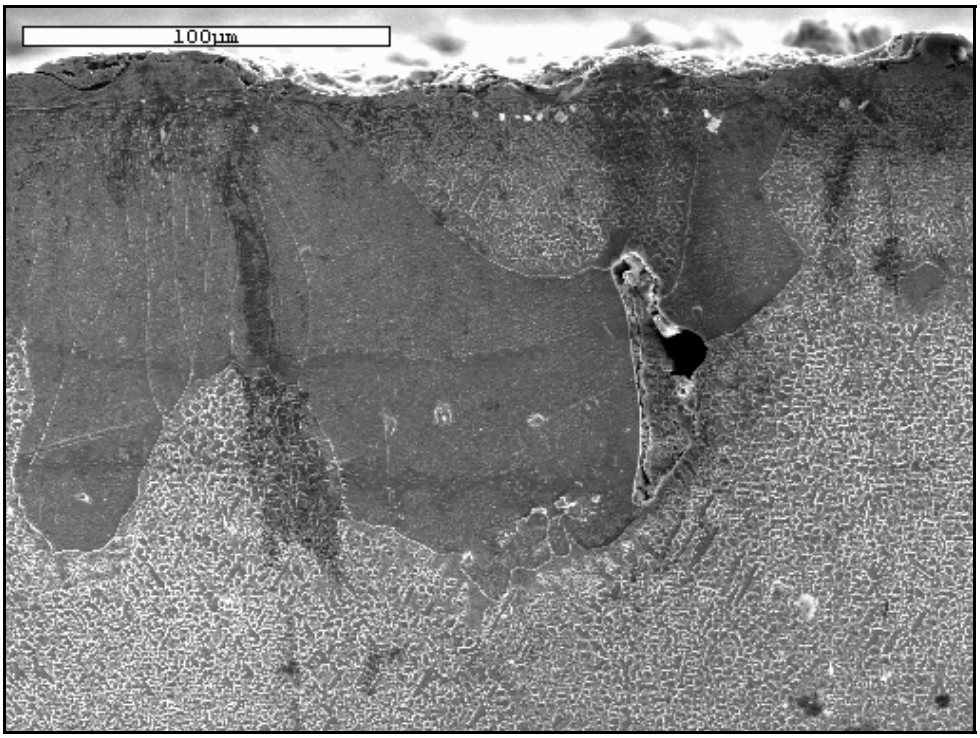

Figure 46 - SEM of large eutectic colony at surface (450X).

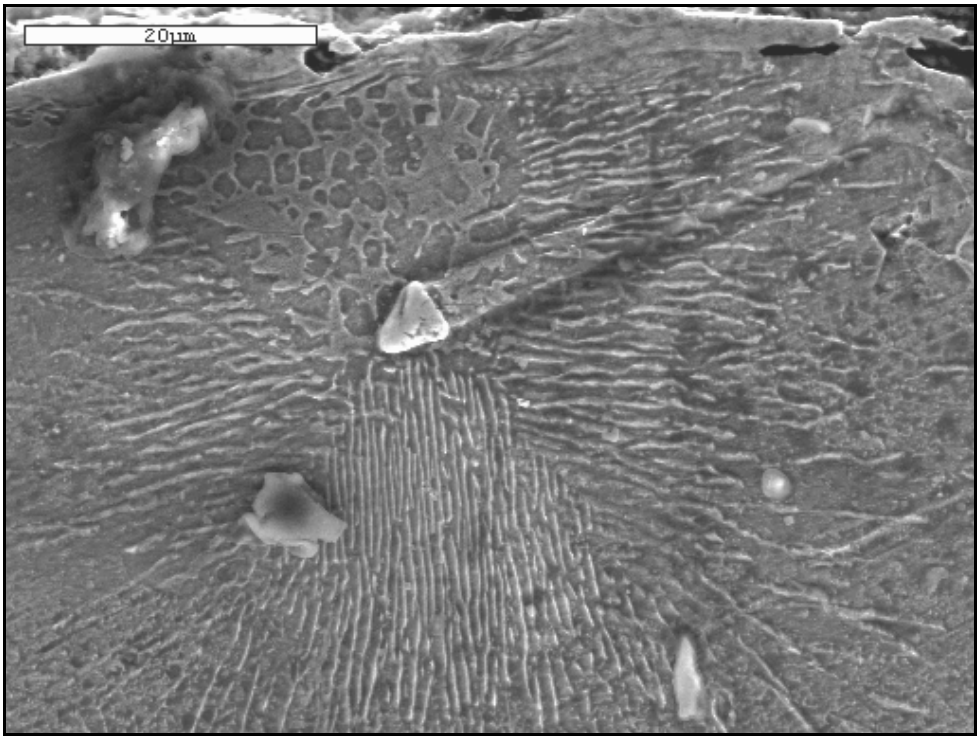

Figure 47 – SEM of carbide in the center of large eutectic colony near casting surface (1800X).

Further analysis of the surface was performed and Figure 48 shows a better resolved image of the surface γ layer beside a carbide near the surface. In this figure, the γ layer shows a "smearing" feature, with the smearing angled towards the carbide. To ensure that these waves were not entirely topological, a backscattered image was taken of Figure 48 (see Figure 49). The smearing, or "waves," are lower in atomic number than the surface layer, and have the same contrast as γ'. A closer look at these waves can be seen in Figure 50, where the γ' appears to be smeared in one direction and then back in another.

Unfortunately, cross-sections of the bare surface not at 90° did not reproduce this feature. A shallow cut towards the sample at approximately 15° was performed to tie together the images of the virgin surface with the cross-sections. Figure 51 shows a

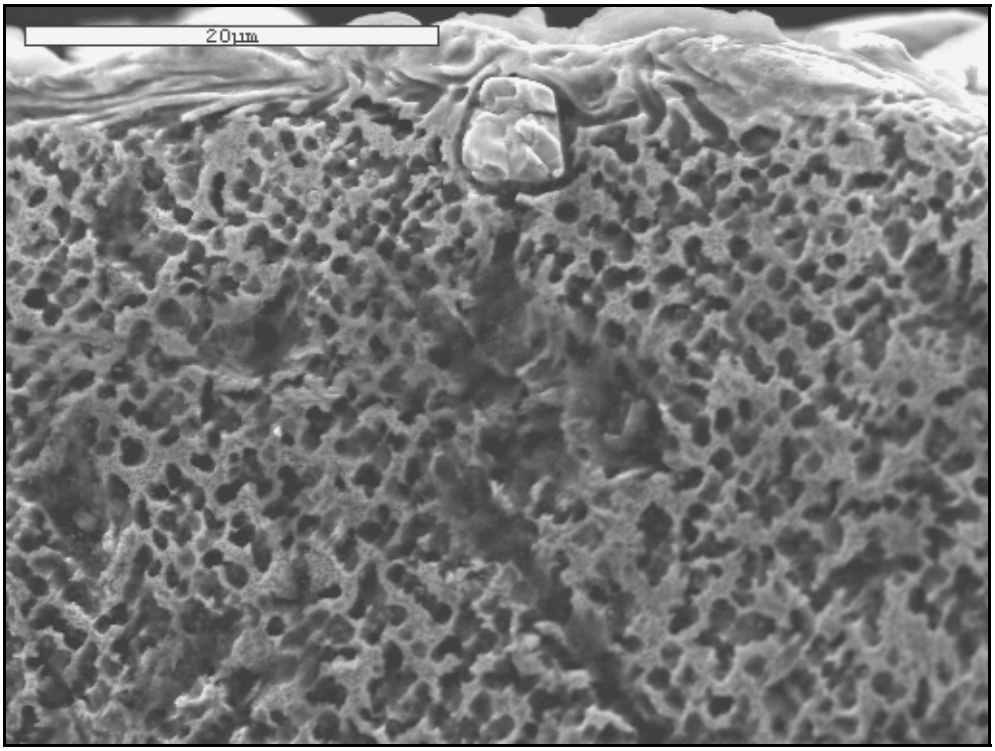

Figure 48 – SEM of carbide near surface (2500X).

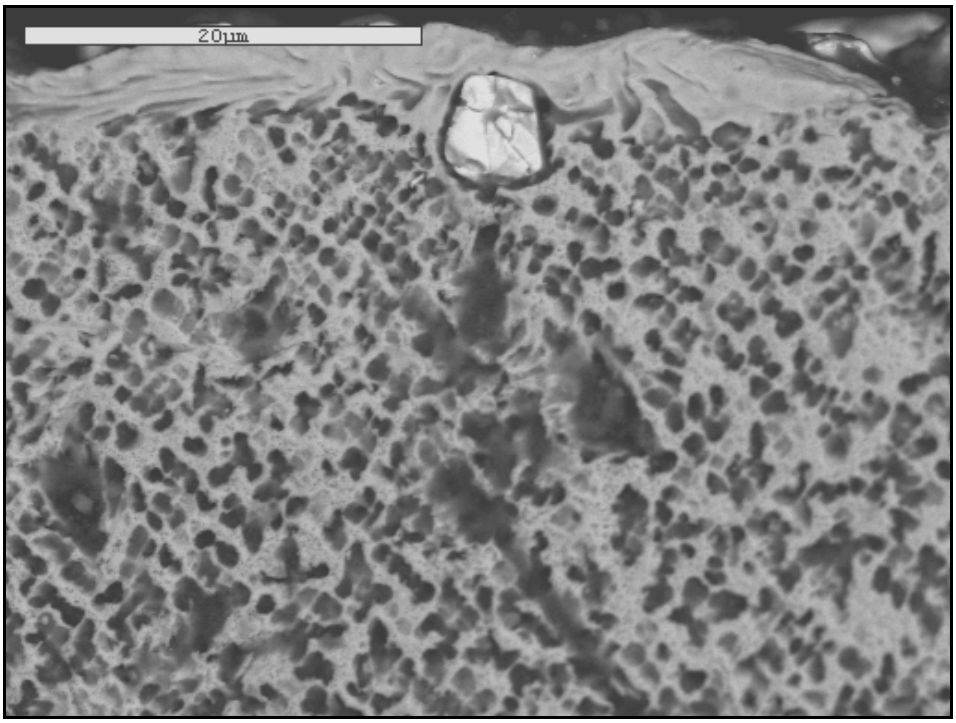

Figure 49 - BSE SEM of Figure 42 (2500X).

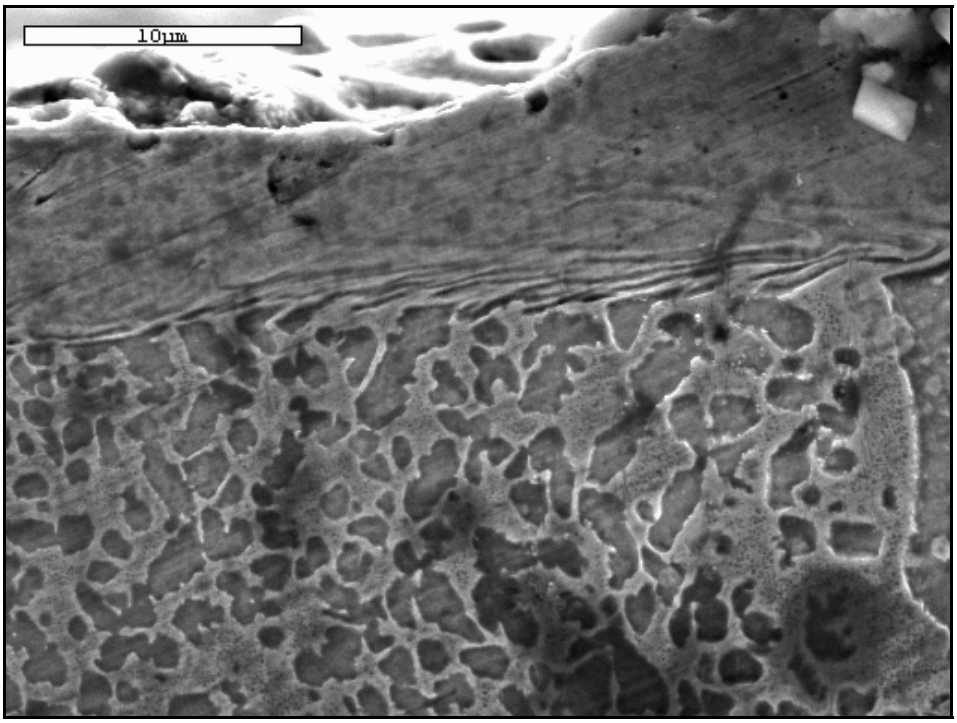

Figure 50 – SEM of casting surface showing the "smearing" of the γ + γ' morphology (3500X).

backscattered image where alumina is covering carbides and the casting. It appears that on the unpolished surface, bare γ' is seen. ZrO_2 was found on top of Al_2O_3 in a few regions, along with what appeared to be trace particles of Si. There was smooth surface γ' sparsely seen on this sample, possibly covering the bare γ' from Figure 51 (see Figure 52). It is likely that since this microstructure is seen so infrequently, it is a eutectic colony at the surface. Figure 53 shows more of the bare cuboidal γ' on the surface. The flat areas are polished. EDS of the crevices between the cuboidal γ' showed higher levels of O than the surrounding γ'.

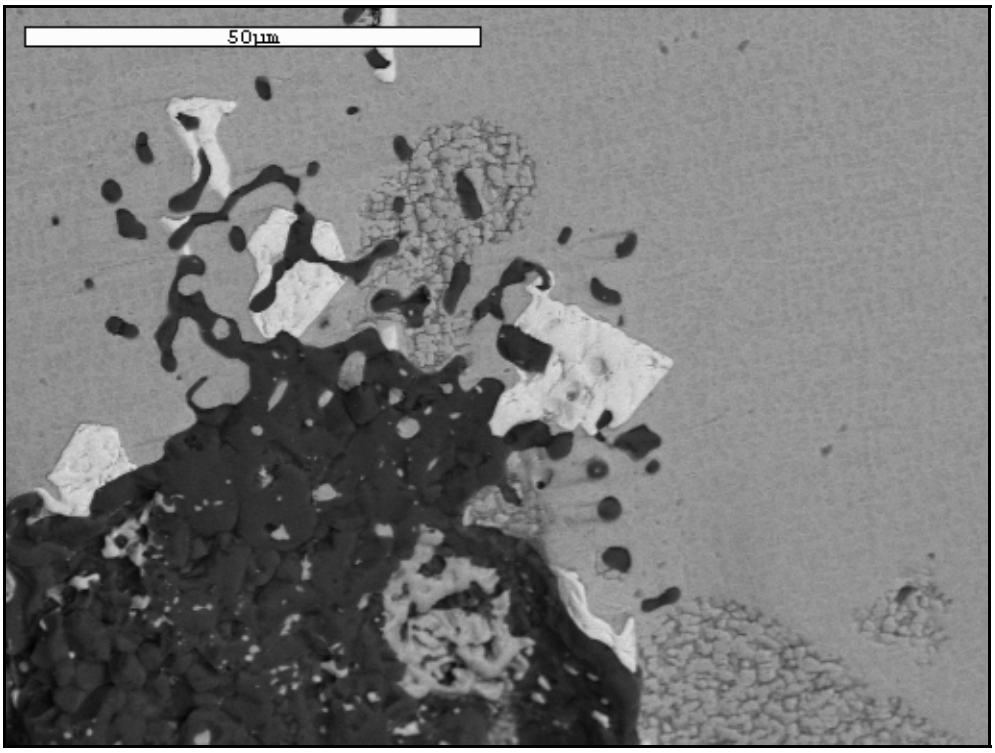

Figure 51 - BSE SEM of bare surface of DS-2 near polished regions. The dark phase is alumina, the white phases are MC carbides, and the grey is the casting. An unpolished part of the casting (lower right) shows bare γ' (3000X).

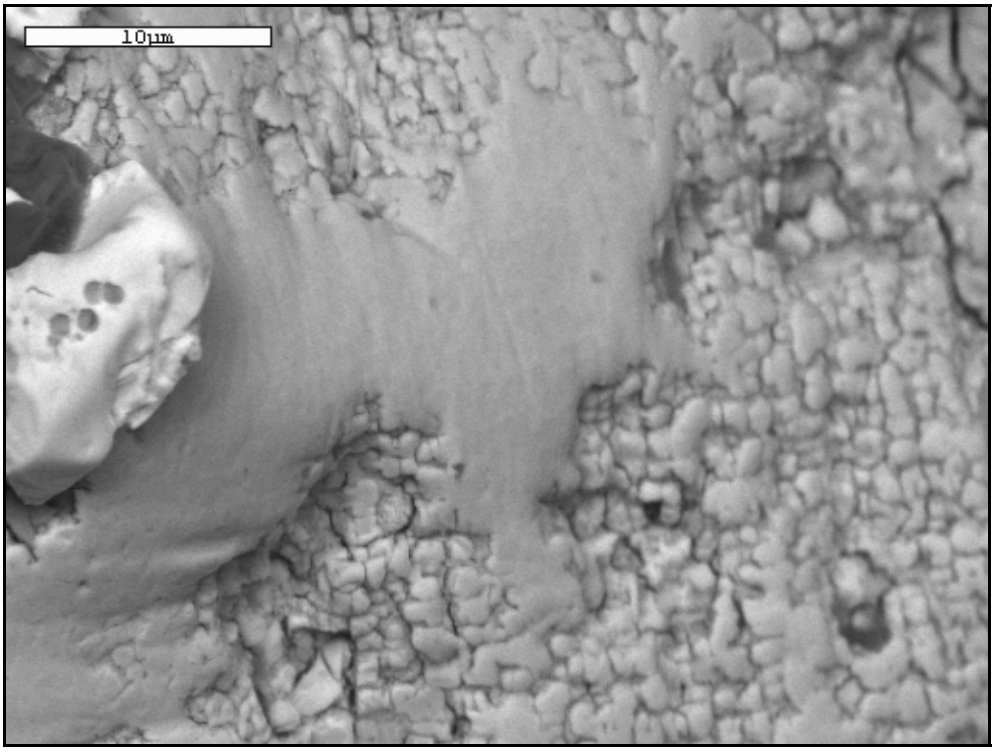

Figure 52 - BSE SEM of unpolished DS-2 surface. The surface γ'layer can be seen covering the bare γ' seen in Figure 51.

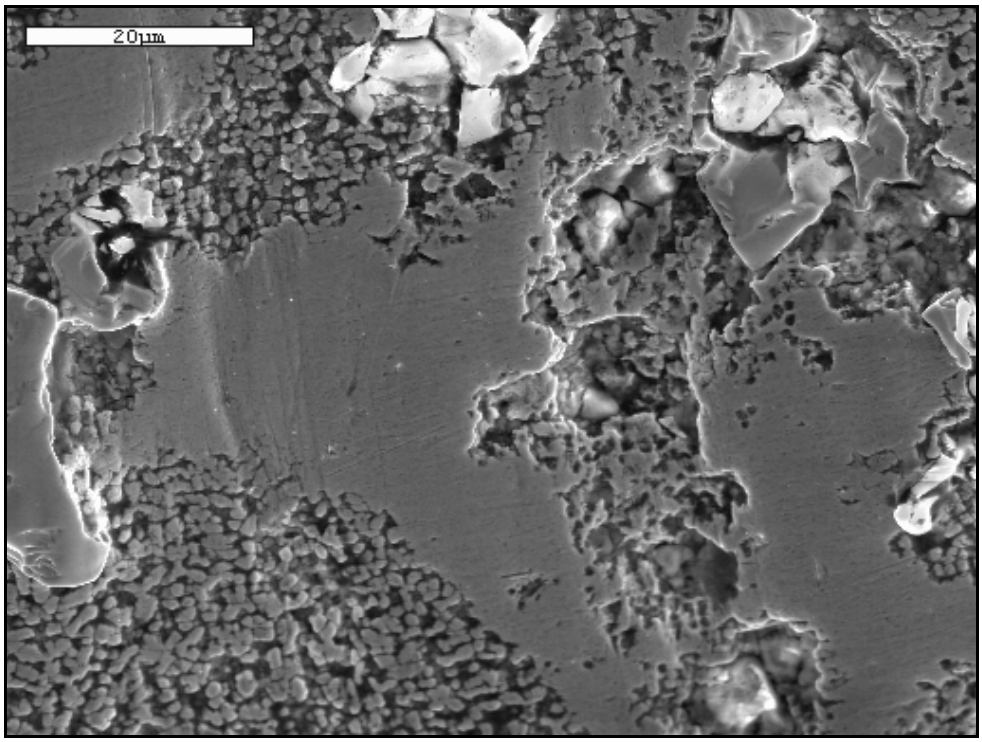

Figure 53 - SEM of virgin surface near polished surface. Bare cuboidal γ' can be seen, along with MC carbides that appear bright. The flat regions are polished areas (1200X).

4.2. Stereology Results

As previously stated, there appeared to be large quantities of eutectic, carbides, and porosity in both castings in and near the freckled regions. To quantify this observation, stereological techniques were used to determine the volume percent of these constituents in both castings and in the various regions in these castings. Stereological measurements were performed at several magnifications until the lowest standard deviation in the measurements was found—point counts for carbides were performed at 1000X in the optical microscope and SEM, and point counts for eutectic, porosity, and η (if present) were performed at 125X primarily on the optical microscope.

4.2.1. Stereology on DS-1 Casting

The constituents observed in the DS-1 alloy were eutectic, porosity, carbides, and η phase. Due to the small number of freckle chains on the DS-1 castings, only Cuts 1 and 3

had significant data. Figure 54 shows the volume percent differences of eutectic in the freckled regions of the casting. These areas include the freckled grains, grain boundaries, and immediate surrounding regions of less than 30 μm near the chains. Figure 55, 56, and 57 show the stereology results of carbides, η, and porosity from the DS-1 castings. The regions labeled "matrix" are regions at least 1 mm from any freckle chain and should represent the rest of the DS casting.

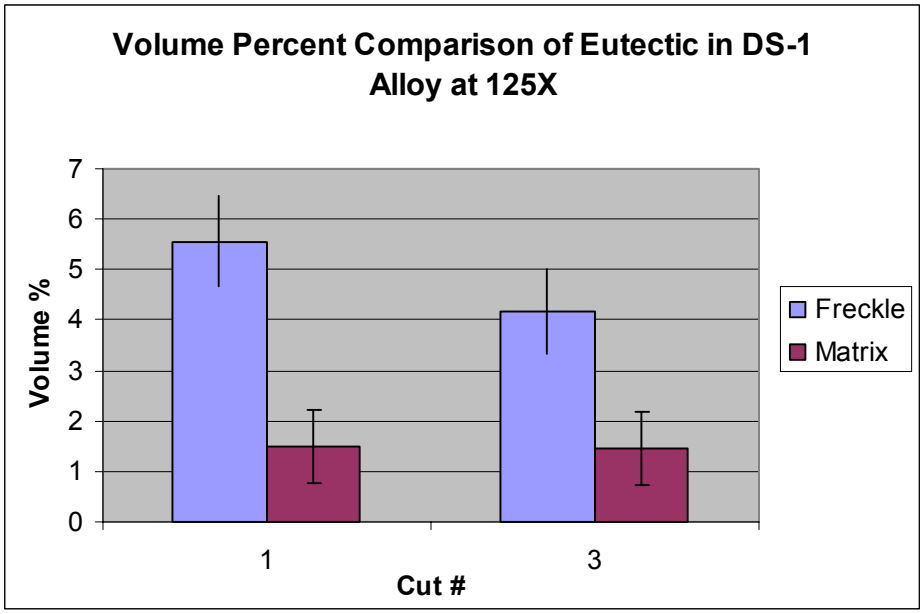

Figure 54 - Volume percent of DS-1 eutectic at 125X found through stereology.

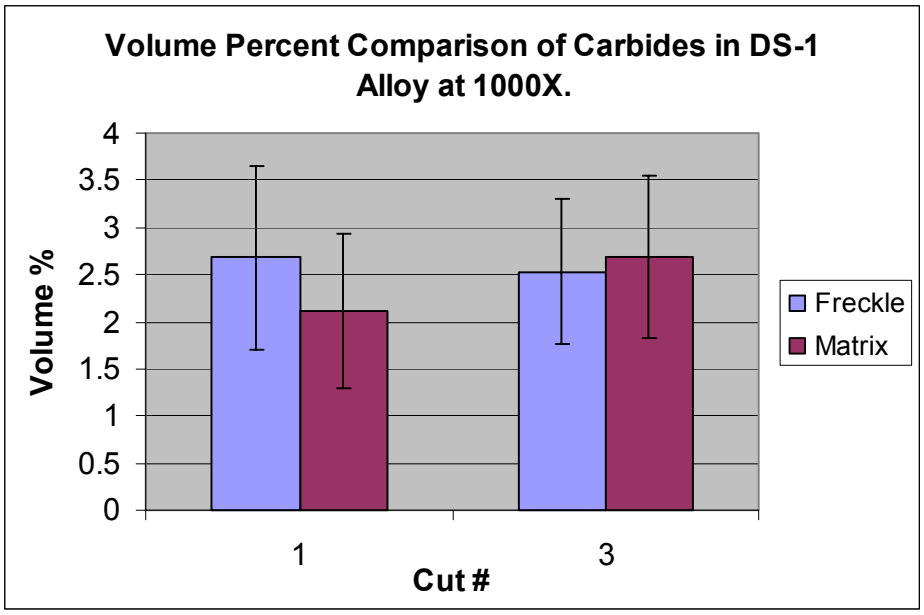

Figure 55 - Volume percent of MC carbides in DS-1 at 1000X found through stereology.

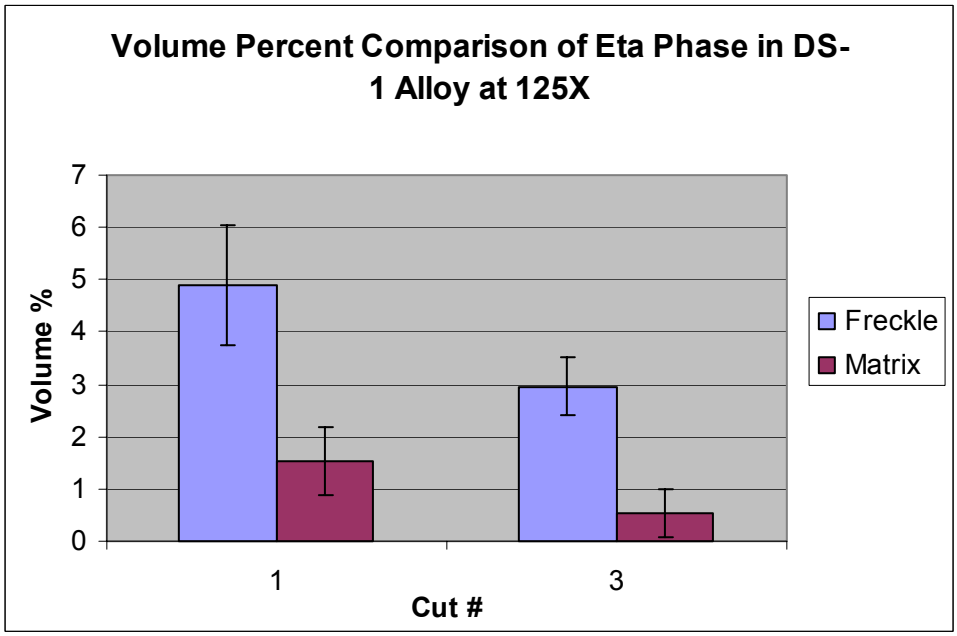

Figure 56 - Volume percent of DS-1 η phase at 125X found through stereology

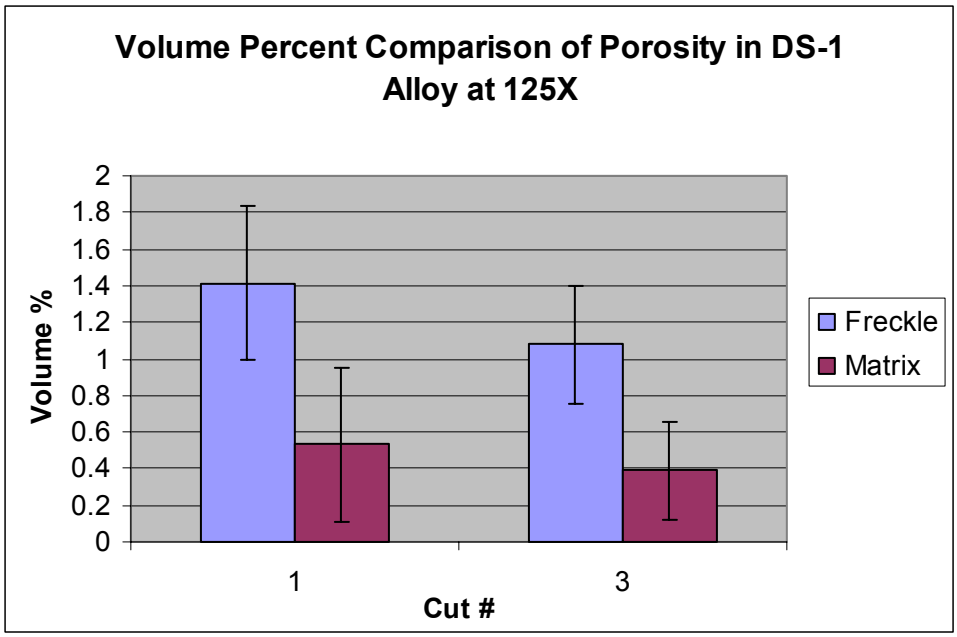

Figure 57 - Volume percent of DS-1 porosity at 125X found through stereology.

From the above figures, it is clear that there is more eutectic and η in and around the freckle grains. There is also more porosity in these regions. Statistically, however, it is not possible to determine if there are more or fewer carbides present in the freckled or matrix regions. In fact, on Cut 3, there appeared to be more carbides present in the matrix than in the freckled regions.

4.2.2. Stereology on DS-2 Casting

While there was no η in the DS-2 alloy, there were eutectic, porosity, and carbides and it was possible to collect data from all three cuts (the same labeling conditions were used for these stereological results). Figure 58 shows the volume percent of carbides, and Figures 59 and 60 show the results for eutectic and porosity, respectively.

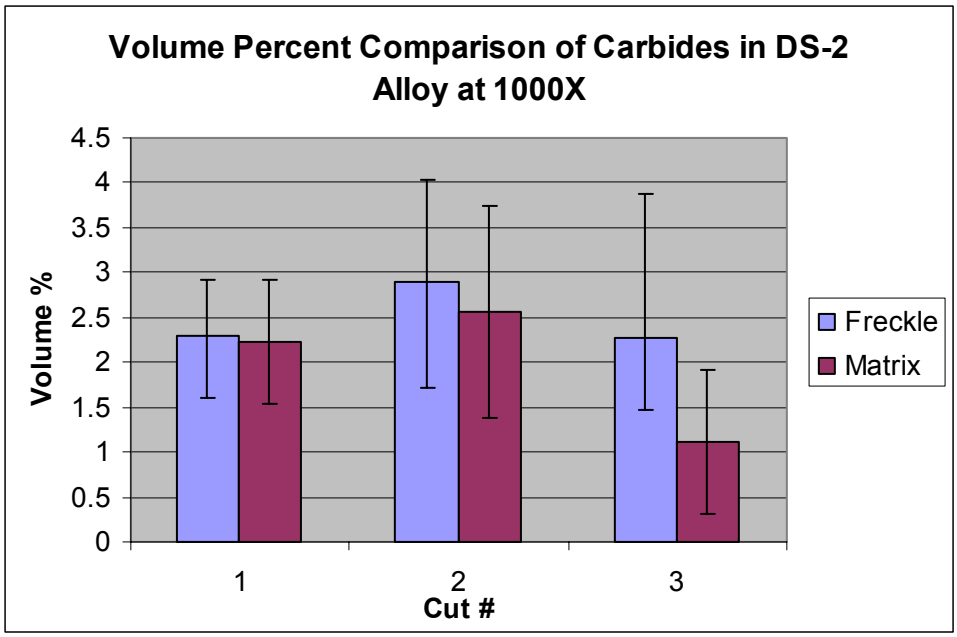

Figure 58 - Volume percent of MC carbides in DS-2 at 1000X found through stereology.

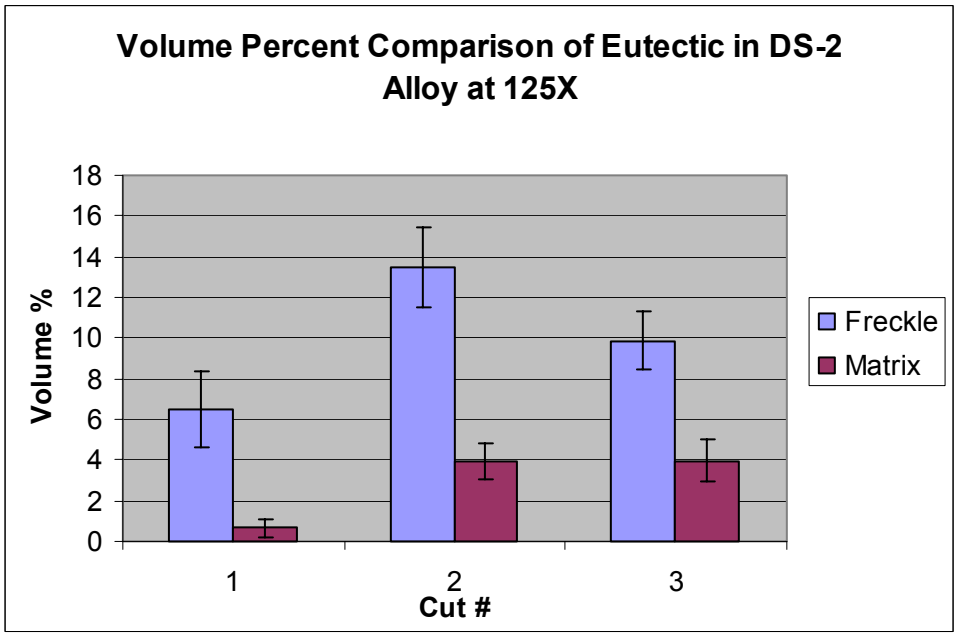

Figure 59 - Volume percent of DS-2 eutectic at 125X found through stereology.

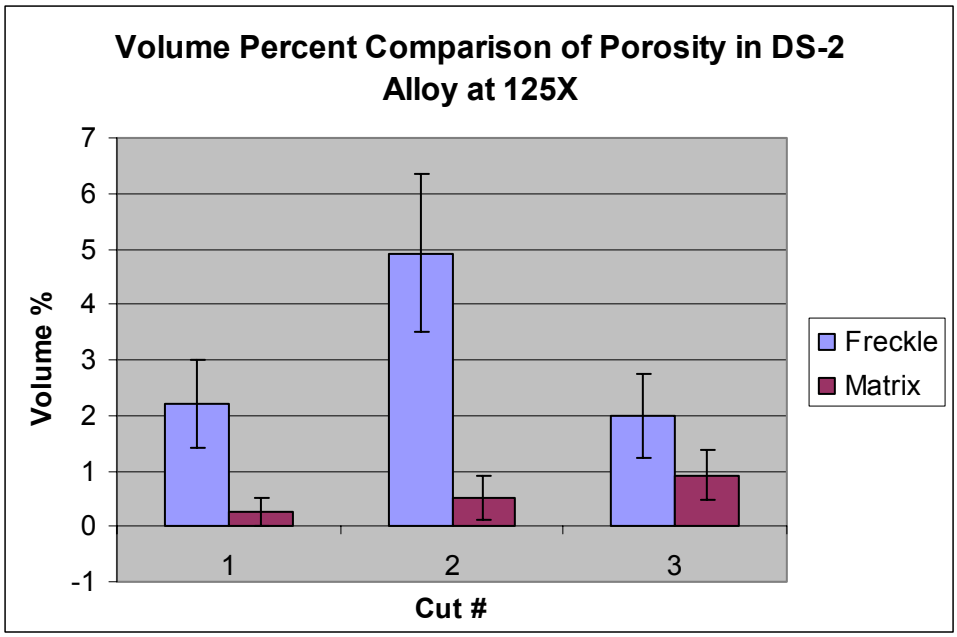

Figure 60 - Volume percent of DS-2 porosity at 125X found through stereology.

The results for the microconstituents of the DS-2 castings were similar to the stereological volume percents of those for the DS-1 alloy. The percentage of carbides seemed higher in the freckled regions, but this could not be proven statistically. Furthermore, the percentage of eutectic and porosity in the freckled regions was markedly higher than in the matrix, especially in the cross sections (Cuts 2 and 3). While the amount of eutectic present in DS-2 freckles was up to twice as high as in the DS-1 alloy, the ratio of eutectic in the freckled regions to the matrix was similar (approximately six times).

4.2.3. Stereology for Individual Freckle Grains

One of the goals for this project was to compare and contrast the amount of the various phases in the freckled regions with those in the matrix, but also to contrast the volume percent of constituents found inside the freckle grains themselves (excluding the grain boundaries and phases at the grain boundaries). However, this process proved difficult for several reasons. First, while it was relatively simple to distinguish the freckle

chains from the rest of the casting, it was difficult to distinguish the individual grains inside the chains. For example, the freckle grain boundaries are usually partially covered with η (if present) and eutectic, but these phases are also present in between dendrite arms. Freckles that can be distinguished with the naked eye do not necessarily contrast the same way at higher magnifications in an optical microscope or in an SEM. This is especially a problem at magnifications greater than 100X. At and near the grain boundaries, it is difficult to determine if a phase is inside or outside a grain, or if it is between two grains.

Therefore, individual freckle grains that could be distinguished yielded far less data than was found in the previous battery of tests. There were simply not enough grains to produce a sizeable amount of data. Statistically, conclusions should not be drawn from the results. Nevertheless, the results found are shown in Figure 61 (eutectic in DS-1), Figure 62 (η in DS-1), and Figure 63 (eutectic in DS-2). In all figures, the mean volume percent of the individual freckle grains is essentially the same as that of the freckled regions, but with a higher deviation. While one may hypothesize that the freckled region and individual freckle grains have identical volume fractions of eutectic and η, it cannot be proven in this study due to the small sampling population.

Besides quantifying volume percent of constituents in the two castings, PDAS was measured on the same specimens with Cut 3, since this is normal to the primary growth direction. The PDAS for DS-1 is 528 μm (±91 μm) and 493 μm (±86 μm) for DS-2. No critical PDAS for freckle formation could be calculated because no castings of the same compositions without freckles were available. However, both were larger than the aforementioned critical PDAS for CMSX-2—320 μm.[35]

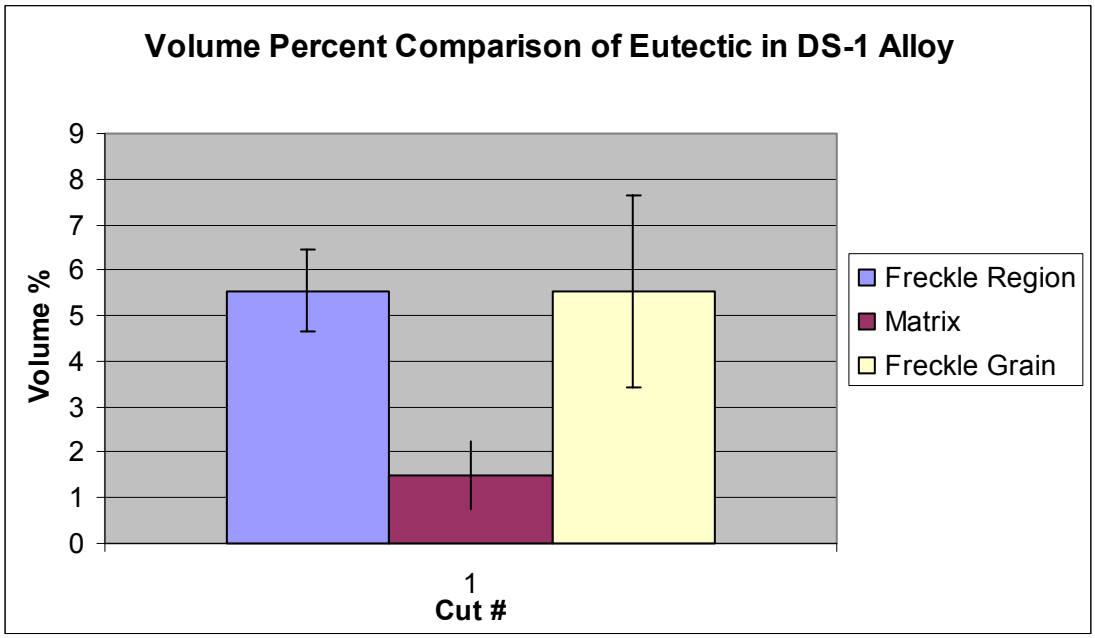

Figure 61 - Volume percent of eutectic in DS-1 alloy at 125X. This figure compares freckle regions with individual freckle grains.

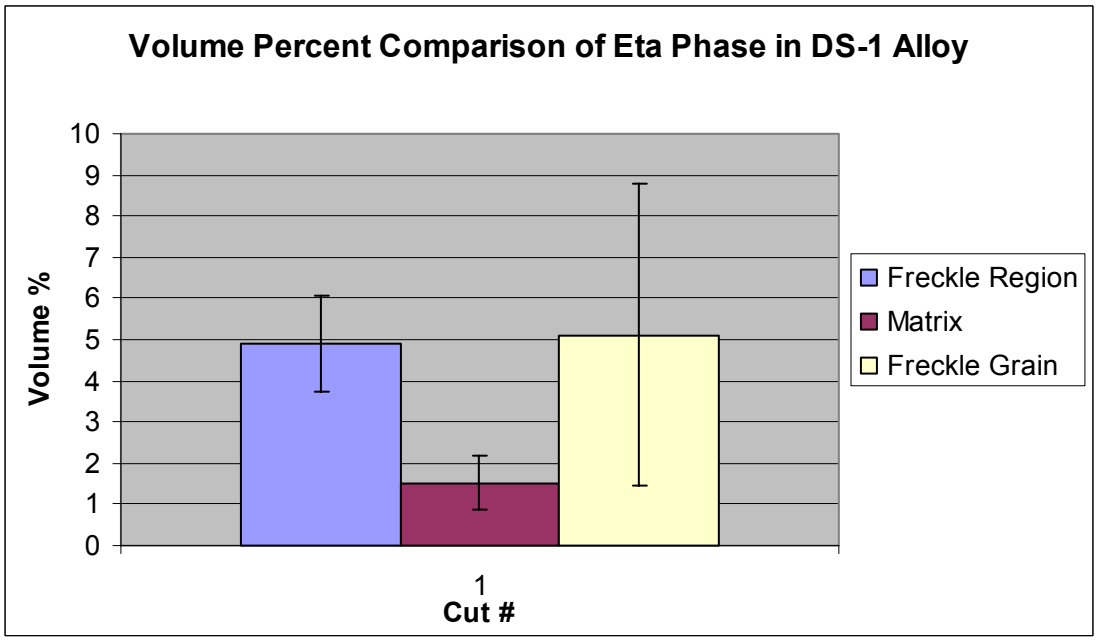

Figure 62 - Volume percent of η in DS-1 alloy at 125X. This figure compares freckle regions with individual freckle grains.

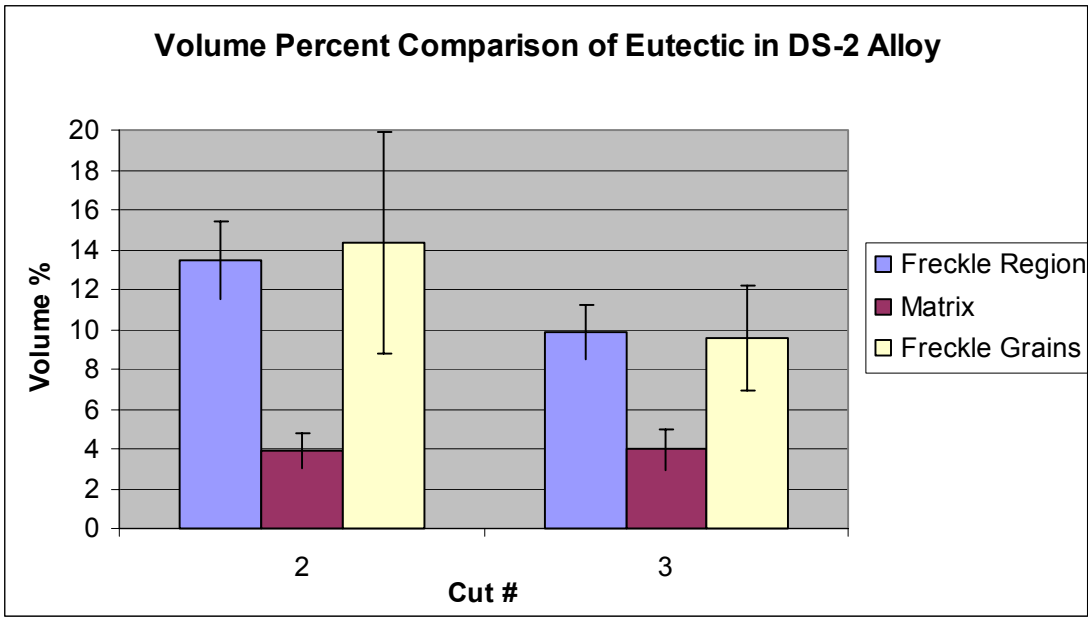

Figure 63 - Volume percent of eutectic in DS-2 alloy at 125X at cuts 2 and 3. This figure compares freckle regions with individual freckle grains.

4.3. EBSD

EBSD patterns were generated from the freckle and matrix grains in the DS-1 casting in order to determine the orientations of several different phases, and to find what orientation relationships, if any, existed between individual freckle grains and the rest of the casting. EBSD was first used to establish the orientation of this part of the casting, and to relate any orientation relationships or misorientations of the various constituents in matrix.

This task was first performed on the $\gamma + \gamma'$ eutectic to ensure that it was indeed oriented with the dendrite arms for the rest of the casting. In order to do this, the orientation of the matrix was first found. Figure 64 shows an EBSD map of the matrix region from Cut 1. This Kikuchi map is labeled; the green crosshairs towards the top indicate the direction normal to the sample, and the cyan crosshairs towards the center indicate the direction of the electron beam. The normal direction of this sample seems to

be in a <120> direction, which is close to a <110>. This result tends to agree with the fact that the secondary dendrite arms in this part of the sample are rotated away from perfectly orthogonal. In theory, this angle should be around 26°.

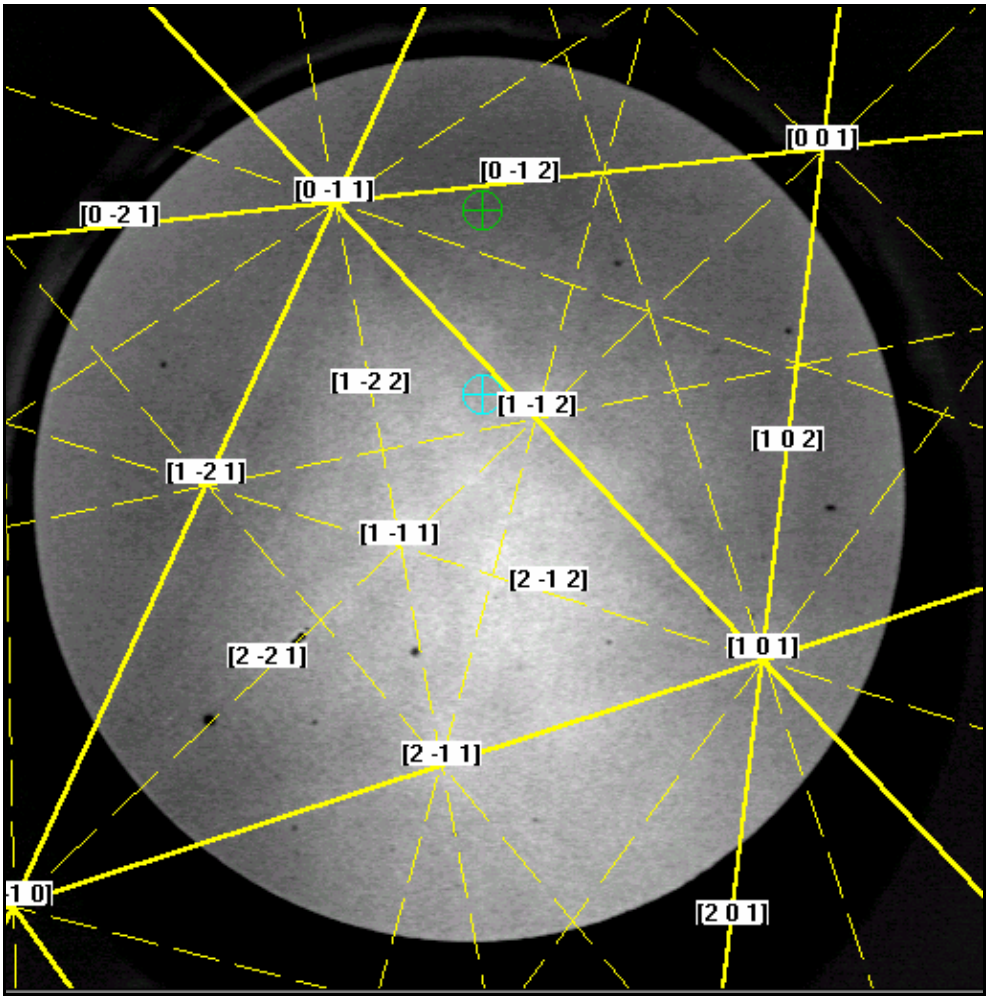

Figure 64 - EBSD Kikuchi map of γ + γ' matrix in DS-1 casting.

Next, EBSD data was compiled from various matrix points, and also various eutectic regions. The eutectic was carefully measured by putting a point probe on each section of a eutectic "fan." The results were similar to the matrix EBSD map in Figure 64, and were compiled as a pole figure in Figure 65. This pole figure is viewed from a [001] normal direction where RD is the rolling direction (which is the same as the growth direction for this sample), and TD is the transverse direction (see Figure 66).[41] Besides

showing the orientation of the matrix and the eutectic, Figure 65 shows that the orientation of eutectic is identical to that of the rest of the matrix. In moving the electron beam from one side of a eutectic "fan" to the other (in other words, across each γ' cell), the EBSD map rotated slightly. However, this rotation was too small to be shown on a pole figure.

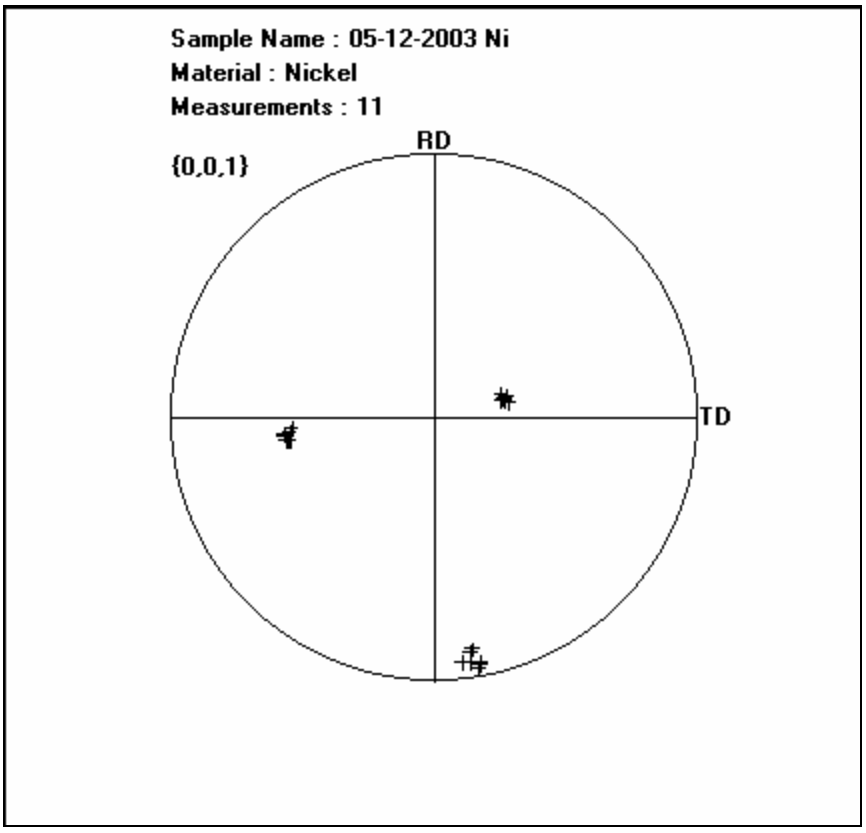

Figure 65 – A [001] Pole Figure of matrix and eutectic regions.

EBSD was also used to find the relationship between the η phase and the eutectic. If a relationship exists between the η and the eutectic, then that relationship would hold true between the η and the matrix. Figure 67 shows η to the right of a eutectic "fan." The EBSD map of the eutectic is shown in Figure 68, and the map of the η phase is

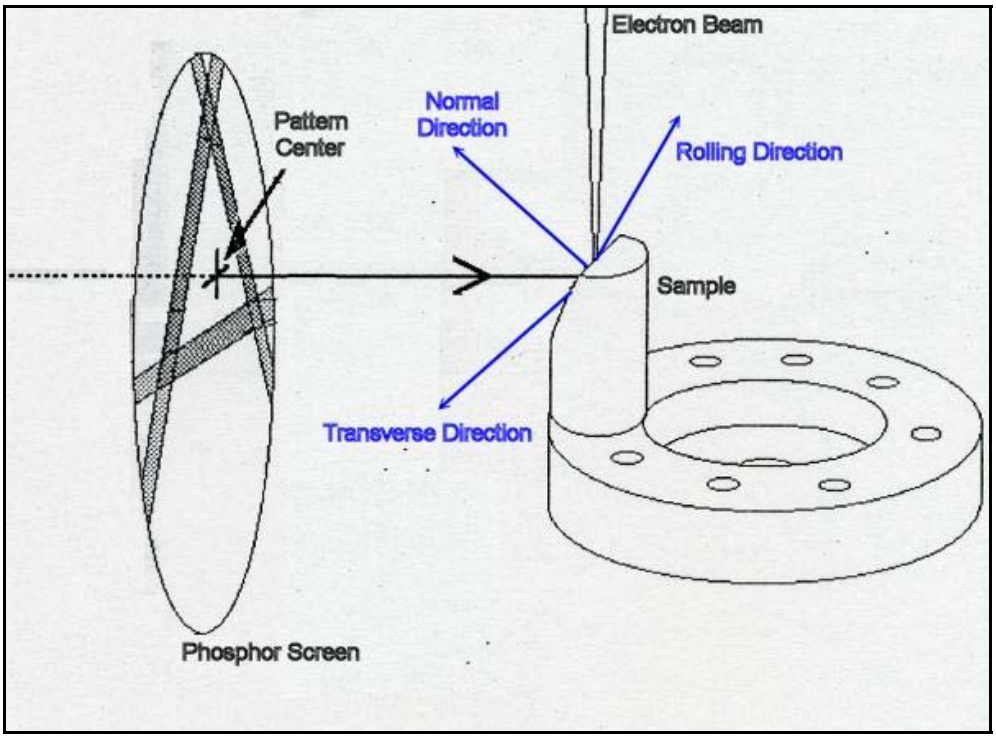

Figure 66 - Schematic of Oxford OPAL system showing directions in the pole figure from Figure 65.

shown in Figure 69. While the orientation of eutectic was relatively fixed throughout the sample, the η orientation changed from piece to piece. However, the basal plane of the η (seen as the thick line on the bottom of Figure 69) matches up with the close-packed (111) plane of the γ' (similar position in Figure 68). Many directions match up as well, such as <112> and $<01\bar{1}0>$, and the <011> and $<11\bar{2}0>$ directions.

Figure 70 shows a part of a freckle chain taken in the optical microscope. Figure 70 shows the same freckle chain, with the individual freckle chains color coordinated. EBSD was performed on each of these freckle grains along with a few random spots not in a particular freckle grain, but in the freckle chain region. The Kikuchi maps of each grain, along with the [001] pole figure of each grain are shown as Figures 71 to Figure 90. Table 4 shows the misorientations of each grain, and the common zone axis between the freckle and the rest of the casting.

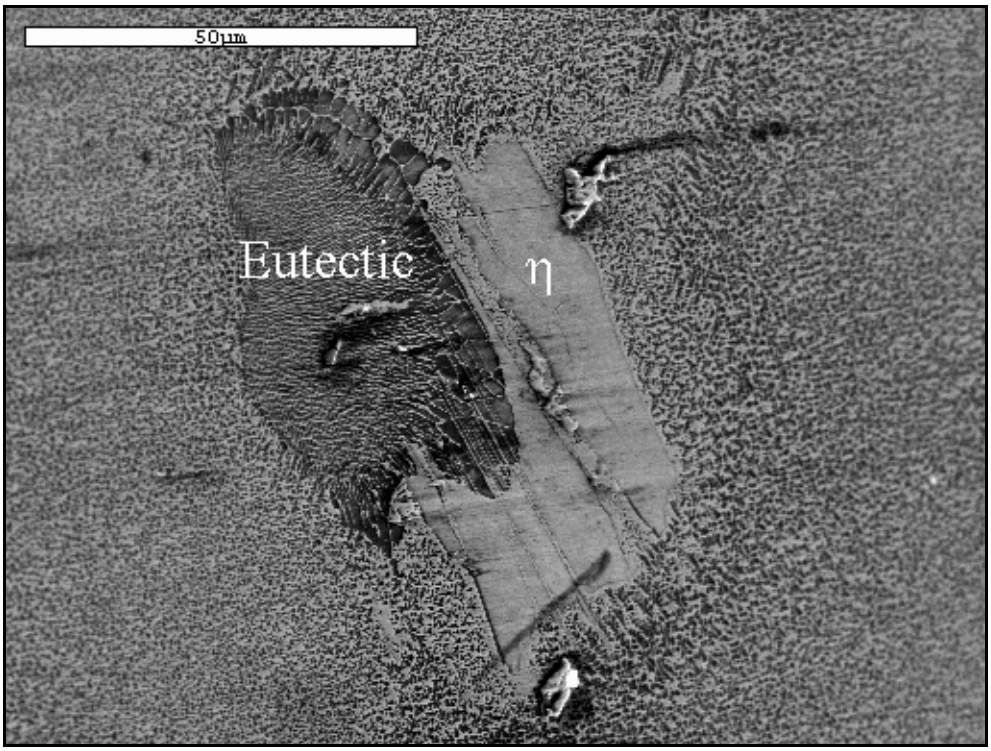

Figure 67 – SEM of η adjacent to eutectic colony (950X).

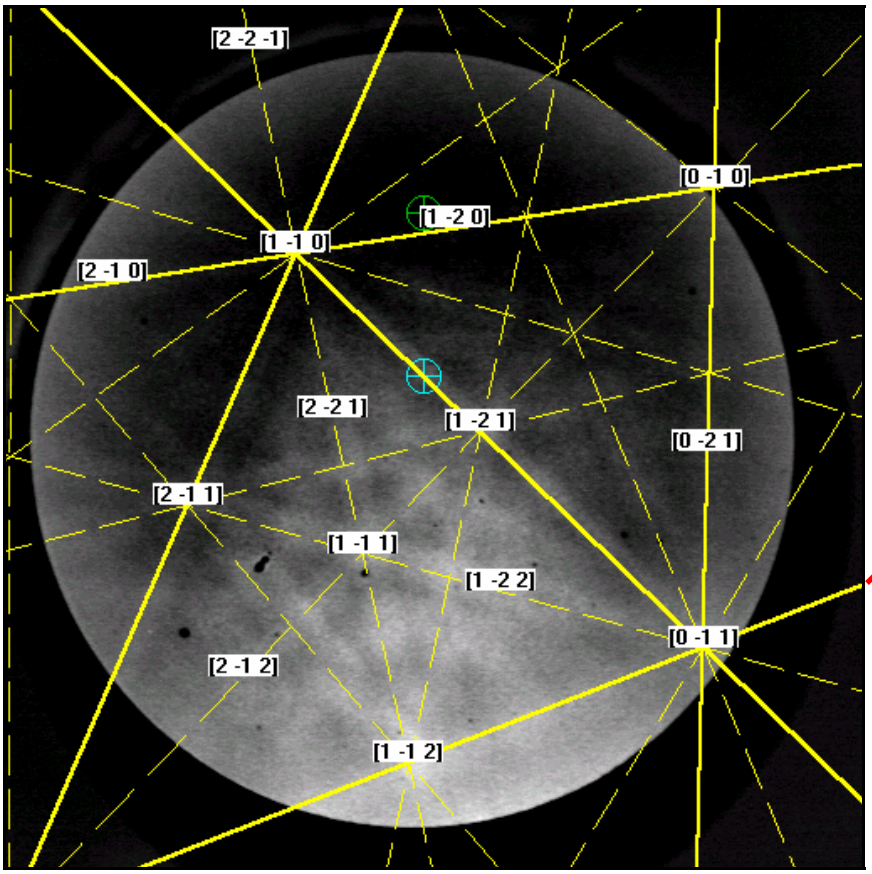

Figure 68 - EBSD Kikuchi map of eutectic from Figure 67.

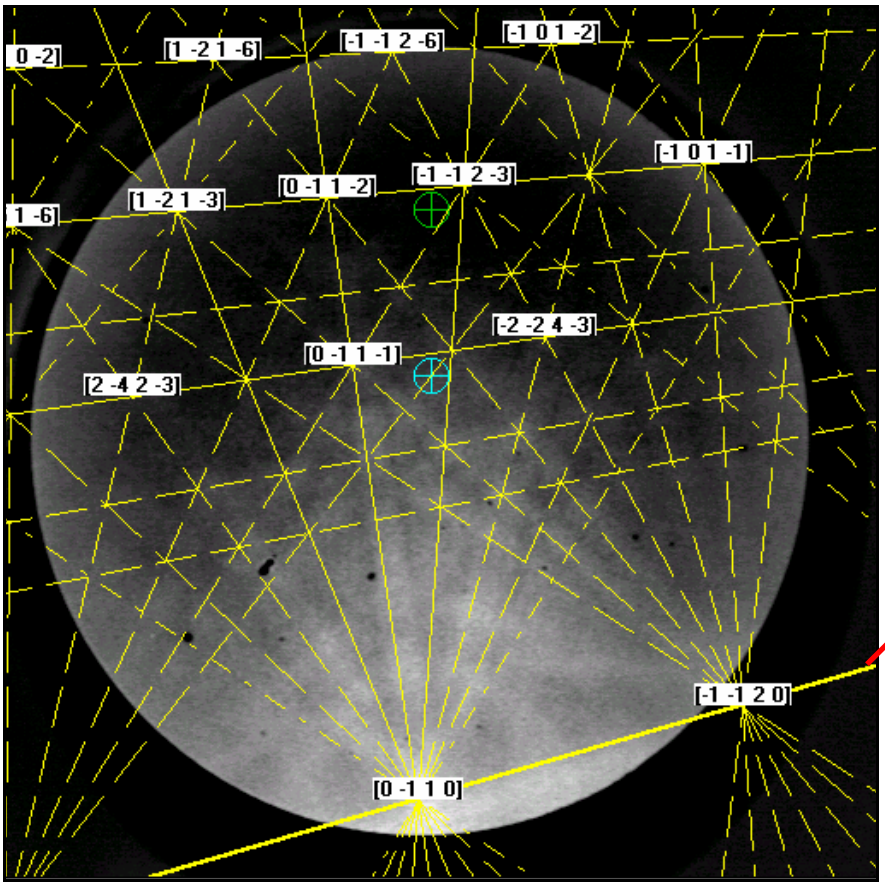

Figure 69 - EBSD Kikuchi map of η from Figure 67.

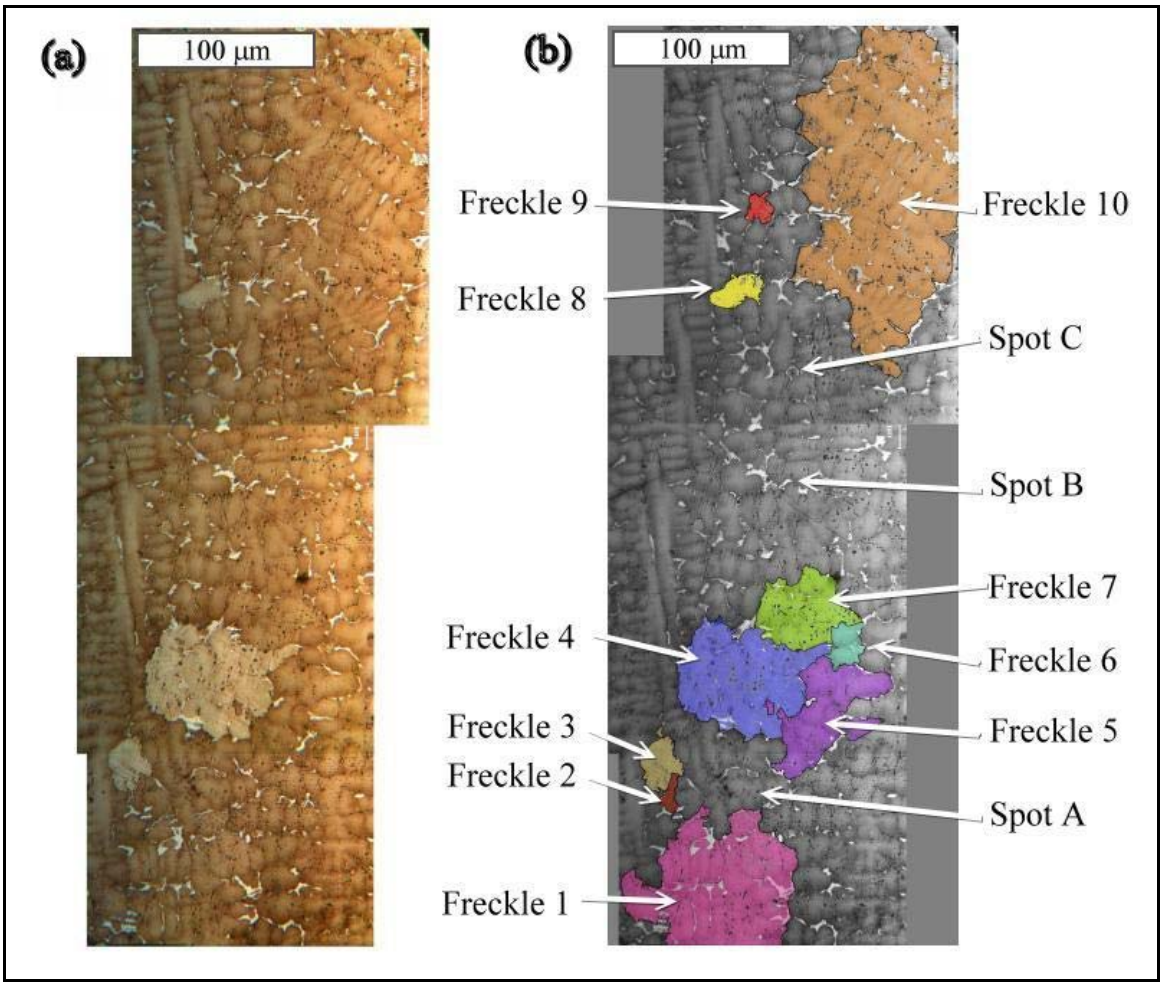

Figure 70 - Optical image of DS-1 freckle chain. (a) The unaltered image at 50X. (b) Individual freckle chains are numbered and colored.

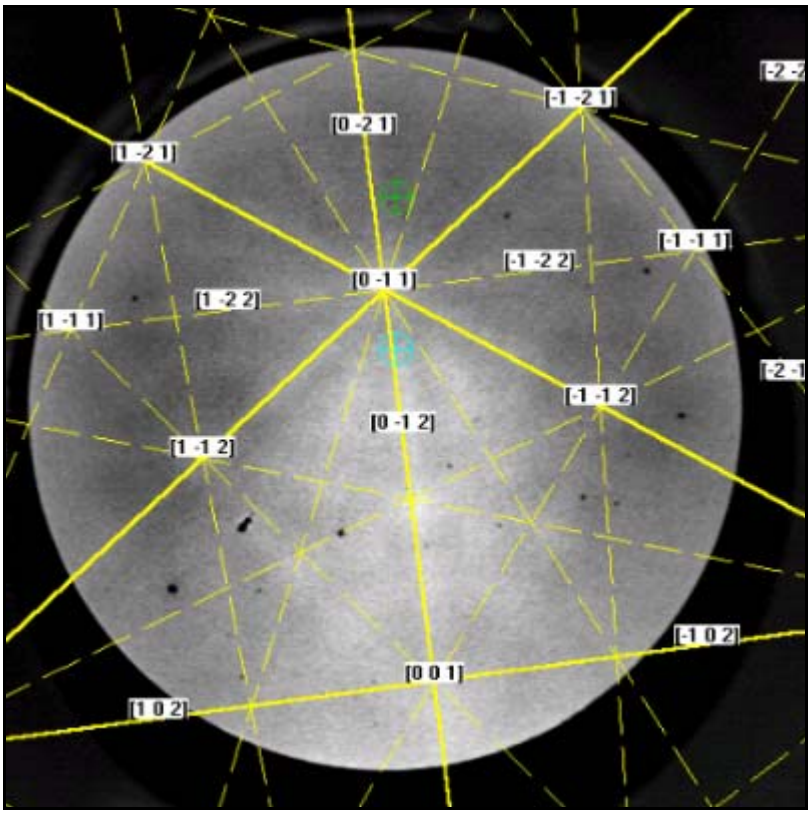

Figure 71 - EBSD Kikuchi map of a spot probed in Freckle 1.

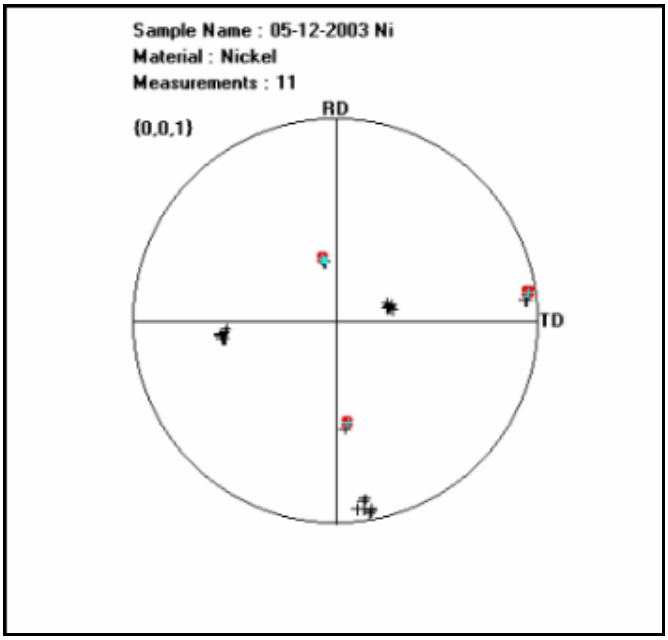

Figure 72 - The [001] Pole figure of freckle 1 in relation to the matrix. The freckle grain results are highlighted red

.

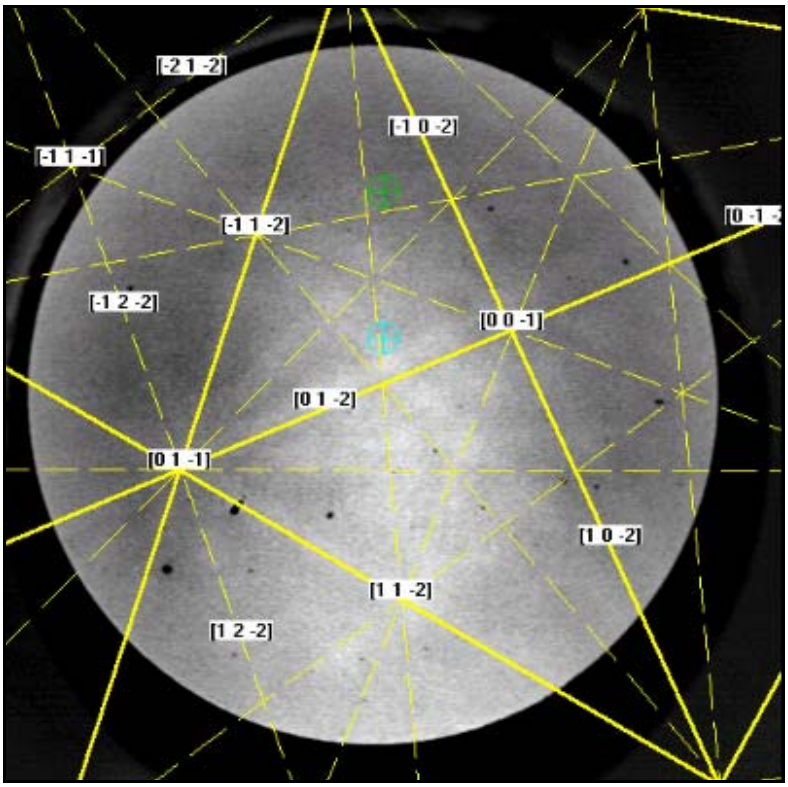

Figure 73 - EBSD Kikuchi map of a spot probed in Freckle 2.

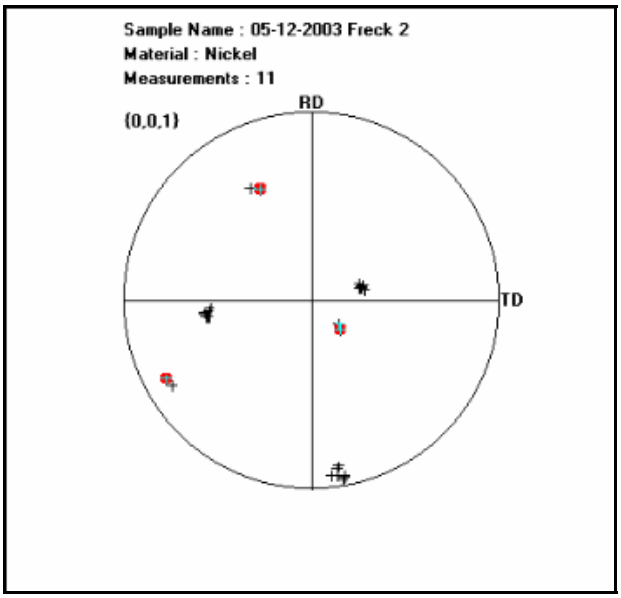

Figure 74 – The [001] Pole figure of freckle 2 in relation to the matrix. The freckle grain results are highlighted red.

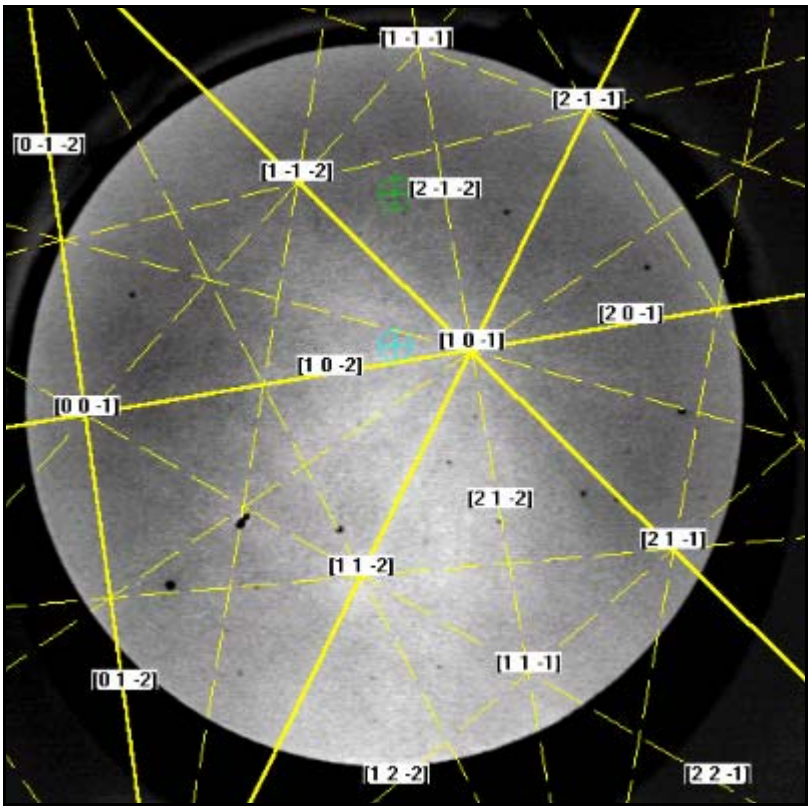

Figure 75 - EBSD Kikuchi map of a spot probed in Freckle 3.

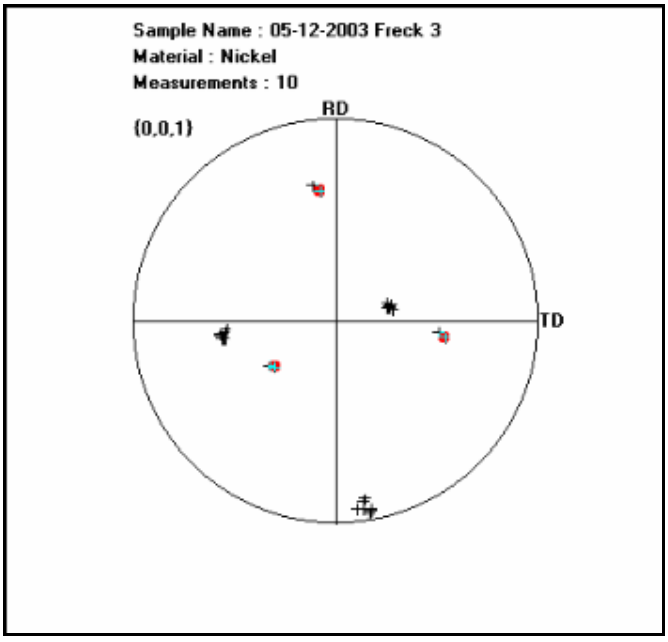

Figure 76 – The [001] Pole figure of freckle 3 in relation to the matrix. The freckle grain results are highlighted red.

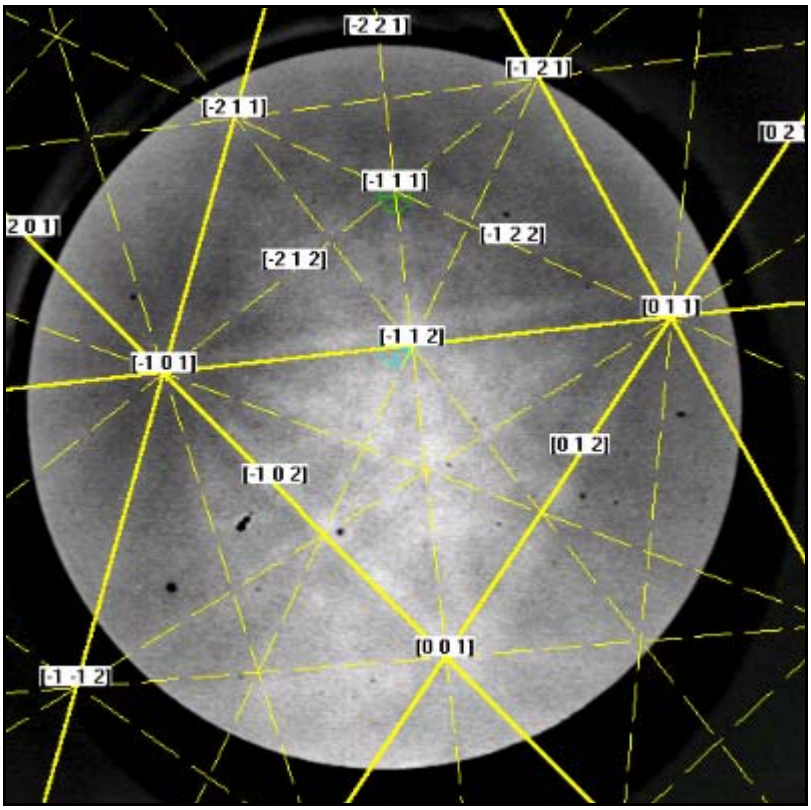

Figure 77 - EBSD Kikuchi map of a spot probed in Freckle 4.

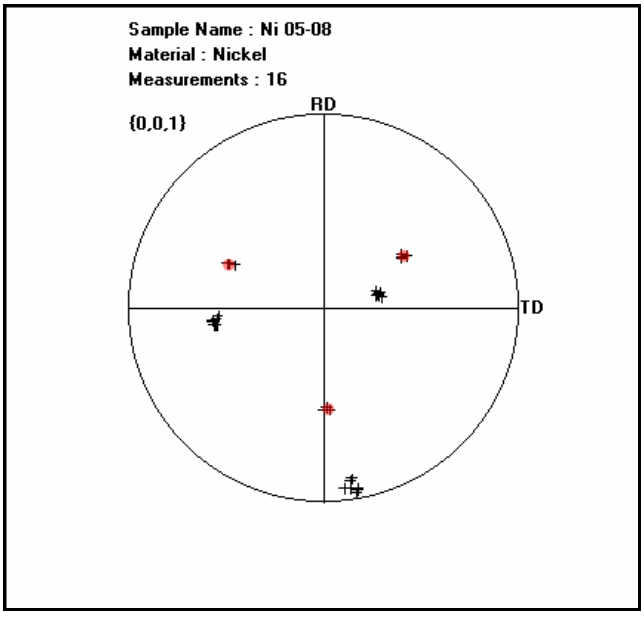

Figure 78 – The [001] Pole figure of freckle 4 in relation to the matrix. The freckle grain results are highlighted red.

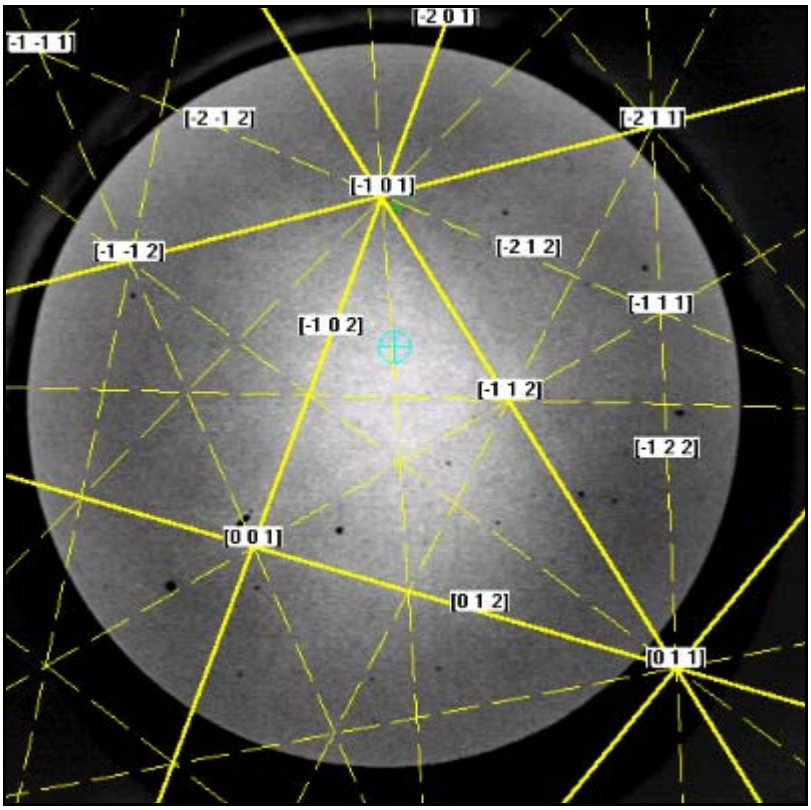

Figure 79 - EBSD Kikuchi map of a spot probed in Freckle 5.

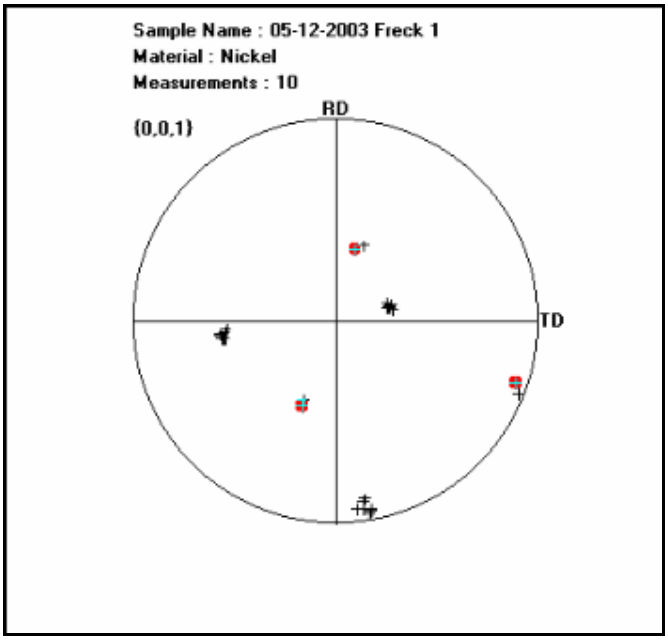

Figure 80 – The [001] Pole figure of freckle 5 in relation to the matrix. The freckle grain results are highlighted red.

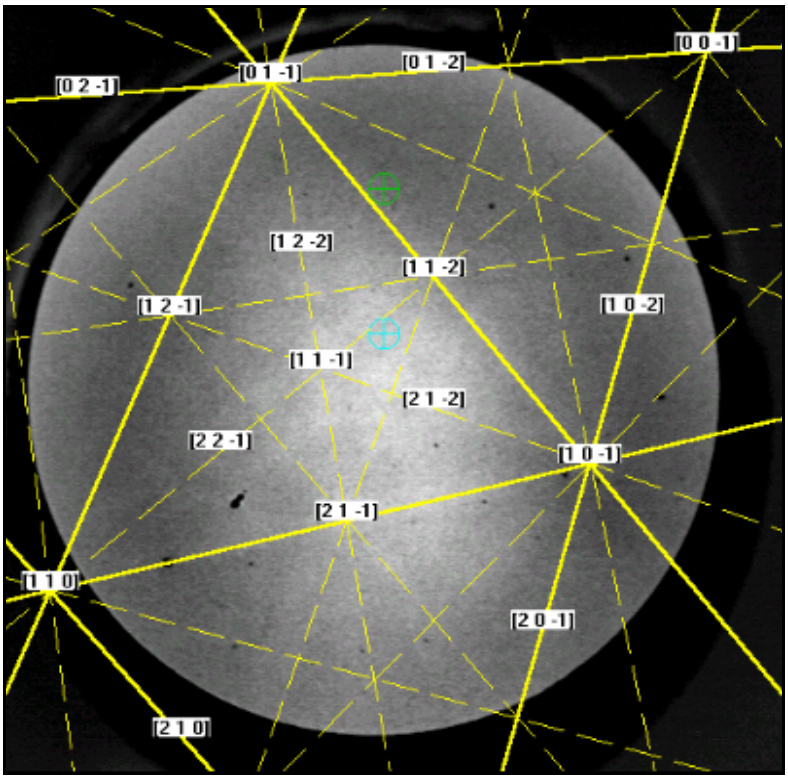

Figure 81 - EBSD Kikuchi map of a spot probed in Freckle 6.

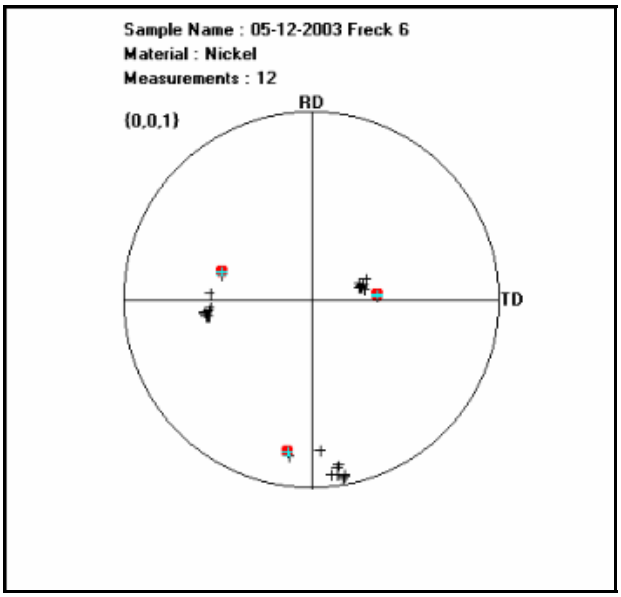

Figure 82 - The [001] Pole figure of freckle 6 in relation to the matrix. The freckle grain results are highlighted red.

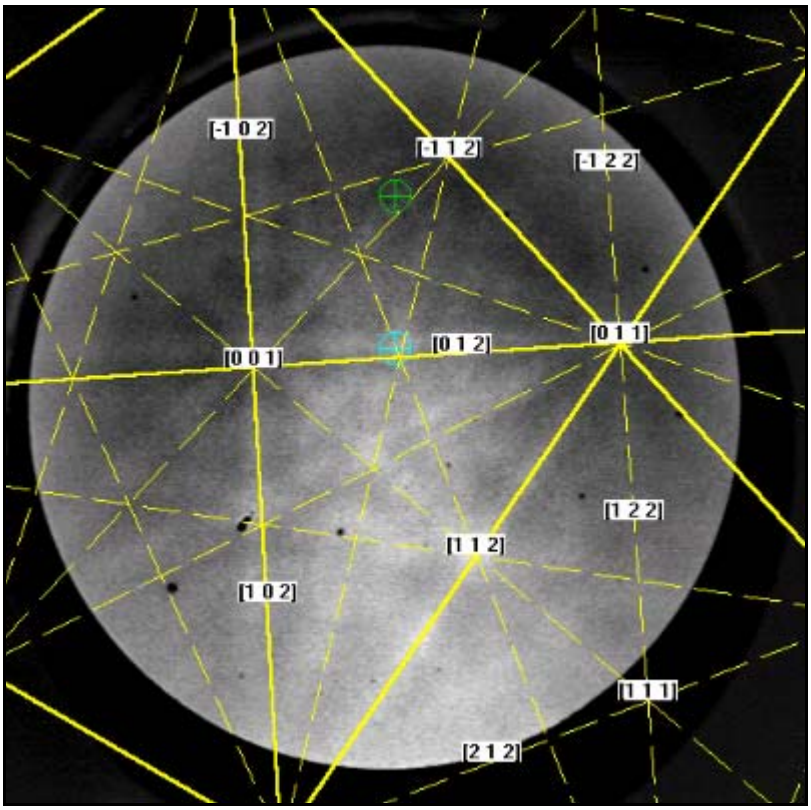

Figure 83 - EBSD Kikuchi map of a spot probed in Freckle 7.

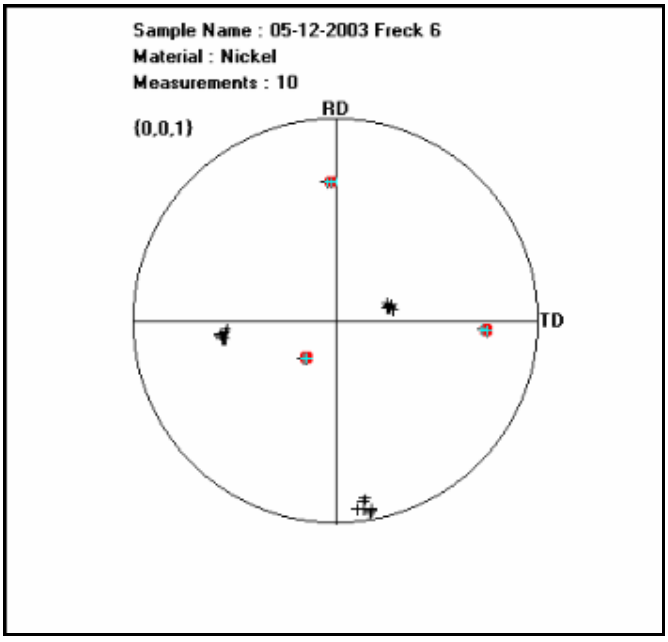

Figure 84 – The [001] Pole figure of freckle 7 in relation to the matrix. The freckle grain results are highlighted red.

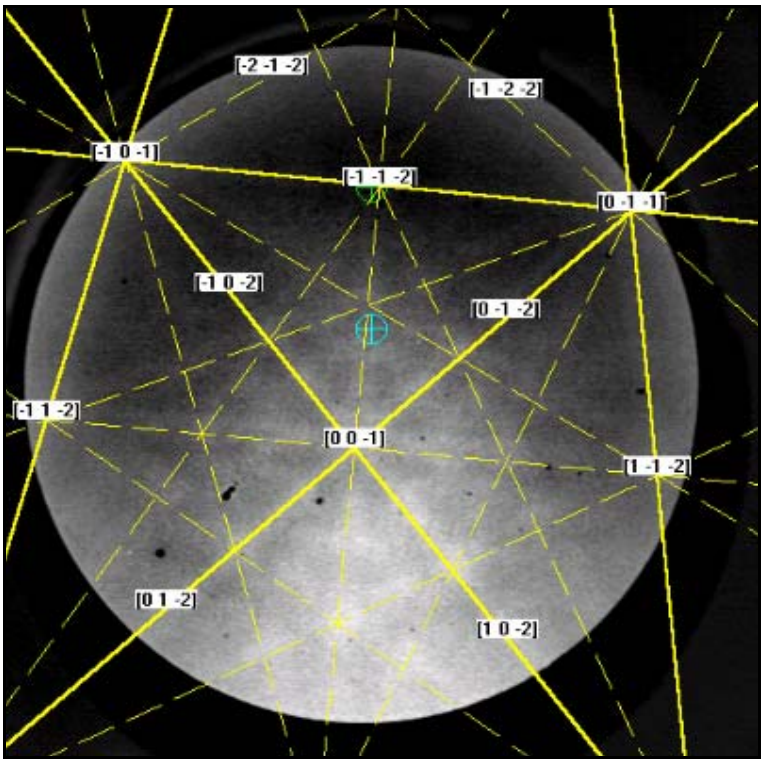

Figure 85 - EBSD Kikuchi map of a spot probed in Freckle 8.

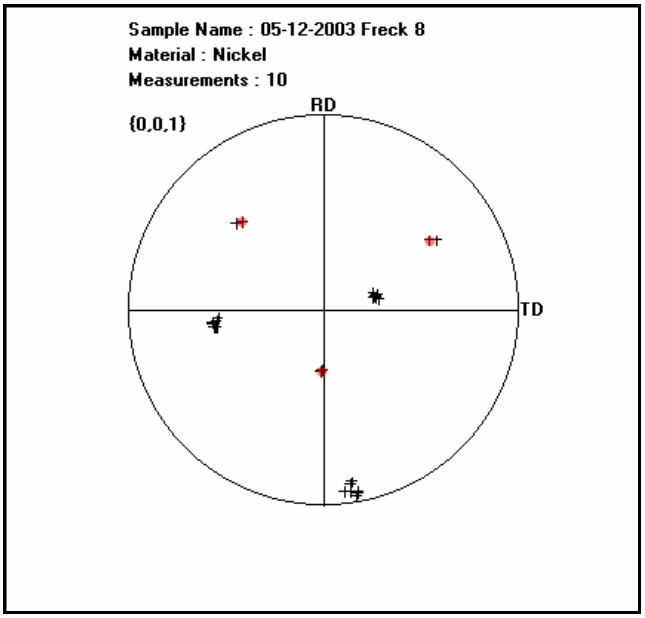

Figure 86 - The [001] Pole figure of freckle 8 in relation to the matrix. The freckle grain results are highlighted red.

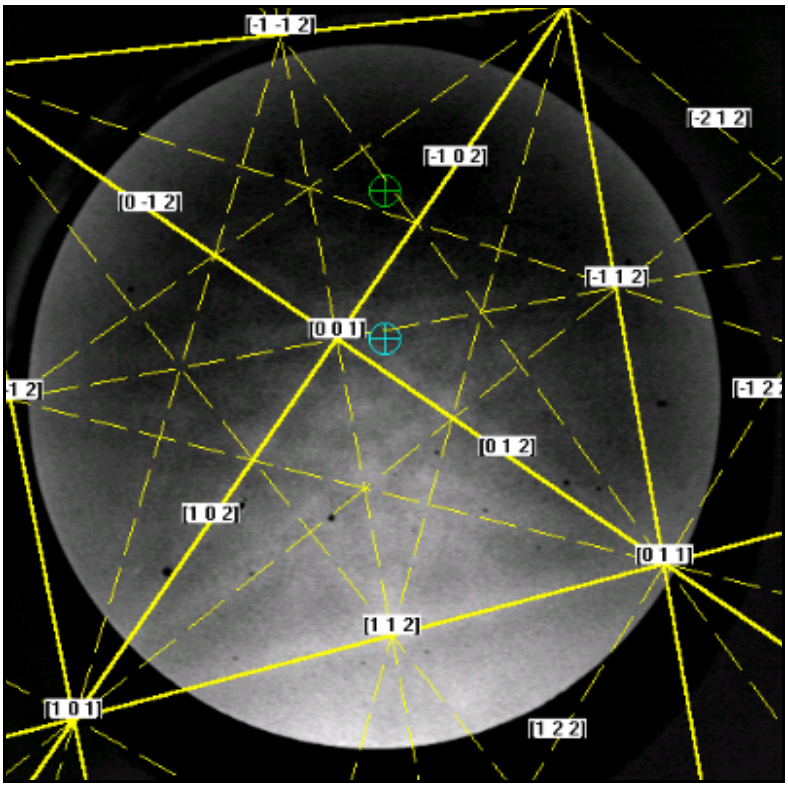

Figure 87 - EBSD Kikuchi map of a spot probed in Freckle 9.

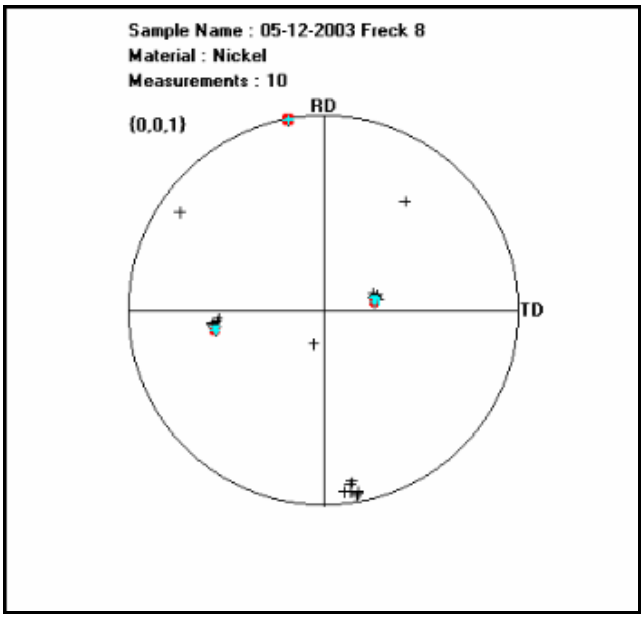

Figure 88 - The [001] Pole figure of freckle 9 in relation to the matrix. The freckle grain results are highlighted red.

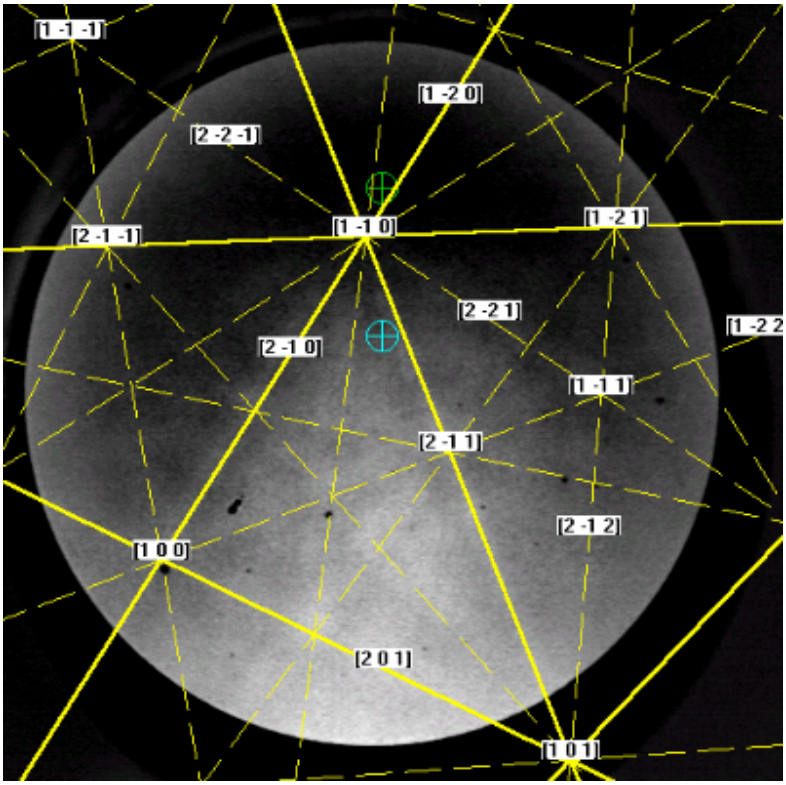

Figure 89 - EBSD Kikuchi map of a spot probed in Freckle 10.

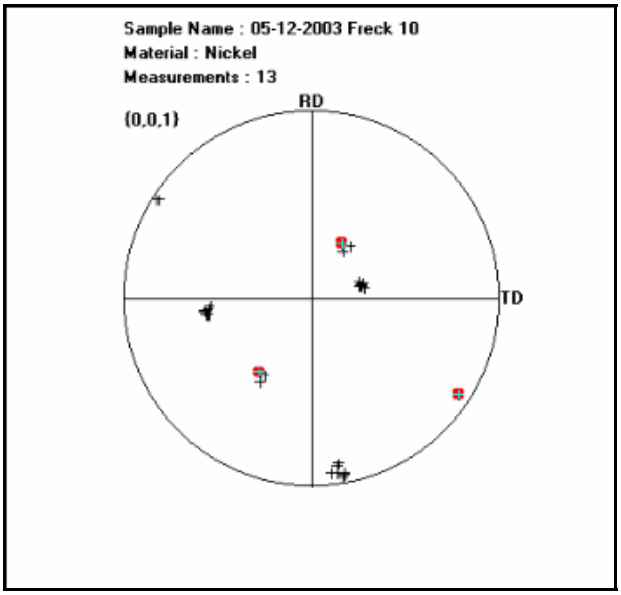

Figure 90 – The [001] Pole figure of freckle 10 in relation to the matrix. The freckle grain results are highlighted red.

Table 4 - Misorientations and common zone axes of DS-1 freckle grains.

Freckle Number	Angle of Misorientation	Common Zone Axis
1	47°	[7,-19,19]
2	35°	[16,14,17]
3	32°	[14,-17,16]
4	38°	[2,-2,-1]
5	54°	[-15,21,-11]
6	13°	[5,-9,26]
7	46°	[-23,9,-11]
8	59°	[14,16,3]
9	60°	[15,16,-17]
10	47°	[14,-23,-3]

These orientations show that there is little if any relationship between the freckles and the matrix regions. This is further backed up by the fact that the common zone axes between the freckle grains and the matrix have high indices. Spots A, B, and C showed the same orientation as the matrix.

4.4. Nanoindenter Results

The Triboindenter was used to identify both the hardness and modulus of the microconstituents. No differentiation was made between the freckles and the matrix since the scale of these grains is too large (for example, one would be comparing η in freckles with η in the matrix). Rather, the following measurements were performed on

- η phase
- Matrix γ phase
- Cuboidal γ' phase in the matrix
- Eutectic γ' phase
- Plates of γ in eutectic

The hardness values for the η phase were higher than in the matrix γ (see Figure 91). Likewise, the hardness of the eutectic γ' was higher than the matrix γ (see Figure 92). The η may be harder than the eutectic γ', but this cannot be statistically determined. As shown in Figure 93, the γ inside the eutectic regions was found to have a higher hardness than the matrix γ. When doing a similar comparison with the γ', no real difference was seen (see Figure 94). The variance in the matrix γ' was high because the indent was often larger than the small γ' precipitates, especially at higher loads. This may have also happened with the eutectic γ.

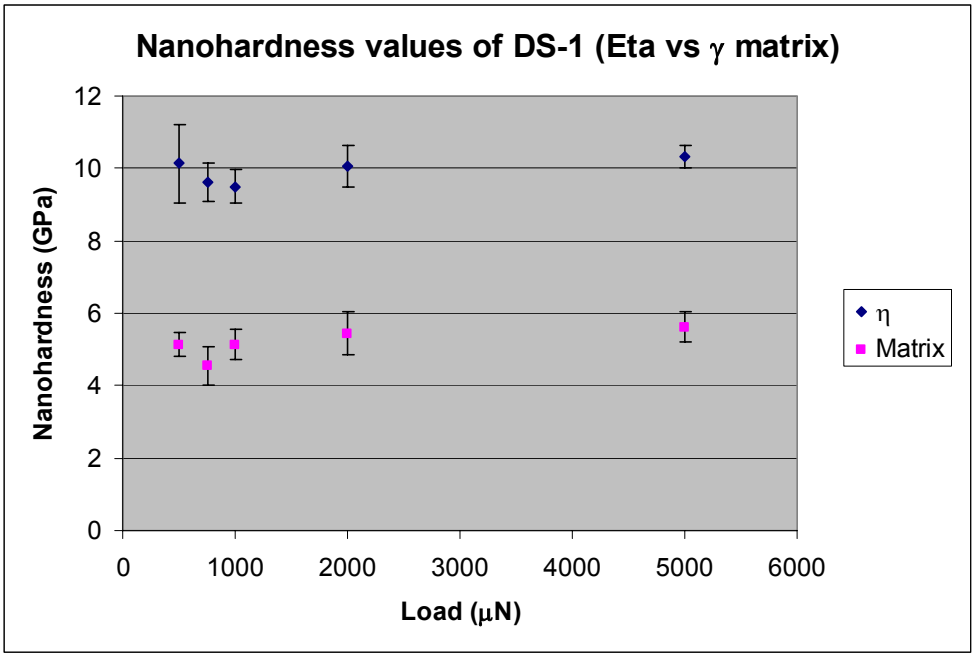

Figure 91 - Nanohardness comparison of η and matrix γ.

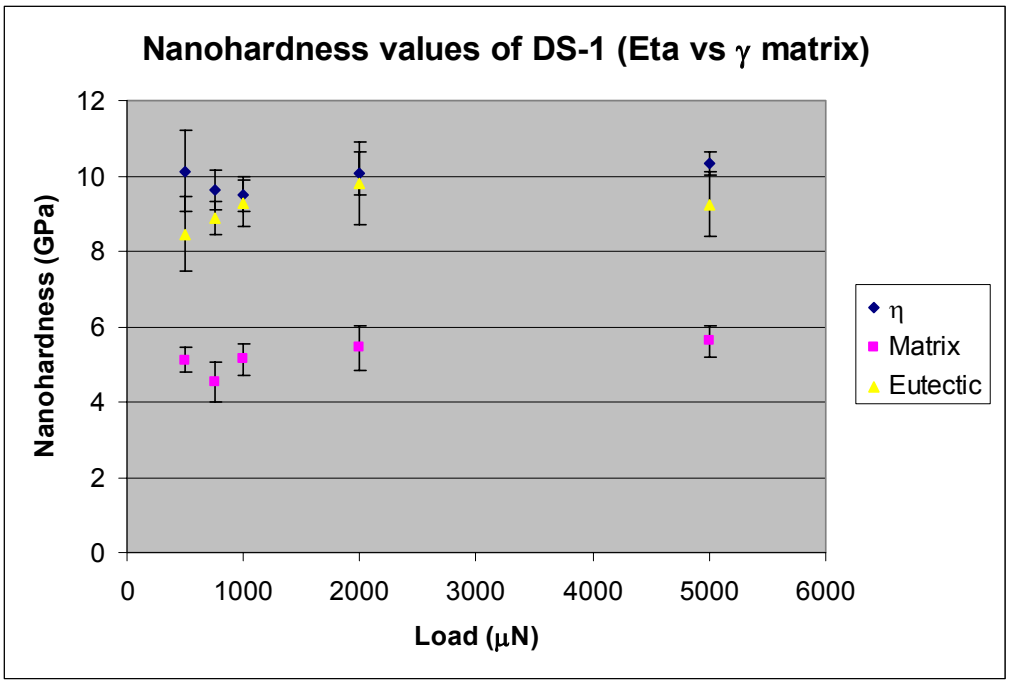

Figure 92 - Nanohardness comparison of η, eutectic γ', and matrix γ.

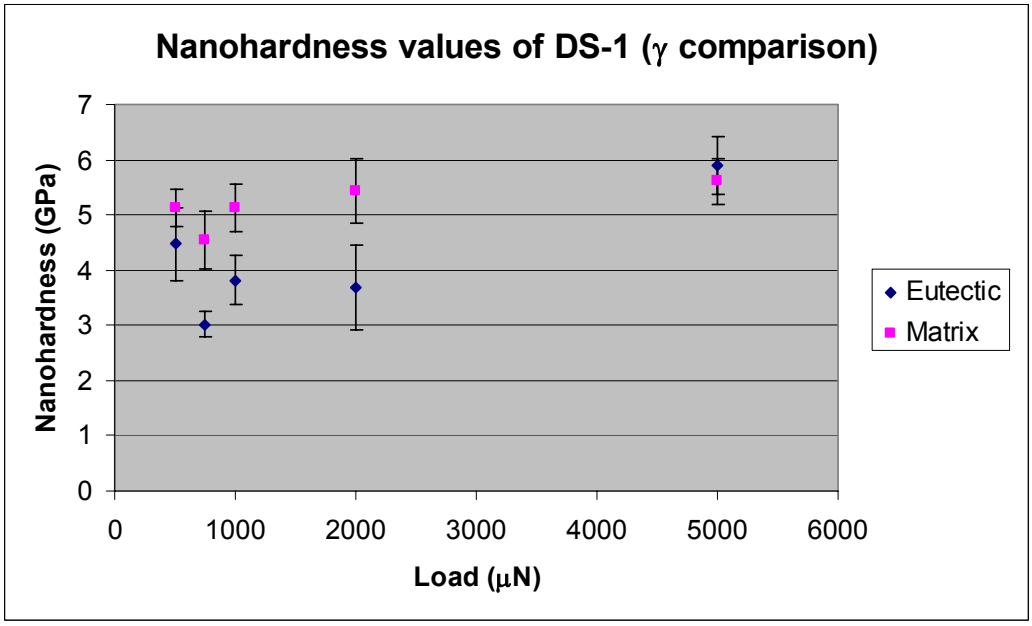

Figure 93 - Nanohardness comparison for γ in the eutectic colonies and in the matrix. The indent at 5000 μN may have been too large to get an accurate measurement.

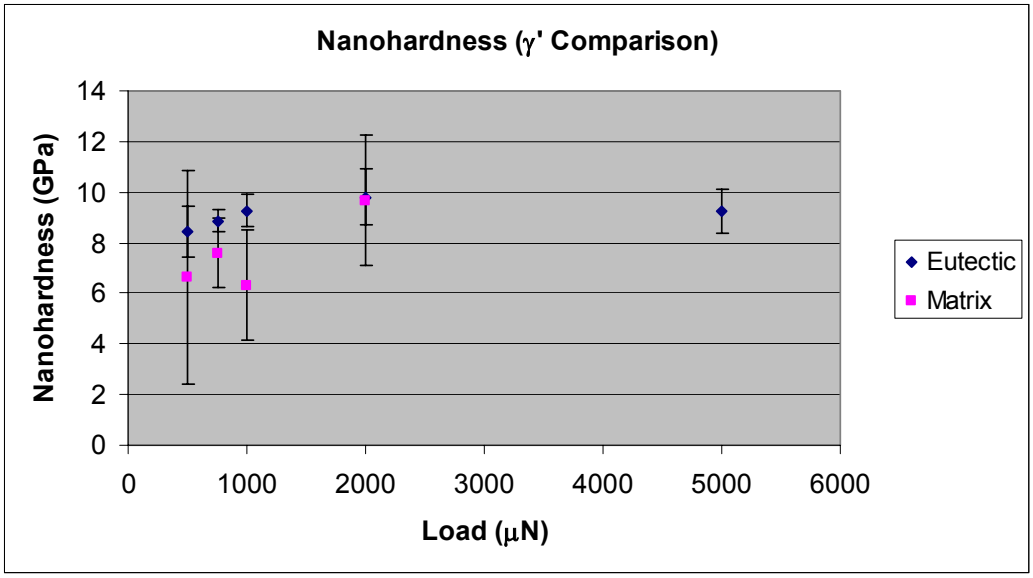

Figure 94 - Nanohardness comparison of the γ' in the eutectic colonies and in the matrix. No precise result could be found for the matrix γ' at 5000 μN due to the large indent size.

Dynamic testing was also performed to create modulus maps of various regions. Figure 95 shows the complex modulus, which is a composite of the stored and loss modulus, for an area of known η phase. Figure 96 shows the complex modulus matrix region. The higher modulus areas indicate higher stiffness, and it is shown that η has the highest stiffness, and that γ is stiffer than γ'. The numbers shown are more relative than absolute. When compared to the relaxed modulus results obtained from the static mode of the nanoindenter, the γ' is stiffer than the γ (see Figure 97). A similar comparison between eutectic γ' and matrix γ revealed no real difference between the moduli of either phases (see Figure 98).

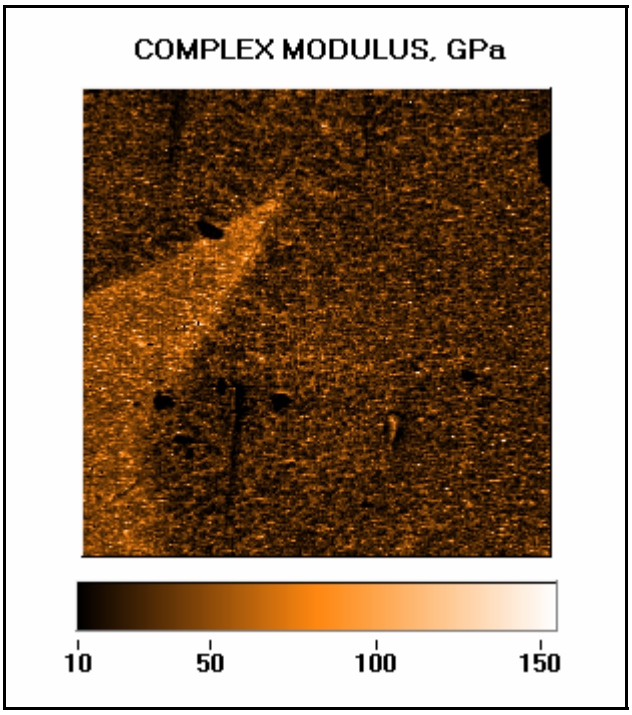

Figure 95 - Complex modulus map of DS-1 sample; η phase is shown on the left.

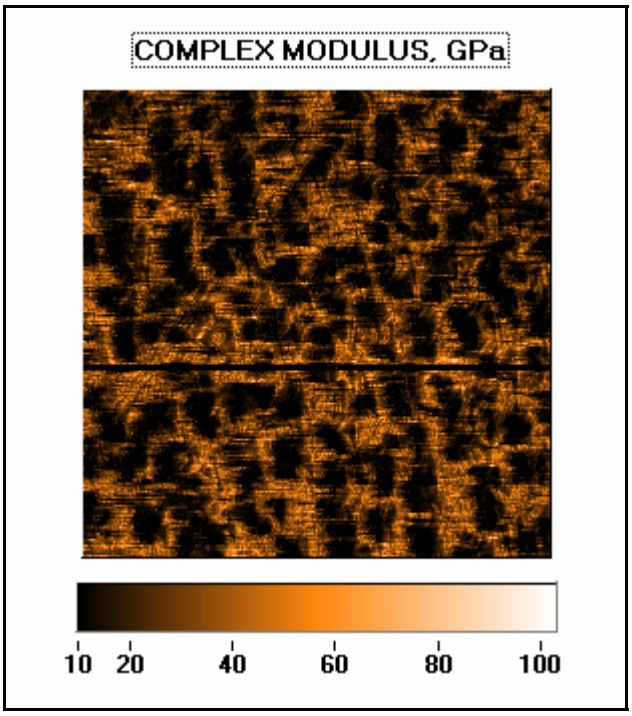

Figure 96 - Complex modulus map of DS-1 sample in the matrix regions showing cuboidal γ'.

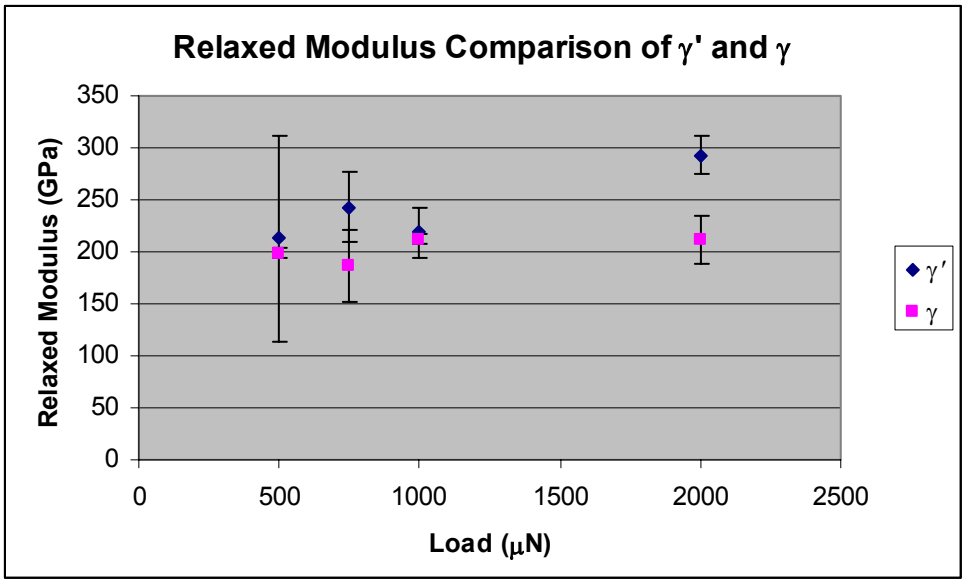

Figure 97 - Relaxed modulus comparison of γ' and γ from the matrix regions.

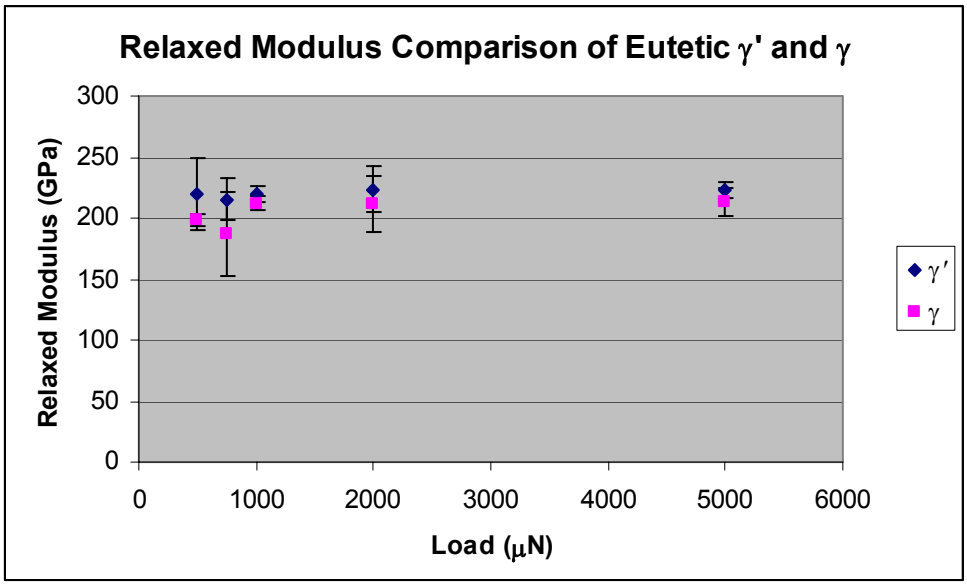

Figure 98 - Relaxed modulus comparison of matrix γ and eutectic γ'.

CHAPTER 5
ANALYSIS AND DISCUSSION

It has been clearly demonstrated that freckle formation in castings is detrimental to the properties desired from the DS process. The samples analyzed in this study were actually commercial castings that were scrapped because they displayed freckle chains. In this chapter, the data obtained from this project will be correlated with previous findings to create a better understanding of the formation of the deleterious freckle grains.

5.1. Analysis of Phases

The microstructures of both DS-1 and DS-2 alloys are consistent with the expected microstructure of DS castings. Both underwent unidirectional dendritic growth and both contained interdendritic regions of eutectic $\gamma + \gamma'$. The primary dendrites contained the typical γ and cuboidal γ' microstructures desired by the industry. Elements that usually segregate out of the dendrite core, i.e., those that have a fractional partition coefficient less than one (e.g., Al, Ti, Ta) were found at higher concentrations in the eutectic regions, while the solid-solution strengtheners with partition coefficients greater than one (e.g., Cr, W, Co, Mo) were enriched in the primary dendrite cores. This segregation and the large quantities of alloying additions lead to constitutional supercooling and the resulting dendritic solidification in these alloys.

Many of the phases described in previous literature for freckled castings and superalloys in general were observed and identified in both alloys. In DS-1, η was identified by multiple characterization techniques. Backscattered SEM showed this phase to have higher atomic number contrast than the γ or γ', but less than the MC

carbides while the EDS data indicated a phase with mostly Ni and Ti. TEM analysis confirmed the D0_{24} structure of the η, its proximity to the eutectic γ' and the expected orientation relationship. In addition, hardness and modulus tests with the nanoindenter confirmed that this phase was harder and stiffer than other phases, which again pointed to η. However, no η was found in DS-2 likely because of a lower Ti/Al ratio than that of DS-1. The η had an orientation relationship with the eutectic γ':

$$\begin{aligned} &\{\bar{1}\,1\,1\} \parallel (0001) \\ &<0\,1\,\bar{1}> \parallel <1\,1\,\bar{2}\,0> \end{aligned} \tag{8}$$

Since the eutectic γ' had an identical orientation with the γ matrix, this relationship holds true for the matrix and η as well, and agrees with previous findings.[42] The TEM images showing the stacking faults would suggest this η is prone to faulting where the stacking faults in the η are local regions of γ' and vice-versa. The areas where η appeared alone (not adjacent to a eutectic colony) are likely from a sectioning effect of the sample preparation.

Besides η, γ' was observed in various morphologies throughout the freckle grains in both alloys. While this included the common cuboidal γ' in a γ matrix and the γ + γ' eutectic, elongated and rectangular γ' was also observed at the freckle-freckle and freckle-matrix boundaries. The rectangular grain boundary γ' could be a film or plate with holes surrounding a freckle grain. While there is literature that suggests that a film of grain boundary γ' frequently occurs during service and improves rupture properties,[2] the morphology observed in this project has not been previously documented.

Carbides were also found in both alloys. The all of those identified were primary MC carbides, which in DS-1 and DS-2 appeared to be (Ta,Ti)C. Secondary, $M_{23}C_6$,

carbides were not found in either casting, likely because no heat treatments had been performed on these castings. Some TCP phases, most likely σ, was found in DS-1. Statistically and quantitatively, no more carbides were found in the freckled regions than in the matrix, as was previously reported.[23,24,43] However, there appeared to be an increase in carbides on the virgin surface of the DS-2 casting although there was no obvious difference between the surface of the freckle regions and that of the general casting.

These constituents correspond well with the results found by Genereux with midradius VAR ingot freckles.[24] While freckles from both ingots and castings are characterized by an increase in elements that partition to the interdendritic liquid and result in the increased presence of η, carbides, and γ', the morphologies of the phases and overall microstructures are different (see Figures 99 and 100 for images of VAR freckles[23]). Freckles in castings are chains of equiaxed grains surrounded by and containing a larger percentage of η and γ' than the rest of the casting, whereas the freckles in ingots are regions of the ingot with an increased percentage of these phases. The freckles in ingots usually result in cracking in the ingot during forging. For those ingots where freckling does not cause this problem, the freckles are not retained in the final product due to extensive hot working of the material. Freckles in castings, though, initiate creep failure from their grain boundaries. The extensive porosity and segregation near the freckles found in this study may indicate that freckles could also be initiation sites for other failure mechanisms not necessarily related to creep, such as fracture or fatigue cycling.

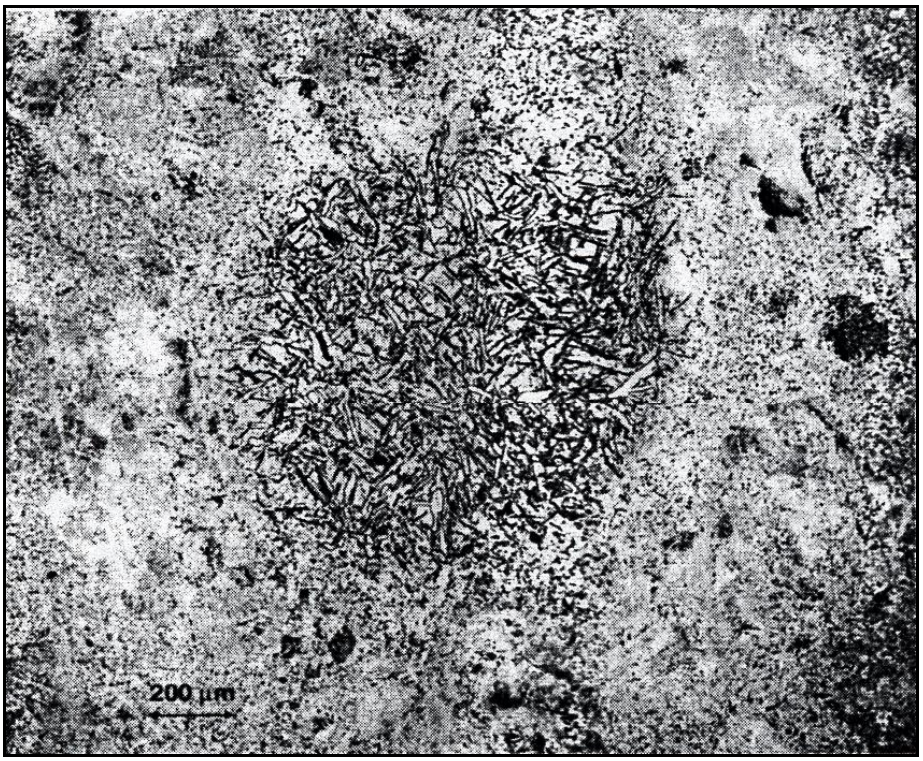

Figure 99 - Transverse optical image of freckle in an ingot of Gatorized Waspaloy. The freckle is the darker region in the middle.

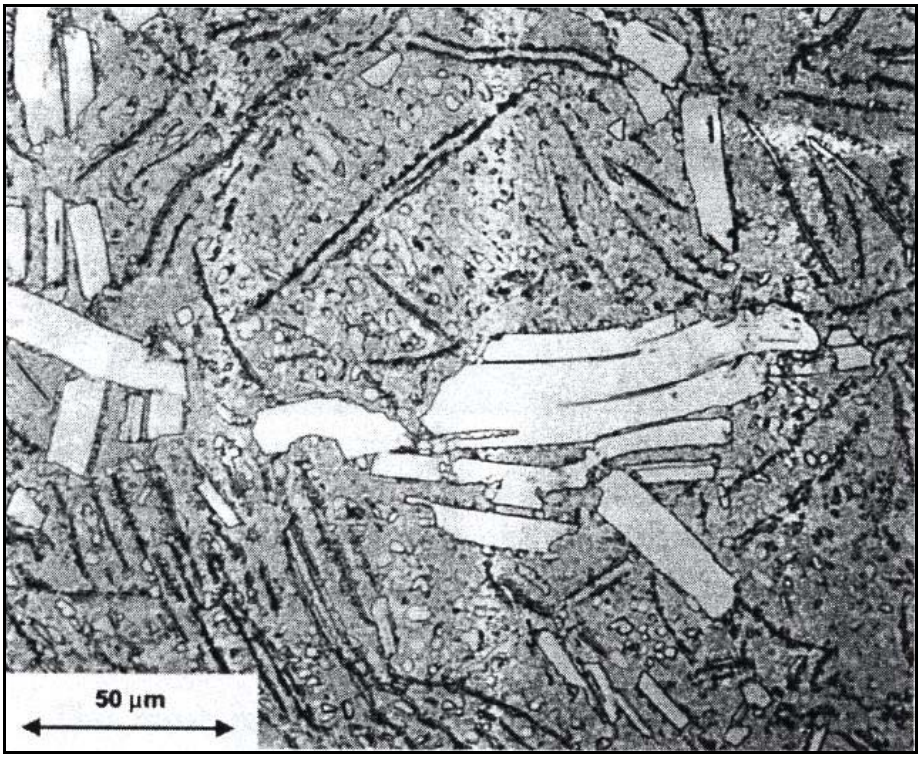

Figure 100 - Optical image of Figure 99 at higher magnification. The white phase is η, and the dark thin plates are γ'.

The hardness and modulus results seem to correlate well to accepted literature. The hardness of η and γ' is higher than that of the γ. However, the elastic modulus of the matrix γ' was shown to be lower during the dynamic modulus mapping. Static tests of relaxed modulus showed no statistical difference between the two phases. Previous authors[2,44] reported that the γ phase should have a higher Young's modulus than the γ'-Ni_3Al (207 GPa for annealed Ni and 179 GPa for pure Ni_3Al). The similar modulus values from static testing likely result from noise (e.g., indents were too large). An indent that was too large in the matrix would interact with the interface between γ and γ', resulting in an increase in hardness and modulus values.

5.2. Freckle Formation

There is little from the results gathered in this project that would dispute the mechanism of thermosolutal convection as the cause of freckle grains on the surface of DS and SX castings. However, several qualitative hypotheses have been backed up with quantitative data, and more information on the virgin surfaces of these castings has been provided.

There appeared to be more freckle chains in the DS-2 castings than in the DS-1. These chains were straighter than the bowed freckles chains in DS-1, and they were more closely spaced. This, along with the higher PDAS in DS-2 and larger casting diameter, corresponds to more convective jets occurring in DS-2 than in DS-1. However, it should be noted that the location of these samples in the original castings is unknown, and the number of freckle chains decreases as one goes form the chill to the top of the casting.[23,25]

As was previously observed, the freckle regions were found to be enriched in the elements that segregate to the interdendritic regions (Al, Ti and Ta).[6] Even so, as was also observed, many of the larger freckle chains exhibited a dendritic structure similar in size and spacing to the matrix regions. This would tend to support the notion that freckle chains are caused from the dendrite arms of the mushy zone being ripped off by the low-density plumes arising from the mush. At the same time though, these freckle grains exhibited a compositional shift towards the interdendritic liquid composition. Since the dendrite arms have the least solute (Ta, Ti, Al) and the plume emanating from the mush has the maximum amount of solute, this mechanism of freckle formation seems questionable.

The measured PDAS for both alloys was above the reported critical values for freckle formation from previous research.[25,35] Large PDAS indicate that the cooling rate (the product of G and R) was low, and extensive macrosegregation of elements in the casting occurred. Therefore, conditions were suitable for the onset of thermosolutal convection. Furthermore, the dendritic structure of freckle grains was similar to that of the matrix. Most likely, the dendrites torn away from the mushy zone were large enough to nucleate new equiaxed grains, but small enough as to contribute minimally to the freckle composition. This would be especially true if partial remelting of the dendrite arms occurred as would be expected if the arms are convectively transported to higher temperature regions. The random orientation of these grains seen from EBSD, which agrees with previous work,[45] shows that the nucleation of these grains is not dependent on the matrix.

It is clear that the freckled regions contain greater amounts of elements that partition to the liquid during solidification and, in turn, more eutectic and η (if present) appear in these areas than in the rest of the casting. The eutectic "fans" at high-angle grain boundaries display an orientation relationship with the grain adjacent to the web-like γ + γ' portion rather than the coarser lamellar regions. Furthermore, in DS-1, η usually appeared adjacent to the lamellar regions of the eutectic colonies and displayed an orientation relationship (see Equation 8) with the eutectic colony. The structure of the eutectic colony is described best by Figure 24, which appears to be a longitudinal section of the colony, and Figure 26, which appears to be a transverse section. This indicates that in these multicomponent superalloys, there is no exact eutectic point, but rather a trough or other geometric construction that describes the solidification of the γ + γ' colony. This agrees with previous work that showed eutectic growth in superalloys over a 5°C temperature range.[19] It is likely that in the both alloys, the web-like regions solidify first. This region is actually small cells of γ'. At some point, some of the cells grow and reject elements that segregate to the dendrite core, causing small γ layer to form between the γ' cells. This growth continues until the last solidification occurs—in DS-1 and alloys with high Ti/Al ratios, the last liquid becomes η. This may stem from the fact that the theoretical solidus for η (1304°C) is lower than that for γ' (1385°C).[3] In alloys where η does not form, the "eutectic" colony completes the solidification process.

An excess amount of porosity was also found between the freckle grains and the matrix, and between the freckles themselves. One possible explanation could be pullout of the large eutectic colonies (and η in DS-1) during grinding and polishing of the sample. However, such pullout should have been seen in the eutectic colonies as well as

in the matrix. Furthermore, if porosity were caused by the removal of eutectic colonies, then the volume fraction of eutectic in these freckle regions would have been lower. Therefore, the porosity must be a real consequence of solidification as has been observed in previous studies of freckle chains.[2,23,43] It is unlikely the porosity is caused by gases since all processing occurs in a vacuum, but rather when the liquid feeding to the advancing solid is slowed by the meandering dendrite arms in the mushy zone[2]. Solidification shrinkage, or macroshrinkage, occurs at the last regions of solidification[2] and could also be a factor in the formation of porosity. More porosity was observed in DS-2 than DS-1 likely because the remaining liquid could not freeze as η, but had to continue the growth of established eutectic colonies.

The morphology and quantity of γ' found between freckle-freckle and freckle-matrix boundaries were not seen at the DS boundaries in either casting. Therefore, the grain boundary γ' is a freckle-related microstructure and is likely caused by excess solute in the freckle chains and grain boundary diffusion of solute to enable coarsening of this γ'. This mechanism also can cause the "elongated" γ' in the regions surrounding the grain boundaries in the freckled regions. Excess solute and grain boundary diffusion cause the cuboidal γ' near these boundaries to coarsen more than in other regions. Both the excess solute and grain boundary transport are necessary to create this morphology, as it was not present at the DS boundaries.

The microstructure and phases present at the surface of the casting appear to be formed by a reaction between the ceramic mold and the liquid metal. This situation is not limited to freckled regions, but does involve surface mechanisms that may influence freckles. Large amounts of MC carbides and alumina were present on the surface and, in

most cases, the alumina layer covered the other phases present. Some zirconia was seen, but only covering alumina. It is likely that a reaction occurred[46] between silica in the ceramic mold and Al in the molten metal:

$$2\ Al + 3\ SiO \rightarrow Al_2O_3 + 3\ Si \qquad (9)$$

This would explain the trace Si amounts seen on the surface (although this Si may have been from SiC used while grinding). These and any amounts of Si would be so minute as to only contribute to background in EDS and have little or no effect of the composition and microstructure of the casting—freckle or matrix. A similar mechanism at the surface causing the formation of an alumina layer in CMSX4 and PWA 1483 castings was shown to eventually lead to the formation of scale.[47] Large amounts of carbides were seen on the surface as well, which is a reaction of the Ti and Ta in the liquid metal with C. Whether the C is exclusively from the alloy, or if it is from an outside source, such as residual C left from dewaxing of the ceramic mold, is unknown. It is likely that there was an alumina layer between the casting and the mold along the entire surface of the casting before the ceramic was knocked off. During the removal process, the majority of alumina remained adhered to the casting while some was still stuck to the mold, leaving the casting surface that was observed. Upon removal of the ceramic shell, some of the γ appears to have been removed as well. Because of the oxide found between the surface cuboidal γ', it is likely that the γ oxidized faster than the γ'. This corresponds with a lower Al concentration in the γ, making it less resistant to oxidation than the γ'. It is unlikely that γ would have been pulled away from γ' unless it had oxidized prior to the removal of the mold.

CHAPTER 6
CONCLUSIONS

The objective of this study was to characterize freckle defects in directionally solidified superalloy castings and to understand their mechanism of formation. The following conclusions can be drawn from this study:

- The freckle grain regions have higher concentrations of those elements that inversely segregate (Al, Ta, and Ti) similar to the interdendritic composition. This indicates that the freckles are a product of interdendritic fluid emanating from within the mushy zone.

- Freckled regions have higher volume percentages of eutectic, porosity, and η (if present) than the rest of the casting.

- No orientation relationship occurs between the individual freckle grains and the rest of the casting.

- Dendrite arms torn from the mushy zone in thermosolutal convection are large enough to nucleate freckle grains in the interdendritic plumes, yet small enough to have a minimal effect on the freckle composition when the arms partially remelt.

- During the last stages of solidification, web-like γ + γ' eutectic colonies form from the remaining interdendritic fluid. However, a true eutectic transformation does not occur, but rather small cells of γ' that reject elements that form γ. During this growth, some of the cells grow forming a coarse lamellar structure. If the Ti/Al ratio is high enough, this solidification concludes with the formation of η whose basal plane is oriented with the {111} of the eutectic.

- Porosity that forms in and around the freckle grains is caused by a lack of interdendritic fluid feeding the area around the freckles and is also caused by solidification shrinkage of the casting and freckles. Along with the eutectic colonies, this porosity will greatly reduce the toughness and fatigue of the casting.

- Elongated and intergranular γ' occurring at the freckle grain boundaries is a product of higher solute concentrations and grain boundary transport. Both these mechanisms allow for unique, coarser morphologies of γ' at the freckle-freckle and freckle-matrix boundaries.

- Not exclusively present in freckle regions, a thin layer of Al_2O_3 is formed at the surface of the DS castings from a reaction between the ceramic mold and liquid metal. After γ' precipitation, the alumina grows preferentially in the γ rather than the γ'. Upon removal of the shell, some alumina is left behind and some is detached leaving bare cuboidal γ'.

LIST OF REFERENCES

1. C. T. Sims, N. S. Stoloff, W.C. Hagel: *Superalloys II*, John Wiley & Sons, New York, NY (1987)

2. J.R. Davis, ed: *Heat Resistant Materials*, ASM International, Materials Park, OH (1997)

3. H. Baker, ed: *ASM Handbook Volume 3—Alloy Phase Diagrams*, ASM International, Materials Park, OH (1992)

4. F. Rhines: *Phase Diagrams in Metallurgy: Their Development and Application*, McGraw-Hill, York, PA (1956)

5. G.E. Dieter: *Mechanical Metallurgy*, McGraw-Hill, York, PA (1961)

6. T.M. Pollock, W.H. Murphy, E.H. Goldman, D.L. Uram, J.S. Tu: *Superalloys 1992*, S.D Antolovich, R.W. Stusrud, R.A MacKay, D.L. Anton, T. Khan, R.D. Kissinger, D.L. Klarstrom, eds., TMS Warrendale, PA, pp. 125-134 (1992)

7. G.K. Bouse: *Superalloys 1996*, R.D Kissinger, D. Deye, D.L. Anton, A. Cetel, M. Nathal, T.M. Pollock, D. Woodford, eds., TMS, Warrendale, PA, pp. 163-177 (1996)

8. R. Darolia, D.F. Lahrman, R.D. Field: *Superalloys 1988*, S. Reichman, D.N. Duhl, G. Maurer, S. Antolovich, C. Lund, eds., TMS, Warrendale, PA, pp. 255-264 (1988)

9. S.T. Wlodek: *The Stability of Superalloys*, 1999 TMS Annual Meeting, San Diego, CA, 1999

10. R.A. Horton: *ASM Handbook Volume 15—Casting*, ASM International, Materials Park, OH, pp. 253-270 (1992)

11. S. Tin, T.M. Pollock, W.T. King: *Superalloys 2000*, R.D. Kissinger, T.M. Pollock, R.R. Bowman, K.A. Green, M. McLean, S.L. Olson, J.J. Schirra, eds., TMS, Warrendale, PA 201-210 (2000)

12. D. Porter, K. Easterling: *Phase Transformations in Metals and Alloys*, Chapman and Hall, London (1995)

13. W. Kurz, D.J. Fisher: *Fundamentals of Solidification*, Trans Tech Publications Ltd, Brookfield, VT (1989)

14. V.A Wills, D.G. McCartney: *Mat. Sci. Eng. A*, Vol. A145, pp. 223-232 (1991)

15. M. Vijayakumar, S.N. Tewari, J.E. Lee, P.A. Curreri: *Mat. Sci. Eng. A*, Vol. A132, pp. 195-201 (1991)

16. N. D'Souza, M.G. Ardakani, M. McLean, B.A. Shollock: *Met. Trans. A*, Vol. 31A, pp. 2877-2886 (2000)

17. W.R. Sun, J.H. Lee, S.M. Seo, S.J. Choe, Z.Q. Hu: *Mat. Sci. Eng. A*, pp. 143-149 (1999)

18. R. Hamar, I. Cournes, S. Hamar-Thibault: *High Temperature Alloys for Gas Turbines and Other Applications*, pt. 1, pp. 767-776 (1986)

19. S.N. Tewari, M. Vijayakumar, J.E. Lee, P.A. Curreri: *Mat. Sci. Eng. A*, Vol A141, pp. 97-102 (1991)

20. S. Minakawa, I.V. Samarasekera, F. Weinburg: *Met. Trans. B*, Vol 16B, pp. 595-604 (1985)

21. M.C. Flemings, G.E. Nereo: *Trans. AIME*, Vol. 239, pp. 1449-1461 (1967)

22. J.S. Kirkaldy, W.V. Youdelis: *Trans. AIME*, Vol. 212, pp. 833-840 (1958)

23. A.F. Giamei, B.H. Kear: *Met. Trans*, Vol. 1, pp. 2185-2192 (1970)

24. P.D. Generaux, C.A. Borg: *Superalloys 2000*, R.D. Kissinger, T.M. Pollock, R.R. Bowman, K.A. Green, M. McLean, S.L. Olson, J.J. Schirra, eds., TMS, Warrendale, PA pp. 19-27 (2000)

25. S.M. Copley, A.F. Giamei, S.M. Johnson, M.F. Hornbecker: *Met. Trans.*, Vol. 1, pp. 2193-2204 (1970)

26. S.D. Fellicelli, J.C. Heinrich, D.R. Poirier: *J. Crystal Growth*, Vol. 191 pp. 879-888 (1998)

27. J.R. Sarazin, A. Hellawell: *Met. Trans. A*, Vol. 19A pp. 1861-1871 (1988)

28. T.M. Pollock, W.H. Murphy: *Met. Trans. A*, Vol. 27A, pp. 1081-1094 (1996)

29. S. Tin, T.M. Pollock, W.H. Murphy: *Met. Trans. A*, Vol. 32A, pp. 1743-1753 (2001)

30. C. Frueh, D.R. Poirier, S.D. Fellicelli: *Met. Sci. Eng. A*, Vol. A328 pp. 245-255 (2000)

31. F.P. Incropera, D.P. DeWitt: *Fundamentals of Heat and Mass Transfer*, John Wiley and Sons, New York (1996)

32. P. Auburtin, A. Mitchell: *Liquid Metal Processing and Casting AVS Conf.*, AVS, Santa Fe, NM, pp. 18-34 (1997)

33. J.C. Heinrich, S. Fellicelli, D.R. Poirier: *Num. Heat Transfer, Part B*, Vol. 23, pp. 461-481 (1993)

34. H. Combreau, G. Lesoult: *Modeling of Casting, Welding, and Advanced Soldification Processes VI*, T.S. Piwonka, V. Voller, L. Katgerman, eds., TMS, Warrendale, PA, pp. 201-208 (1993)

35. M.C. Schneider, J.P. Gu, C. Beckermann, W.J. Boettinger, U.R. Kattner: *Metall. Mater. Trans. A*, Vol. 28A, pp. 1517-1531 (1997)

36. P. Auburtin, T. Wang, S.L. Cockcroft, A. Mitchell: *Met. Trans. B*, Vol 31B, pp. 801-811 (2000)

37. C. Beckermann, J.P. Gu, W.J. Boettinger: *Met. Trans. A*, Vol. 31A, pp. 2545-2557 (2000)

38. G. F. Van Der Voort: *Metallography: Principles and Practice*, McGraw-Hill, New York (1984)

39. R.T. DeHoff: *Materials Microstructure*, University Copy Center, Gainesville, FL (2001)

40. J.I. Goldstein: *Scanning Electron Microscopy and X-Ray Microanalysis*, Plenum Press, New York (1994)

41. *Link Opal Operator's Guide*, Oxford Instruments PLC, United Kingdom (1997)

42. R. Zhao, R. Beltran: *Met. Trans. A*, Vol. 32A, pp. 1271-1282 (2001)

43. P. Auburtin, S.L. Cockcroft, A. Mitchell, T. Wang: *Superalloys 2000*, R.D. Kissinger, T.M. Pollock, R.R. Bowman, K.A. Green, M. McLean, S.L. Olson, J.J. Schirra, eds., TMS, Warrendale, PA 225-261 (2000)

44. MatWeb Material Property Data, http://www.matweb.com/, accessed May 2003

45. R. Schadt, I. Wagner, J. Pruehs, P.R. Sahm: *Superalloys 2000*, R.D. Kissinger, T.M. Pollock, R.R. Bowman, K.A. Green, M. McLean, S.L. Olson, J.J. Schirra, eds., TMS, Warrendale, PA 211-218 (2000)

46. Y. Virieux, J. Desmaison, J. Labbe, A. Gabriel: *Key Engineering Materials*, Vol. 132-136, pp. 1657-1660 (1997)

47. K. Kloske: *Investigation of Scale Formation on the Surface of Two Directionally Solidified Nickel-Base Superalloys*, Master's Thesis, University of Florida (2001)

BIOGRAPHICAL SKETCH

Erik Michael Matthew Mueller was born on July 7, 1978, to Michael J. Mueller and his wife Sally Leona in Jacksonville, FL. There he attended Sacred Heart Elementary and Bishop Kenny High School, where he started at defensive line for the football team and threw shotput and discus for the track team. After graduating in 1996, Erik moved to Gainesville, FL, where he attended the University of Florida. His undergraduate research focused on fractal analysis of lead zirconate/lead titanate fracture surfaces under the tutelage of Dr. J. J. Mecholsky. In May 2000, he graduated cum laude with a Bachelor of Science in materials science and engineering with a focus in engineering ceramics, and began an internship at American Technical Ceramics. There he worked on particle size reduction for processing multi-layered ceramic capacitors. He then entered graduate school later that year at the University of Florida and redirected his focus to metallurgy and electron microscopy.